TE CO_2 LASER DYNAMICS

TE CO_2 LASER DYNAMICS

by

JOHN REID, B.A., M.Sc.

A Thesis
Submitted to the Faculty of Graduate Studies
in Partial Fulfilment of the Requirements
for the Degree Doctor of Philosophy

McMaster University
December 1974

© 1977

DOCTOR OF PHILOSOPHY (1974)
(Physics)

McMASTER UNIVERSITY
Hamilton, Ontario

TITLE: TE CO_2 Laser Dynamics

AUTHOR: John Reid B.A. (Oxford University

M.Sc. (McMaster University)

SUPERVISORS: Professor B.K. Garside, Professor E.A. Ballik

NUMBER OF PAGES: 170 , xix

ABSTRACT

The work described in this thesis concerns the investigation of the properties of transversely excited (TE) CO_2 lasers. The introduction of these high pressure CO_2 lasers in 1970 represented a very significant advance in high power laser technology. However, despite concentrated research on this CO_2 laser, many aspects of the laser dynamics are not clearly understood. This is particularly true of the processes, taking place on a time-scale of a microsecond or less, which control the dynamics of TE CO_2 lasers. The work reported here was initiated in 1970, and was aimed at the development of a better understanding of the dynamics of pulsed TE lasers.

The initial investigations were concerned with the small-signal gain in typical pulsed TE CO_2 amplifiers. Two different experimental techniques were used to measure gain; (1) A direct method employing a low pressure cw CO_2 laser as a probe, and (2) An in-cavity technique which enabled very accurate measurements to be made of relative gain. A theoretical model was developed to explain the observed time-dependence of the gain profiles. Particular attention was paid to the behaviour of the lower laser level during the risetime of the gain, as this has been the subject of some recent controversy. The results obtained here unambiguously demonstrate that the lower laser level empties rapidly during the risetime of the gain.

Once the correct gain mechanism was determined, the pumping processes which take place during the discharge current pulse were investigated. The small-signal gain in typical gas mixtures was measured as a function of increasing discharge energy, and a gain saturation effect was observed. Careful experimental investigation revealed that this saturation of gain with increasing energy is not caused by secondary effects such as temperature increases or discharge deterioration, but is a fundamental property of CO_2 discharges. At low input energies, the pumping efficiency of the upper laser level was found to agree with conventional models, but the measured efficiency falls drastically at high input energies. This has important consequences for all high energy TE CO_2 lasers.

In the final section of this thesis, the interaction between the CO_2 gain medium and intense laser radiation is studied. Experimental laser pulses are observed under carefully controlled conditions in a Q-switched cavity. These pulses are compared with the predictions of a theoretical model which explicitly includes rotational relaxation within the sublevels of the 10.4 μ band. It is shown that the effect of rotational coupling dominates the laser dynamics in moderately low pressure CO_2 lasers, and its inclusion in the laser dynamical equations accounts for most of the difficulties encountered with previous models. The excellent fits obtained between theory and experiment enable careful studies to be made of slowly decaying laser pulse "tails". It is shown that these tails are controlled by the various relaxation rates of the lower laser level. The relaxation rates are determined under conditions which are relevant to the laser dynamics.

ACKNOWLEDGEMENTS

I wish to express my appreciation to my supervisors, Dr. B.K. Garside and Dr. E.A. Ballik, for their guidance and support in this work.

I would like to thank Dr. J.J. Lowke of the Westinghouse Research Laboratories for supplying tables of cross-sections of electron excitation in He, CO_2 and N_2. Thanks are also due to my colleague T. Tricker who developed the computer program described in Section 2.5.

This work was supported, in part, by the National Research Council and the Defence Research Board of Canada.

TABLE OF CONTENTS

CHAPTER		PAGE
1	INTRODUCTION	1
2	CO_2 LASER MOLECULAR DYNAMICS	10
	2.1 CO_2 Molecular Structure	10
	2.2 Rotational Structure and Laser Transitions	13
	2.3 Relationship Between Inversion and Gain	14
	2.4 Hot Band Transition	20
	2.5 Electronic Excitation Processes	21
	2.6 Collisional Relaxation Processes	24
	2.7 In-Cavity Time-Delays	30
	2.8 Summary	32
3	EXPERIMENTAL APPARATUS AND PRELIMINARY GAIN MEASUREMENTS	33
	3.1 The Pin-Pin Discharge System	33
	3.2 Gain Measurement Apparatus	38
	3.3 Preliminary Gain Measurements	45
	3.4 Summary	49
4	STUDIES OF THE INVERSION AND LOWER LEVEL RELAXATION IN PULSED TE CO_2 LASERS	50
	4.1 Introduction	51
	4.2 Direct Laser Amplifier Gain Measurements	54
	4.3 In-Cavity Laser Gain Measurements	59
	4.4 Hot Band Lasing Observations	68
	4.5 Direct Measurements of the Bending Mode Temperature	72
	4.6 Discussion and Conclusions	79
	4.7 Summary	84

TABLE OF CONTENTS

CHAPTER PAGE

5 REDUCTION OF THE PUMPING EFFICIENCY IN CO_2 LASERS AT HIGH DISCHARGE ENERGY 85

5.1 Introduction 85
5.2 Experimental Technique 87
5.3 Results and Analysis 88
5.4 Discussion and Conclusions 118
5.5 Summary 121

6 STUDIES OF ROTATIONAL COUPLING AND LOWER LEVEL RELAXATION RATES DURING Q-SWITCHED TE CO_2 LASER PULSES 122

6.1 Introduction 123
6.2 Experimental Technique 126
6.3 Theoretical Model 132
6.4 Rotational Coupling and its Effect on the Main Laser Pulse 139
6.5 Laser Pulse Decay and Lower Level Relaxation Rates 143
6.6 Discussion and Conclusion 150

7 CONCLUSIONS 154

Appendix A THE PARTITION FUNCTION OF CO_2 AND ITS INFLUENCE ON THE LASER LEVEL POPULATIONS 159

Appendix B THE ENERGY IN THE COMBINED BENDING AND SYMMETRIC STRETCHING MODE 164

References 165

FIGURE CAPTIONS

FIGURE		PAGE
1	The vibrational levels of CO_2 relevant to laser operation.	12
2	Detailed transition diagram of laser oscillations in the 10.4 μ and 9.4 μ bands (from Reference 42).	15
3	Relative gains on the P and R branches of the 10.4 μ band, calculated using (2.10) and (2.11). $T = 300°K$ and $N_u/N_\ell = 10.0$.	19
4	Energy levels of the CO_2 molecule, and relaxation mechanisms of the lower laser level.	27
5	Collisional relaxation rates for a 10% CO_2: 90% He mixture at 100 torr total pressure.	29
6	Schematic diagram of the discharge circuit. Also shown are typical current and voltage pulses obtained when a 20 nF capacitor, charged to 20 kV, was discharged through a 3% CO_2: 97% He mixture at atmospheric pressure.	37
7	Schematic diagram of the apparatus used for measuring small-signal gain.	39
8	Schematic diagram of the repetition-rate control unit. The 4-bit binary counters perform simultaneous division of the pulse rate by factors of 2,4,8 and 16 at the A, B, C and D outputs.	42

FIGURE PAGE

9 Typical gain signal superimposed upon the modulated probe laser beam. Gas mixture is 85% He: 5% N_2: 10% CO_2 at 80 torr, and amplifier length is 92 cm. 43

10 Small-signal gain as a function of stored energy 47

11 Measured peak gain for several R and P branch transitions in the 10.4 μ band. The fitted curve (using Equations 2.10 and 2.11) corresponds to $T = 340°K$ and $N_u/N_\ell = 10$. A 10% CO_2: 6% N_2: 84% He mixture at 80 torr total pressure was used, with an input energy of ∿100 J/ℓ-atm. The P(18) peak gain was 2%/cm. Some typical error bars are also indicated. 55

12 Measured peak gain for several P-branch transitions in the 10.4 μ band. The fitted curve corresponds to $T = 410°K$ and $N_u/N_\ell = 10$. Gas mixture and pressure were the same as for Figure 11, but the discharge energy was increased to ∿250 J/ℓ-atm. This gave a peak gain of 1.5%/cm on P(18). 58

13 The ratio of the maximum gain in the R-branch to the maximum gain in the P-branch (R/P) plotted as a function of N_u/N_ℓ, for two different rotational temperatures. Also displayed is a typical experimental error bar of ±5% in the value of R/P. 60

FIGURE PAGE

14 Relative gains on the P-branch transitions of the 10.4 μ band for two different rotational temperatures, calculated using Equation 2.10. 62

15 Time-delay to lasing as a function of relative gain for transitions P(6) to P(38) and R(6) to R(34). Transitions with J-values greater than 20 are represented by X, those with J-values less than 20 by ○. P(20) is represented by □ . The time-delay curve is plotted for two different rotational temperatures, 330°K and 360°K. (N_u/N_ℓ was taken as 10 in each case). The data for 360°K has been shifted 5 μs to the right. Discharge mixture is 10% CO_2: 90% He at 75 torr total pressure, with an input energy ∿90 J/ℓ-atm. 63

16 Determination of N_u/N_ℓ using the data of Figure 15. As N_u/N_ℓ is varied, the P and R branch temperatures are fitted separately, using Equations 2.10 and 2.11. The error bars represent fitting errors. 65

17 Time variation of the gain on P(18) as measured directly with a cw probe laser (solid line) and as deduced from the time - delay data of Figure 15 (dashed line). Discharge conditions are given in the caption of Figure 15. Zero time corresponds to the peak of the discharge current pulse. 67

FIGURE PAGE

18 Variation of the ratio N_u/N_ℓ during the risetime of the gain. The four time-delay curves are generated by varying the excitation conditions and cavity loss for a 10% CO_2: 90% He mixture at 35 torr total pressure. The horizontal bars on each curve represent the maximum variation in the time-delay of the R-branch line with the highest gain. Also indicated is the corresponding range of N_u/N_ℓ. The gain peak occurs approximately 27 μs after the peak of the current pulse (0 μs). 69

19 Variation of the bending mode temperature, T_1, during the risetime of the gain. The two time-delay curves are generated by varying the cavity loss for a 10% CO_2: 90% He mixture at 35 torr total pressure. The horizontal bars on each curve represent the maximum variation in the time-delay of the P(20) transition of the hot band. The arrow indicates the time-delay obtained on P(18) of the 10.4 μ band when the total gain in the amplifier has been reduced by a factor of 4. The gain peak occurs approximately 27 μs after the peak of the current pulse (0 μs). 71

20 Gain curves for three different excitation energies in a 10% CO_2: 90% He mixture at 35 torr total pressure. The curves are normalised to a constant initial gain "step". Zero time corresponds to the end of the current pulse. Curves A, B and C correspond to discharge input energies of 8, 16 and 110 J/ℓ-atm respectively, giving peak gains of 0.13, 0.28 and 1.0%/cm. 75

FIGURE PAGE

21 Comparison of measured and calculated gain curves for 10% CO_2: 90% He at 35 torr total pressure. The dashed line is the calculated gain curve using a V-T relaxation time of 10 μs, and an initial value for T_1 of 630°K. The solid line is the gain curve obtained directly from oscilloscope photographs. 76

22 A plot of the initial value of the temperature of the combined bending and symmetric stretch modes (T_1) as a function of discharge energy. The gas mixture was 10% CO_2: 90% He at 50 torr total pressure. These results are typical of those observed over a range of CO_2:He gas mixtures. 78

23 Gain saturation characteristics of a 3% CO_2: 97% He mixture at 150 torr. The solid curve is the measured gain; representative error bars are given for two points. The dashed curve shows the population of the upper laser level as a percentage of the total number of CO_2 molecules present (N_{tot}). Excitation efficiency at low energies is indicated by the straight line. 90

24 The variation of discharge voltage with gas pressure. The voltage was measured at the time of the current pulse peak, and was independent of storage capacitor and charging voltage. 92

FIGURE PAGE

25 Peak gains as a function of pressure and discharge length. ○, Δ, X correspond to lengths of 23 cm, 46 cm, and 92 cm, respectively. 94

26 Small-signal gain of a 10% CO_2: 90% He mixture at various pressures. The energy axis has been scaled by pressure; see text for details. 96

27 Spatial variation of gain for a 3% CO_2: 10% N_2: 87% He mixture at 100 torr. Two gain distributions are shown, the one on the left (curve 1) corresponds to an input energy of 120 J/ℓ-atm. The other gain distribution (curve 2) corresponds to an input energy of 350 J/ℓ-atm. Representative gas temperatures are also shown. 99

28 Spatial variation of gain for a 10% CO_2: 90% He mixture at 150 torr. The solid curve is the gain variation calculated using the indicated spatial energy distribution. Experimental points are also displayed. 101

29 Carbon monoxide production in a 10% CO_2: 90% He mixture at 150 torr. 103

30 Small-signal gain and gas temperature as a function of energy. Temperatures measured by the absorption method (X) and rotational gain method (Δ) are both indicated. (see Section 5.3e). 106

FIGURE PAGE

31 Gain saturation characteristics of a 10% CO_2: 90% He mixture at 150 torr. The solid curve is the measured gain; representative error bars are given for two points. The dashed curve shows the population of the upper laser level as a percentage of the total number of CO_2 molecules present (N_{tot}). Excitation efficiency at low energies is indicated by the straight line. 110

32 Excitation efficiency in the 10% CO_2: 90% He mixture as a function of discharge energy. The results of using the two possible dependences of linewidth ($\Delta\nu$) on temperature are shown. 113

33 Gain saturation characteristics of a 3% CO_2: 10% N_2: 87% He mixture at 100 torr. The solid curve is the measured gain; representative error bars are given for two points. The dashed curve shows the population of the upper laser level as a percentage of the total number of CO_2 molecules present (N_{tot}). Excitation efficiency at low energies is indicated by the straight line. 117

34 Schematic diagram of the apparatus used to observe Q-switched laser pulses. 127

FIGURE PAGE

35 Two experimentally observed laser pulses together with the small-signal gain profile. A 10% CO_2: 90% He gas mixture was employed, at a total pressure of 36 torr. Pulse 1 is obtained when no Q-switch is used; lasing occurs early in the risetime of the gain. Pulse 2 is typical of the pulses obtained when lasing is arranged to take place at, or just beyond, the peak of the gain. Note that an expanded time-scale is employed in plotting Pulse 2. The peak intensity of Pulse 2 is 5 times that of Pulse 1. 130

36 Laser pulse and gain, calculated employing a model not including rotational coupling. All vibrational relaxation rates used in the calculations are chosen to correspond to a 10% CO_2: 90% He mixture at 27 torr total pressure; the values of Rate 1 and the V-T rate used are those determined in Section 6.5. All other parameters are chosen to correspond to the experimental cavity with an amplifier length of 92 cm. Lasing takes place at the peak of the time-dependent gain. 136

37 Laser pulse and gain calculated employing a model including the finite rotational level coupling time (τ_R = 10 ns). All other parameters are the same as for Figure 36. The dashed line indicates the time-dependence of $g_\alpha K(J)\Delta N$. Note the large departure from rotational equilibrium at the time of the laser pulse peak. The threshold gain is 0.24%/cm, the same as in Figure 36 138

FIGURE PAGE

38 Computed laser pulses (solid lines) for a range of τ_R values. All other theoretical parameters are chosen to correspond to the experimental conditions appropriate to Pulse 2 of Figure 35. This pulse is indicated on each plot as a series of experimental points. The ratio of the initial inversion to the threshold inversion ($\Delta n_i:\Delta n_t$)is 4:1. The peak intensities of plots A, B and C are in the ratio 8:3:1. 140

39 Comparison of computed (solid lines) and observed laser pulses for two widely different gas pressures in a 10% CO_2: 90% He mixture. At 72 torr, the experimentally measured $\Delta n_i:\Delta n_t$ ratio is 4:1, and at 27 torr it is 2:1, the cavity decay time is 33 ns. Identical values are used in the calculations. A rotational relaxation rate of $3.6\text{x}10^6$ s^{-1} $torr^{-1}$ is used in each calculation, and all vibrational relaxation rates are similarly scaled with pressure. 142

40 Computed laser pulses at high pressure in a 10% CO_2: 90% He mixture. The dashed lines are the results obtained from a model which does not include rotational coupling; the solid lines are the results obtained when a rotational relaxation rate of $3.6\text{x}10^6$ $s^{-1}torr^{-1}$ is included. The cavity decay time is set at 15 ns (corresponding to a 1 m cavity with two mirrors of 80% reflectivity), and lasing occurs at the peak of the time-dependent gain. This peak gain is set at 1%/cm, and the amplifier length at 80 cm. 144

FIGURE PAGE

41 Computed laser pulses (solid lines) for a range of τ_{VT} values. All other parameters correspond to the experimental conditions appropriate to Pulse 1 in Figure 35; this pulse is indicated on the central plot as a series of experimental points. 146

42 Computed laser pulses (solid lines) for a range of τ_1 values. All other relaxation rates are chosen to correspond to a 10% CO_2: 90% He mixture at the experimental pressure of 72 torr. The experimental pulse indicated in the central plot was obtained by Q-switching the cavity to give lasing at the gain peak(1%/cm, amplifier length 92 cm). To better demonstrate the behaviour in the laser pulse tails, the laser intensities have been plotted on a logarithmic scale. 148

43 Comparison of computed (solid lines) and observed laser pulses for two widely different gas pressures in a 10% CO_2: 90% He mixture. In each case, lasing took place just after the peak of the time-dependent gain (1%/cm, amplifier length 92cm). Rate 1 is set at $4.6x10^4$ s^{-1} $torr^{-1}$ in each calculation, and all other relaxation rates are similarly scaled with pressure. 149

LIST OF TABLES

TABLE		PAGE
1	Recent measurements and calculations of the relaxation rate of the lower laser level (10°0) in CO_2	28
2	Relative Excitation Efficiencies	116
3	Vibrational Partition Function of CO_2	161

CHAPTER I

INTRODUCTION

Early in 1964, Patel et al. [1,2] first reported the observation of cw laser action in CO_2 at a wavelength of 10.6 μ. The discovery came at a time when the search for new laser transitions from ionic and molecular species was near its peak, and as a result this particular laser did not attract any special attention. However, it subsequently became evident that the efficiency and average output power of the CO_2 laser system were unique when compared with all other existing lasers. Consequently, very intensive research and development activities on the CO_2 laser were carried out in industrial, government and university laboratories. Prior to 1970, this research concentrated on longitudinally excited discharges in low pressure CO_2 gas mixtures. Continuous laser outputs of many kilowatts were obtained, and efficiencies of 20% could be attained with relative ease [3]. The maximum peak power obtainable in pulsed operation of a conventional longitudinally excited CO_2 laser was $\sim$ 1 MW [4].

The introduction of the transversely excited high pressure CO_2 laser in 1970 represented a very significant advance in high power laser technology. Megawatt outputs were reported in the initial papers [5,6] and powers in the gigawatt range were soon achieved [7]. (Most of the initial work in this field used atmospheric pressure, transversely excited lasers, commonly called TEA lasers. Subsequently, similar systems were operated at pressures both above and below one atmosphere, and the abbreviation TE became more appropriate). High pressure discharges are essential for the production of powerful laser pulses. The output energy from a given laser volume depends on the number of excited molecules present, and therefore on the gas pressure. The laser pulse duration is determined to a large extent by the relaxation times of the excited molecules. Since these times become shorter at higher pressures, the pulse length also depends on pressure. As a result, the peak power increases rapidly with increasing pressure. However, uniform excitation of gases at elevated pressures is not readily achieved, and much work has been carried out in scaling these lasers to higher pressures and larger volumes [8]. Intense interest in TE CO_2 lasers has been generated as their potential for fusion research became apparent.

Despite concentrated research on the CO_2 laser since 1964, many aspects of the laser dynamics are not clearly understood. Since this laser involves a large number of collisional processes (both electronic and molecular), exact analysis is extremely complex. With the advent of the high pressure CO_2 laser came a pressing necessity to develop an understanding of the CO_2 molecular system on a timescale of a microsecond or less. This is essential if a systematic optimisation of the efficiency and energy extraction in TE lasers is to be accomplished. Much of the work carried out on low pressure cw CO_2 lasers can be suitably scaled to apply to TE lasers, but the intense gain-switched pulse is unique to TE laser cavities. The work described in this thesis was initiated in 1970 and was aimed at the development of a better understanding of the dynamics of pulsed TE lasers. At this stage, it is worthwhile outlining the generally accepted model of laser dynamics in CO_2, with particular emphasis on some of the shortcomings and areas of uncertainty which must be resolved before an accurate understanding of pulsed TE CO_2 lasers can be developed.

The strongest transition in the CO_2 laser takes place between the first asymmetric stretching level (00°1) and the first symmetric stretching level (10°0). (A more comprehensive discussion of CO_2 molecular structure, and an energy level diagram, appear in Section 2.1). The conventional model of pulsed gain in CO_2 lasers assumes that both these levels are populated by the discharge current pulse. The subsequent rise and fall-times of the gain reflect the effective lifetimes of the lower and upper laser levels [9,10]. Furthermore, the symmetric stretching vibrational mode of CO_2 is thought to be very strongly coupled to the bending mode. Consequently, the relaxation of the lower laser level is controlled by the energy decay in the bending mode, in particular the vibration-translation (V-T) relaxation of the 01'0 level. The behaviour of the upper laser level (00°1) (and hence the falltime of the gain) is fairly well understood, and its cross-section for collisional de-excitation is known for all the typical laser gases [11]. However, several measurements have been reported recently which cast doubt on the above interpretation of the risetime of the gain. In the first place, some measurements of the lower level relaxation indicate that the coupling between it and the bending mode may be much weaker than hitherto supposed [12,13]. Secondly, measurements of gain in pulsed CO_2 lasers have been employed to show that the lower laser level does not empty during the risetime of the gain [14,15]. It is extremely important that the correct mechanism for the relaxation of the lower laser level be determined, as it affects both the interpretation of the small-signal gain and the modelling of the laser dynamics. Once the risetime of the gain is understood, there remains the further problem of determining the mechanism controlling the emptying of the lower level during an intense laser pulse. Although the rate is of paramount importance in optimising the energy extraction from TE lasers, very little is known about it. Recent measurements and calculations have determined collisional de-excitation rates for the 10°0 level which range over several orders of magnitude, assume different de-excitation mechanisms, and disagree on the effectiveness of helium at relaxing the lower level [12,13,16-20]. The determination of the correct rate and mechanism is crucial to the subsequent development of an appropriate model for the laser dynamics.

A comprehensive model of the pulsed CO_2 laser must also include the pumping mechanisms which take place during the discharge current pulse. Of particular importance in the development of high power lasers is an understanding of the electronic collision mechanisms in CO_2 at high input energies. These pumping mechanisms have been investigated for low input energies [21,22], but in order to maximise the laser energy extraction from a fixed discharge volume, it is important to know the limitations on the maximum useful input energy. Although it is generally accepted that such a limitation does exist, it is not known if it is a fundamental property of the discharge, or is caused by effects of a secondary nature such as temperature increase~~s~~.

An important objective of the current research on TE CO_2 lasers is to produce more intense laser pulses. This requires a detailed understanding of the laser dynamics, particularly the influence of rotational coupling under conditions of high intensity. Rotational coupling in TE CO_2 amplifiers, and its effect on nanosecond pulses, has been the subject of some research [23-26], but the importance of rotational coupling in the typical gain-switched laser has not been appreciated.

It is the objective of the work reported in this thesis to resolve as many of the above issues as possible. The conclusions reached lead directly to a better understanding of the properties of TE CO_2 lasers. These conclusions, and the supporting research, are outlined below.

In Chapter 4, accurate measurements of small-signal gain on many rotational lines enables us to unambiguously identify the pulsed gain mechanism in TE lasers, and also to determine a lower limit on the 10°0 de-excitation rate. Studies of a Q-switched TE laser presented in Chapter 6 allow us to measure the 10°0 de-excitation rate which controls the laser pulse dynamics. It is this rate which determines the energy extraction by the laser pulse.

Calculations of the electronic pumping mechanisms in CO_2 lasers were first carried out by Nigham in 1969 [27] and 1970 [21].

Similar calculations were subsequently made by several authors [22,28,29], and reasonable agreement with experiment was obtained over a limited range at low energies. However, it has invariably been found that the gain in TE lasers ceases to increase with increasing discharge energy beyond a certain point [7,30-34]. This effect has been variously ascribed to a deterioration of the discharge quality, an increase in the discharge temperature, progressive shortening of the upper laser level lifetime, or a combination of all three. In the work described in Chapters 3-5, a stable cw CO_2 laser was used to measure the gain onmany rotational lines in a TE laser. This gave an accurate measure of the gas temperature, and also determined the absolute populations in the upper and lower laser levels. The temperature increases in TE lasers under normal excitation conditions were found to be small, and consequently thermal effects are unable to account for the saturation of gain with increasing input energy. Investigations described in Chapter 5 have shown that this gain saturation is a fundamental property of the discharge, and cannot be explained by the secondary effects mentioned above.

In Chapter 6, the behaviour of the CO_2 molecular system during interaction with an intense radiation field is investigated. It is this behaviour which ultimately limits the energy extracted from the laser medium by the gain-switched laser pulse. Several models of TE laser pulses have been developed [35-38]; basically these models are very similar, and they all assume that the population distribution over the rotational levels of CO_2 remains in equilibrium throughout the pulse. The falltime of the initial gain-switched spike, and the behaviour in the tail of the pulse, are not well described by these conventional theories. Several authors have attempted to compare theory with experiment, but accurate comparisons are difficult as several experimental parameters are generally unknown (particularly the laser level populations at the onset of lasing). Consequently, several adjustable parameters remain in the theory and a many-parameter fit must be attempted. These fits can only reproduce the gross features of the observed pulses; the falltimes and tails are still incorrect [35-38]. Although the rotational coupling rate in CO_2 is much shorter than the typical laser pulse ($\sim$ 1 ns as compared with 200 ns), it is still possible for significant deviations from rotational equilibrium to occur at the peak of intense laser pulses. A rotational coupling term was added to the conventional laser theory, and the modified theory was compared with experiment. The laser system described in Chapter 6 allows a very careful comparison with experiment to be made; all the laser parameters such as gain, cavity loss, laser level populations and gas temperatures are accurately known. It is found that the observed laser pulses can only be explained by the inclusion of rotational coupling in the laser model. Indeed, using the rotational coupling rate as the only adjustable parameter, an excellent fit between theory and experiment is obtained over a wide range of conditions. The rotational coupling rate obtained in this way agrees with other more direct measurements of rotational coupling in CO_2 [39-41]. Rotational coupling dominates the laser dynamics at pressures below

300 torr, and has significant effects even in atmospheric pressure lasers.

Although the research in this thesis is concerned entirely with CO_2 molecular lasers, many of the techniques described in the subsequent Chapters can be applied to other molecular lasers (such as CO or HF). In particular, the laser model adopted in Chapter 6 can be modified to describe other molecular systems. It is apparent that rotational coupling plays an important part in the dynamics of all high power molecular laser systems.

All measurements were made using pin-pin resistive discharges, generally at pressures below 300 torr. The pin-pin discharge is a very effective method of obtaining stable discharges over a wide range of gas mixtures and pressures. Although the excited volume is small, the input energy/unit volume is comparable with that used in the most powerful TE lasers (see Chapter 5). The pin-pin discharge is an almost ideal scientific tool for the investigation of pulsed TE lasers. It was used in preference to double-discharge systems [8], which tend to operate over a very limited range of pressure, mixture and input energy. Electron-beam (E-beam) pumped lasers are very stable, but offer little advantage over the pin-pin discharge for the type of work described in this thesis. The minor advantage of a uniformly excited volume is greatly outweighed by the complexity and cost of the E-beam systems. Although most of this research has been carried out at moderately low pressure, the conclusions reached apply equally to low pressure pin-pin discharges and to the most up-to-date, high pressure, high energy TE

CO_2 lasers. It is hoped that this work will make a significant contribution to the better understanding of modern high energy lasers.

CHAPTER 2

CO_2 LASER MOLECULAR DYNAMICS

This Chapter gives a brief review of the dynamics of the CO_2 molecular laser. It is intended as an introduction to the experimental work of the following Chapters, and also serves as a convenient place to derive many of the expressions used subsequently in this thesis. A brief description of CO_2 molecular structure is given, with emphasis on the energy levels involved in the laser transitions. The 10.4 μ band is considered in detail, and the relationship between gain and inversion is developed for the rotational lines in this band. Next, the electronic excitation processes responsible for establishing an inversion are investigated, and the complicated collisional relaxation processes in CO_2 are discussed. Finally, a simple laser cavity is considered, and the time-delay to the onset of lasing is calculated.

The CO_2 laser has been the subject of several review articles; for a more comprehensive discussion of the material in this Chapter reference should be made to the articles by Cheo [42] and Woods [8].

2.1 CO_2 Molecular Structure

The CO_2 molecule is a linear symmetric molecule which has an axis of symmetry, C_∞, and a plane of symmetry perpendicular to the

C_∞ axis. There are three normal modes of vibration, symmetric stretching ν_1, bending ν_2, and asymmetric stretching ν_3, which are associated with the species Σ_g^+, Σ_u^+ and π_u, respectively. The designations of species for the CO_2 molecule are chosen in the usual way as for electronic states of homonuclear diatomic molecules [43]. The species π_u represents a doubly degenerate vibration, as the bending vibration can be considered to occur with equal frequency in two perpendicular planes. Each vibrational energy level is denoted by (n_1, n_2^{ℓ}, n_3) where n_1, n_2 and n_3 are the number of quanta excited in the ν_1, ν_2 and ν_3 modes respectively, and ℓ denotes the angular momentum associated with the bending vibration. The fundamental frequencies of the three modes are 1337 cm^{-1}, 667 cm^{-1}, and 2349 cm^{-1}. It should be noted that anharmonic corrections to the vibrational energy levels become more important with increasing quantum number. Fortunately, CO_2 laser transitions involve the lowest vibrational levels, namely, $(00^\circ1 \rightarrow 10^\circ0)$ and $(00^\circ1 \rightarrow 02^\circ0)$; therefore the anharmonic corrections are not very large. However, the lower laser levels $(10^\circ0)$ and $(02^\circ0)$ are almost in resonance, which leads to a perturbation of the energy levels, as first recognised by Fermi [44]. This perturbation also leads to a strong mixing of the eigenfunctions of the two levels. Hence these levels are better represented as $[10^\circ0, 02^\circ0]_I$ and $[10^\circ0, 02^\circ0]_{II}$. This nomenclature will not be adopted in this thesis; for convenience $(10^\circ0)$ will represent the lower level of the 10.4 μ band, and $(02^\circ0)$ will represent the lower level of the 9.4 μ

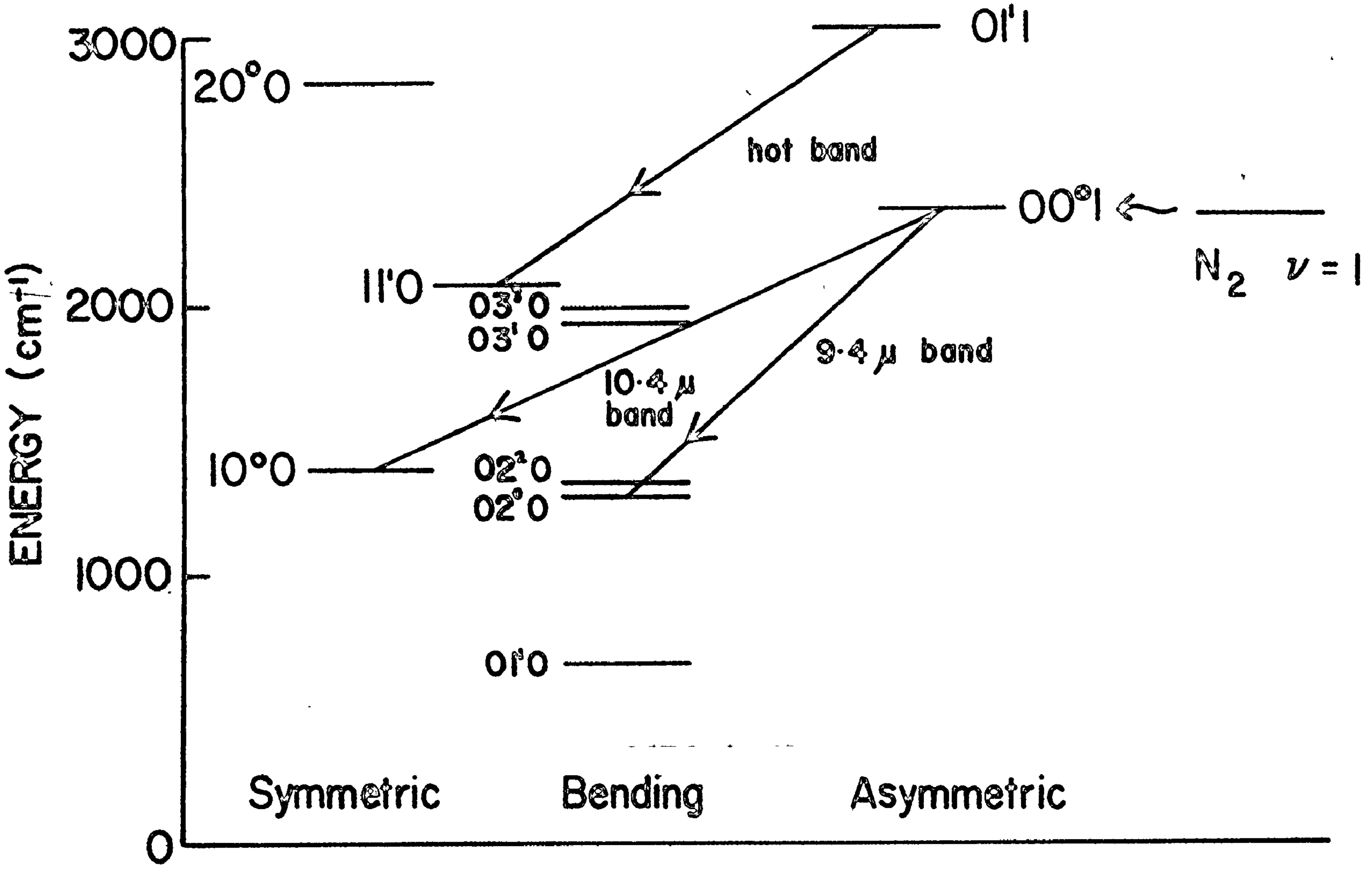
ENERGY (cm^{-1})
3000
2000
1000
0
20^00
11^10
10^00
03^30
03^10
02^20
02^00
01^10
01^11
00^01
N_2 $\nu = 1$
hot band
$10{\cdot}4\,\mu$ band
$9{\cdot}4\,\mu$ band
Symmetric
Bending
Asymmetric

Figure 1: The vibrational levels of CO_2 relevant to laser operation.

band. Figure 1 is an energy level diagram of the low-lying vibrational levels of the CO_2 molecule. The laser transitions are indicated, together with the first vibrational level of the nitrogen molecule, which is an important constituent of most CO_2 lasers.

2.2 Rotational Structure and Laser Transitions

For every vibrational state there exists a set of rotational levels, with slightly different rotational constants for each vibrational level. The energy levels are given by the well-known formula [42] as

$$E(J) = BJ(J+1) + DJ^2(J+1)^2 + --- \qquad (2.1)$$

where E is the rotational energy of the level with the rotational quantum number J, and B is the rotational constant. The $DJ^2(J+1)^2$ and higher - order terms enter (2.1) because of the non-rigidity of the molecule and other effects which are small compared with the first term. The population density, n_J, of the various rotational levels can be described by the Boltzmann distribution

$$n_J = N\left(\frac{hcB}{kT}\right) g(J) \exp\left(-\frac{E(J)}{kT}\right) \qquad (2.2)$$

where g(J) is the statistical weight and N is the total population density of the vibrational level. In the case of CO_2, the spins of the identical oxygen nuclei are zero. Therefore, the antisymmetric rotational levels are missing entirely [42,45]. Hence, for the upper laser level even rotational levels are absent, while for the lower laser level odd rotational levels are absent. For those levels which are allowed $g(J) = 2J + 1$ [43,45].

The selection rules for the vibration - rotation transitions in the IR spectrum are

$$\begin{array}{lll} \Delta\ell = 0, \pm 1 & \Sigma^{+} \leftrightarrow \Sigma^{-}, \quad g \nleftrightarrow g, \; u \nleftrightarrow u & \\ \Delta J = 0, \pm 1 & (J = 0 \nleftrightarrow J = 0) \; + \nleftrightarrow -, \; s \nleftrightarrow a & \end{array} \qquad (2.3)$$

where s and a designate the symmetric and antisymmetric rotational wavefunction and the symbols $\leftrightarrow$ and $\nleftrightarrow$ represent "allowed" and "not allowed", respectively. Specifically, two of the strongest CO_2 laser bands arise from the vibration - rotational transitions of the $\Sigma_u^{+} - \Sigma_g^{+}$ vibrational bands (00°1 → 10°0) and (00°1 → 02°0). Laser transitions have been obtained from both the P-branch ($\Delta J = -1$) and the R-branch ($\Delta J = +1$) of each band. The Q-branch ($\Delta J = 0$) is not allowed because transitions occur between two Σ states for which $\ell = 0$. Figure 2 gives a detailed transition diagram for laser oscillations in both the P and R branches of the (00°1 → 10°0) and (00°1 → 02°0) bands.

2.3 Relationship between Inversion and Gain

To obtain an accurate knowledge of any laser system, it is important to be able to relate gain coefficients to population inversions.

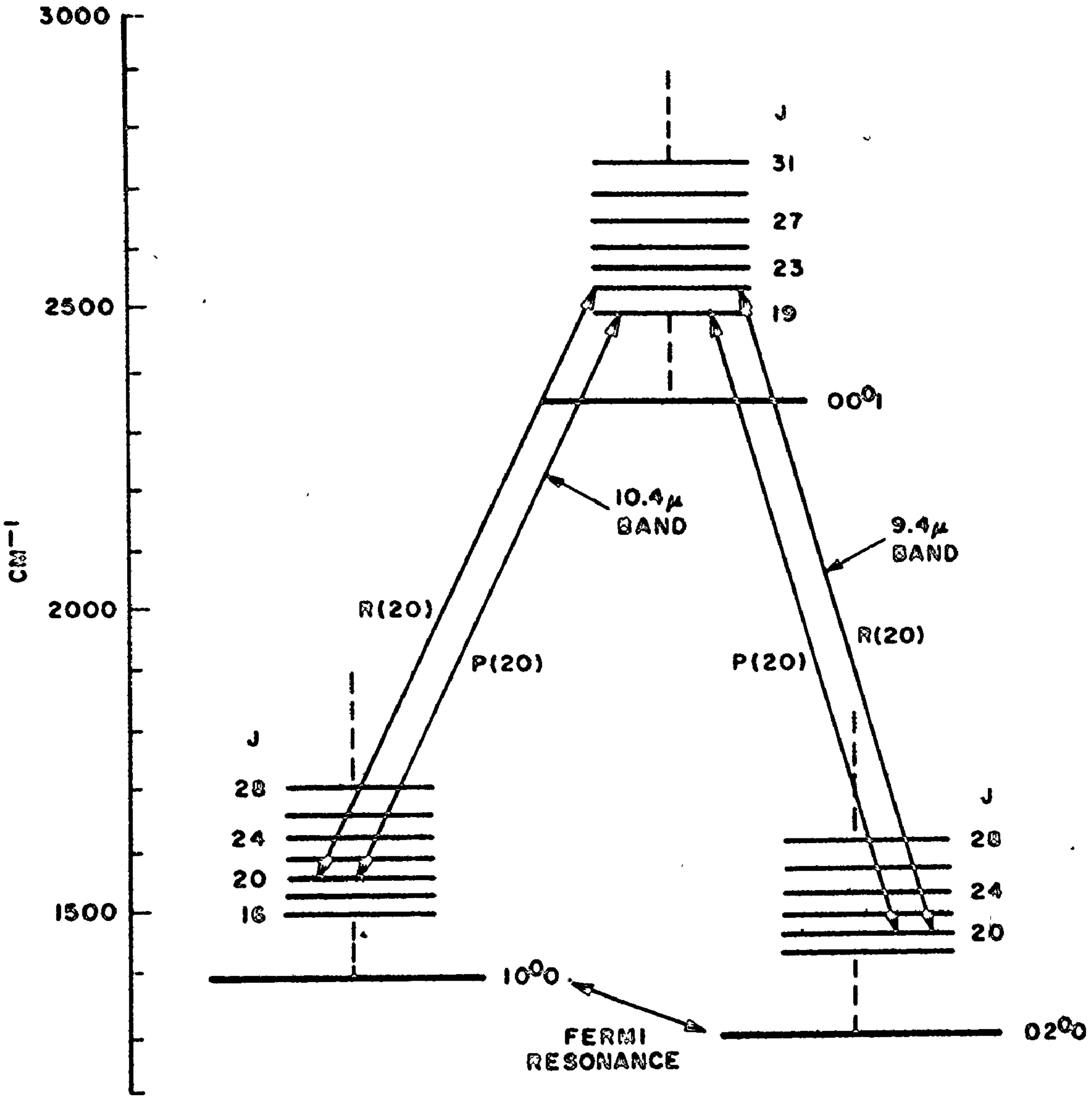

3000
2500
2000
1500
CM⁻¹
J
31
27
23
19
00⁰1
10.4μ BAND
9.4μ BAND
R(20)
P(20)
P(20)
R(20)
J
28
24
20
16
J
28
24
20
10⁰0
FERMI RESONANCE
02⁰0

Figure 2: Detailed transition diagram of laser oscillations in the 10.4 μ and 9.4 μ bands (from Reference 42).

The situation in CO_2 is somewhat complicated by the large number of rotational levels, and consequently a detailed calculation is presented here.

In a gas, the gain coefficient between two levels, u (upper) and ℓ (lower), can be written [46]

$$\alpha(\nu) = \frac{\lambda_o^2}{8\pi} A_{u\ell} \left[N_u - \frac{g_u}{g_\ell} N_\ell \right] g(\nu) \tag{2.4}$$

where λ_o is the wavelength at the centre of the spectral line, $A_{u\ell}$ is the spontaneous transition probability, N_u and N_ℓ are population densities of the upper and lower levels having statistical weights g_u and g_ℓ, and $g(\nu)$ is the normalised lineshape function. The spontaneous transition probability $A_{u\ell}$ is given by [47]

$$A_{u\ell} = \frac{64\pi^2 |R_{12}|^2 S_J F_J}{3h \lambda_o^3 g_u} \tag{2.5}$$

where R_{12} and S_J are the vibrational and rotational contributions to the transition moment, respectively, and F_J is the interaction factor between vibration and rotation. For a P-branch transition $S_J = J$ and for an R-branch transition $S_J = J + 1$, where J corresponds to the lower level. Cousin et al. [48] have accurately determined R_{12} and F_J for both the 10.4 μ and 9.4 μ bands. The number densities, n_J^u and n_J^ℓ, in the upper and lower rotational levels are given by

(2.1) and (2.2)

For gas pressures above 20 torr, the CO_2 transition is pressure broadened and $g(\nu)$ at line centre is given by

$$g(\nu_o) = \frac{1}{\pi\Delta\nu(J)} \tag{2.6}$$

where $\Delta\nu(J)$, the linewidth (half-width at half-maximum), is given, upon rearrangement of the formula derived by Patty et al. [49], by

$$\Delta\nu\ (J) = \frac{C}{(8\pi kT)^{\frac{1}{2}}} \left[P_c + \frac{P_h}{1.69} + \frac{P_n}{1.33}\right] \tag{2.7}$$

C is related to the optical broadening cross-section as defined in the above reference, and P_c, P_h and P_n are the partial pressures of CO_2, He and N_2 respectively. These are the three gases commonly used in CO_2 lasers. Cousin et al. [48] have measured $\Delta\nu$ in pure CO_2, and by fitting a straight line to their data,(2.7) can be modified to

$$\Delta\nu\ (J) = \frac{22.79\Delta_J}{T^{\frac{1}{2}}} \left[P_c + \frac{P_h}{1.69} + \frac{P_n}{1.33}\right] \tag{2.8}$$

where $\Delta\nu$ is in MHz, the partial pressures in torr, and

$$\Delta_J = \begin{cases} 3.42 - 0.0234\,J & \text{P-branch} \\ 3.42 - 0.0267\,J & \text{R-branch} \end{cases} \tag{2.9}$$

Equation (2.8) indicates that $\Delta\nu \propto T^{-\frac{1}{2}}$. Ely and McCubbin show, however, that $\Delta\nu$ varies more closely as T^{-1} in the range 300 - 400°K [50]. This distinction will be considered in Chapter 5; for the time being $\Delta\nu$ will be assumed proportional to $T^{-\frac{1}{2}}$.

Combining the previous equations yields the gain coefficient on the P-branch

$$\alpha_P(J) = \frac{7.13\times10^{-19}\, J\, \{N_u B_u[\exp(-E_u(J-1)/kT)] - N_\ell B_\ell[\exp(-E_\ell(J)/kT)]\}}{\left(P_c + \frac{P_h}{1.69} + \frac{P_n}{1.33}\right)(3.42 - 0.0234J)\,\lambda(J)\, T^{\frac{1}{2}}} \tag{2.10}$$

A similar expression hold for the R-branch

$$\alpha_R(J) = \frac{7.13\times10^{-19}(J+1)\{N_u B_u[\exp(-E_u(J+1)/kT] - N_\ell B_\ell[\exp(-E_\ell(J)/kT)]\}}{\left(P_c + \frac{P_h}{1.69} + \frac{P_n}{1.33}\right)(3.42 - 0.0267J)\,\lambda(J)\, T^{\frac{1}{2}}} \tag{2.11}$$

The values of B_u, B_ℓ and $\lambda(J)$ as given by Chang [51] are used in a computer solution of Equations (2.10)and (2.11). Typical results for α as a function of J,at T = 300°K,are shown in Figure 3. Note that the strongest transition is P(18) at 10.6 μ. Only relative values of gain are indicated in Figure 3. The accuracy of the computer calculation was checked by modifying it slightly to calculate absorption coefficients in pure CO_2 at room temperature. These were compared with the experimental results of Cousin et al. [48]

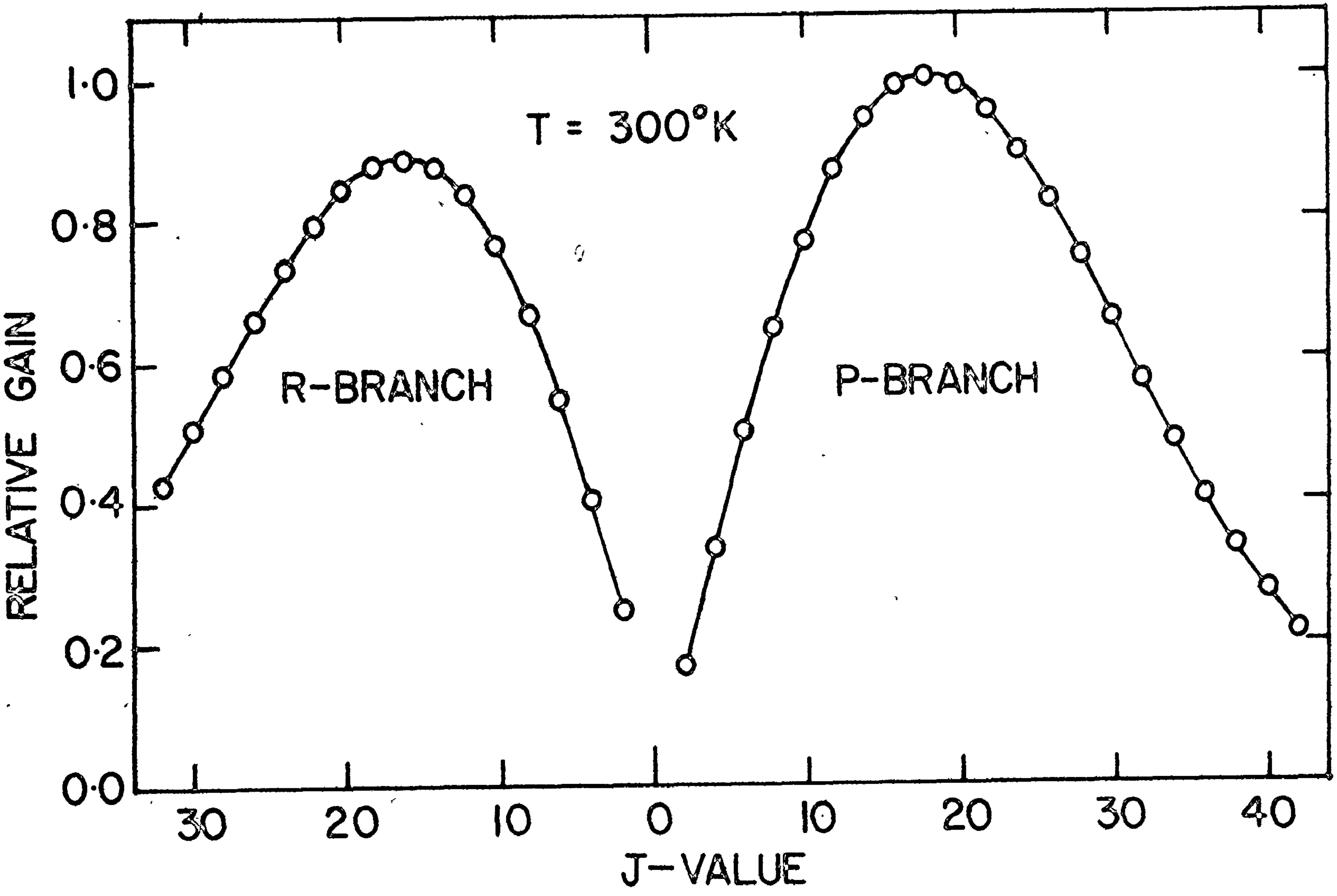

Figure 3: Relative gains on the P and R branches of the 10.4 band, calculated using (2.10) and (2.11). T = 300°K and $N_u/N_\ell = 10.0$

and excellent agreement was obtained. In general, the calculations agreed with experiment to better than 5%. A slighly larger error occurs for P lines with large J values ($>$ 42), where the straight line approximation to $\Delta\nu$ is less accurate. This accuracy is more than adequate for our purposes.

It should be mentioned that the absorption data of Cousin et al. [48] is in good agreement with other measurements [52]. However, some discrepancies arise when absorption data is converted into linewidths and transition moments. No problems arise in the calculation of gain coefficients,provided the data of a given set of measurements is treated self-consistently. This procedure was adopted with the measurements of Cousin et al.

2.4 Hot Band Transition

In addition to the strong transitions observed in the (00°1 → 10°0) and (00°1 → 02°0) bands, several weaker transitions have been observed in CO$_2$ lasers [53,54]. Only one of these will be considered, the hot band transition (01'1 → 11'0) at approximately 11 μ. This transition is equivalent to the 10.4 μ transition, ~~with~~ the addition of a bending mode quantum to each laser level,and is indicated in Figure 1. Only the P-branch has been observed, as the R-branch overlaps the 10.4 μ band. The addition of a bending mode quantum to each laser level increases the complexity of the P-branch transitions. The overall degeneracy of each laser level is increased by a factor of two, and the phenonema of ℓ-doubling ensures that alternate J lines are no longer missing. The transition is now between two states of species π, and the observed spectra feature frequency "staggering" [53,54]. However, if account is taken of the relative degeneracies, the line strength of the hot band transition is similar to that of the 10.4 μ band [48]. Hence, the ratio of the gain in the hot band to that in the 10.4 μ band is a direct measure of the 01'0 population. In Chapter 4, measurements of gain in the hot band are used to estimate the temperature of the bending mode.

2.5 Electronic Excitation Processes

All TE lasers are excited by short current pulses. Energy is transferred to the CO_2 molecules by inelastic collisions with electrons, and by resonant energy transfer from vibrationally excited N_2 [55]. To determine the distribution of the input power transferred to the various vibrational modes requires a knowledge of electron density, electron energy distribution, mean electron energy, and cross-sections for electronic excitation of N_2, CO_2 and He. Because some of these parameters are difficult to measure experimentally, calculated values are heavily relied upon for quantitative predictions of laser performance. Using Holstein's formulations of the Boltzmann equation [56], Nigham has numerically calculated the electron distribution function for a variety of experimentally interesting discharge conditions [21]. With this calculated distribution function and with measured cross-sections, Nigham has determined the fractional power transferred to electronic excitation, ionization, and vibrational excitation of N_2 and CO_2, as a function of the ratio of applied electric field to total particle density, E/N. The calculation assumed spatial uniformity, and that all molecules were in their ground state of energy. In TE CO_2 lasers, because the discharge parameters change on a time-scale which is slow compared to the electron-neutral inelastic collision rate, Nigham's steady-state calculation is applicable for each successive value of E/N taken on by the high pressure pulsed discharge.

In high pressure pulsed CO_2 lasers, typical values for E/N are in the range 2-8 x 10^{-16} V-cm^2 [57,58], resulting in average electron energies of 2-4 eV. A number of authors have measured electron cross-sections for vibrational and electronic excitation of CO_2 in this energy range [59-62]. Halke and Phelps [59] have reported a cross-section for excitation of the lowest bending mode (01'0) in CO_2, along with cross-sections for excitation of the asymmetric stretching vibrations (00°1), (00°2) and (00°3). In addition, they reported cross-sections for electronic excitation and electron impact ionization. More recent work by Boness and Schulz [60,61] and by Andrick et al. [62] have further clarified the low-energy measurements in CO_2, showing that an inelastic process near 3 eV represents the combined excitation of several low-lying bending and symmetric stretching modes. The resonant nature of the cross-sections in the 3-5 eV range indicate that the vibrational excitation of these modes proceeds via the temporary formation of a negative ion state [63]. Cross-sections for direct excitation of the CO_2 (01'0) level and for direct excitation of the CO_2 (00°1) level have also been determined [21].

Using an equation balancing energy deposition from the electric field against the net rate of vibrational and electronic excitation, Nigham has calculated the fraction of the electron power transferred to the individual vibrational and electronic processes. The results are given as a function of gas mixture with E/N as a parameter. For full details, reference should be made to the original paper [21], but one important feature will be mentioned. For the E/N values used in TE lasers, considerable energy can be transferred to the (01'0) level and the combined bending and symmetric stretching modes, and hence to the lower laser level. This energy must decay by collisional relaxation before the peak inversion (gain) is attained.

A very efficient excitation mechanism involves the transfer of energy from vibrationally excited nitrogen molecules to ground state CO_2 molecules by way of the process

$$CO_2\ (00^\circ 1) + N_2\ (\nu = 0) \longleftrightarrow CO_2\ (00^\circ 0) + N_2(\nu = 1) + 18.6\ \mathrm{cm}^{-1} \tag{2.12}$$

This rate is relatively fast ($2 \times 10^4\ \mathrm{s}^{-1}\ \mathrm{torr}^{-1}$ [11]) and N_2 has large cross-sections for vibrational excitation by inelastic collision with electrons [64-66]. Hence N_2 is a common constituent of TE laser mixtures. Despite the improved efficiency and larger gains obtainable with N_2 mixtures, the N_2-CO_2 energy transfer process tends to obscure the dynamics of the CO_2 molecular system. For this reason, the majority of the investigations in this thesis are carried out on mixtures containing only He and CO_2.

Several authors have carried out calculations similar to those of Nigham [22,28,29,67]. Lowke et al. [22] have used the most recent cross-section data, and included the effect of energy loss to elastic collisions in their calculation. We have followed the work of Nigham and Lowke et al. and set up a computer program to calculate electron distribution functions and fractional energy transfers in He: N_2: CO_2 mixtures. The cross-sectional data was supplied in tabulated form by J.J. Lowke of the Westinghouse Research Laboratories. This computer calculation is used in later Chapters to compare theoretical fractional energy transfers with experiment.

2.6 Collisional Relaxation Processes

Excitation processes taking place during the current pulse were discussed in the previous section. Once the current pulse, and hence the excitation, has ceased, many of the CO_2 molecules in the discharge will be excited to low-lying vibrational states. These molecules must eventually relax to the ground state; the various relaxation processes will be considered in this section.

In a comprehensive study, Statz et al. have calculated the Einstein A coefficients in CO_2 for all relevant transitions [68]. All the spontaneous rates are very slow (of the order of a second), and hence collisionally-induced vibrational relaxation dominates energy relaxation processes in CO_2 lasers (in the absence of lasing). These relaxation rates will be considered for a 10% CO_2: 90% He mixture at 100 torr total pressure, which is typical of the mixtures used in this work. Collisional relaxation rates are proportional to pressure and can be simply scaled to higher and lower pressure. Processes of the type $2CO_2\ (00°1) \longleftrightarrow CO_2\ (00°2) + CO_2\ (00°0) + 25\ cm^{-1}$, which result in a redistribution of energy within the asymmetric stretching mode, have a relaxation time of about 20 ns at 100 torr [11,69]. Relaxation rates of the upper laser level (00°1) to all other levels are well known for all typical laser gases. CO_2 has a rate constant of 330 s^{-1} $torr^{-1}$ and He a constant of 80 s^{-1} $torr^{-1}$ [11,70]. The relaxation rates increase with temperature, tending to double at ~450°K [11]; however, this is relatively unimportant for TE lasers as the temperature rise generally does not exceed 50°C. (Some E-beam lasers achieve large temperature increases, and for these lasers the temperature dependence of the relaxation rates may become important).

As indicated in the Introduction, the rates controlling the relaxation of the lower laser level are still the subject of some controversy. The energy in the lower laser level is generally supposed to relax by a two stage process: (1) A relatively fast relaxation to the lowest bending mode level, possibly via the 02°0 and 02²0 levels. This is represented by Rate 1 in Figure 4; specific decay mechanisms are represented by 1(a), 1(b) and 1(c). (2) A slower relaxation of the lowest bending mode level via CO_2 (01'0) + He ⟷ CO_2 (00°0) + He + 667 cm^{-1}, with a rate constant of 3.5 x 10^3 s^{-1} $torr^{-1}$ [11]. This is the V-T rate of Figure 4. However, recent work by Bulthuis and Rosser et al. has cast some doubt on this interpretation [12,13]. Table 1 lists the most recent calculations and measurements of the relaxation rates of the lower laser level. We have tried to interpret experimentally measured rates in terms of the fast and slow rates mentioned above. It is obvious from Table 1 that the situation is very confused.

The rotational sublevels within the upper and lower laser level exchange energy on a subnanosecond timescale for atmospheric pressure gas mixtures. This very fast rate implies that almost every collision is effective at maintaining thermal equilibrium amongst the rotational levels. For a 10% CO_2: 90% He mixture at 100 torr, the rotational relaxation time is approximately 1.5 ns [39-41]. Although this rate is very fast, rotational equilibrium can be significantly disturbed by the effect of intense stimulated emission (see Chapter 6). Figure 5 is a simplified version of Figure 1 indicating the important collisional relaxation processes for a 10% CO_2: 90% He mixture at 100 torr. The lower level relaxation rates are obtained from the work described in the subsequent Chapters.

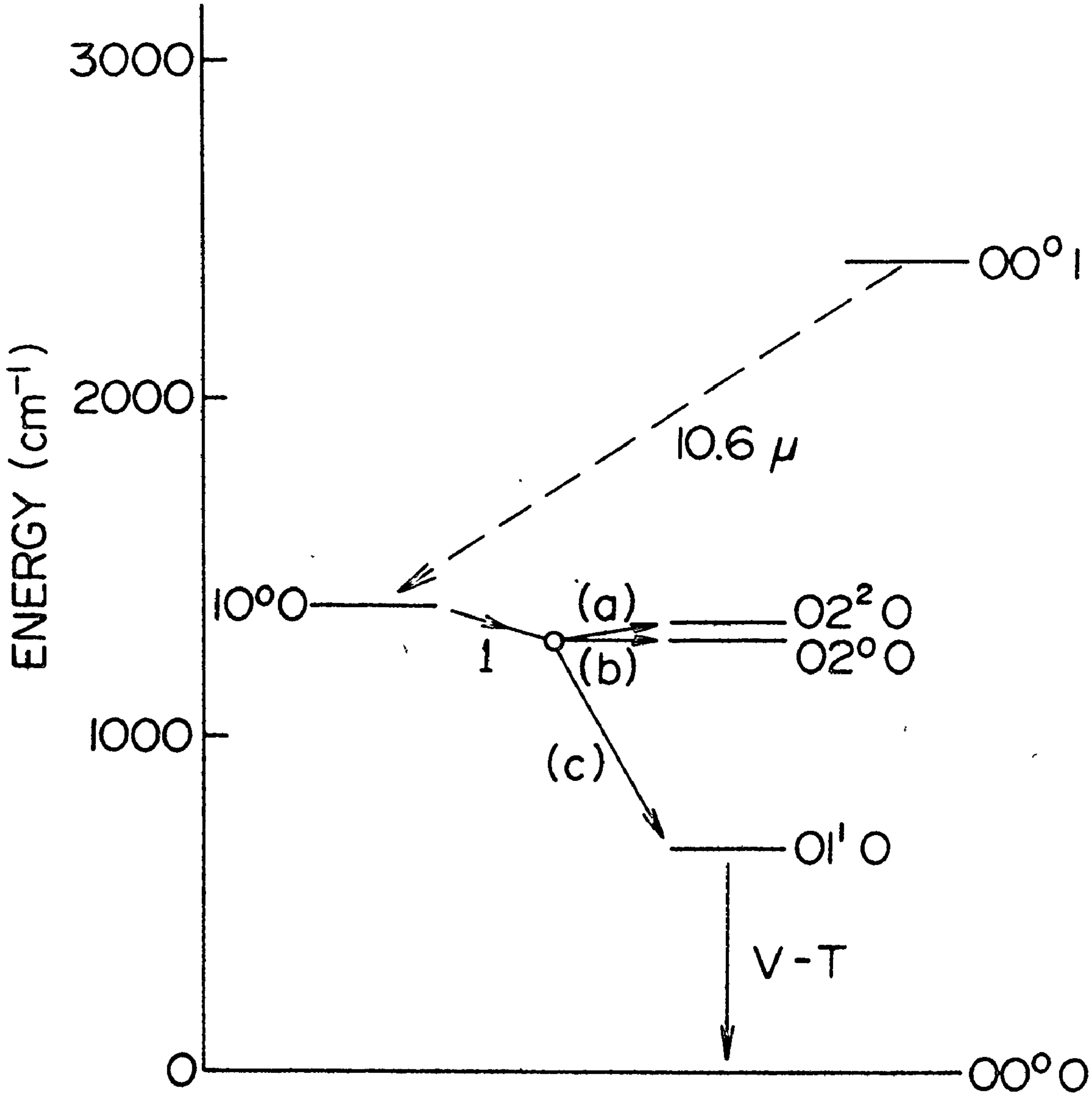
ENERGY (cm^{-1})
3000
2000
1000
0
00°1
10.6 μ
10°0
(a)
(b)
1
02²0
02°0
(c)
01¹0
V-T
00°0

Figure 4: Energy levels of the CO_2 molecule, and relaxation mechanisms of the lower laser level.

TABLE I

Recent measurements and calculations of the relaxation rate of the lower laser level (10°0) in CO_2.

Relaxation Mechanism	Collision Partner	Reference	Rate s^{-1} $torr^{-1}$
1	CO_2	Sharma [20] Calc.	$\sim 6 \times 10^5$
1	CO_2	Seeber [19] Calc.	$\sim 2 \times 10^5$
1(b)	CO_2	Stark [18] Expt.	1.4×10^5
1(b)	He	"	7.5×10^3
1(b)	CO_2	Rhodes [16] Expt.	$> 10^6$
1(a) plus 1(c)	CO_2	"	4×10^5
1(b)	CO_2	DeTemple [17] Expt.	$\sim 10^6$
1(a) plus 1(c)	CO_2	"	$\sim 10^5$
1	CO_2	Manes [37] Expt.	1.3×10^6
1	CO_2	Bulthuis [12] Expt.	$\sim 1.5 \times 10^4$
1	He	"	$< 10^3$
V-T	He	"	$< 10^3$
1	CO_2	Rosser [13] Expt.	$\sim 10^3$
1	He	"	$<< 10^3$
V-T	CO_2	Taylor [11] Review	200
V-T	He	"	3.5×10^3

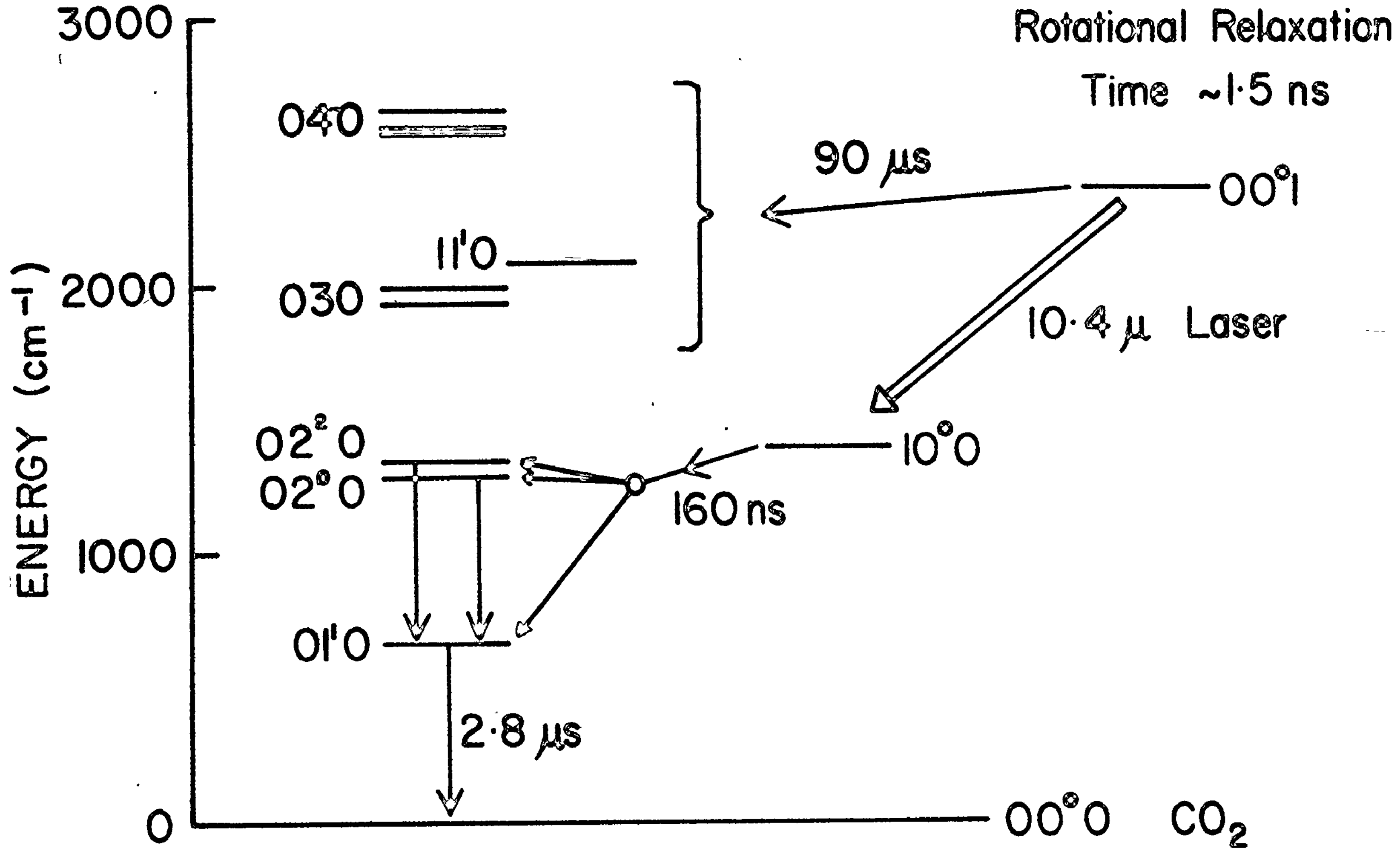
ENERGY (cm⁻¹)
3000
2000
1000
0
040
11'0
030
02²0
02°0
01'0
00°0 CO₂
Rotational Relaxation
Time ~1·5 ns
90 μs
00°1
10·4 μ Laser
10°0
160 ns
2·8 μs

Figure 5: Collisional relaxation rates for a 10% CO_2: 90% He mixture at 100 torr total pressure.

2.7 In-Cavity Time-Delays

To this point, this Chapter has been concerned with the properties of the CO_2 molecular system, and the mechanismsfor establishing an inversion. We shall now briefly consider the behaviour of a TE gain medium when placed in a laser cavity. In TE lasers, the pulsed gain has usually reached a value greatly exceeding the cavity loss at the time of lasing. This leads to the occurrence of an intense gain-switched laser pulse [8]. The period from the current pulse to the onset of this laser pulse will be considered in this section. (The onset of lasing is arbitrarily defined as the time at which the laser intensity rises to ∿5% of its peak value. This intensity is sufficient to be easily detected, but the effects of stimulated emission on the laser level populations are still small. The behaviour of the intense laser pulse, and the resulting gain saturation, will be considered in Chapter 6). The formulae deduced in this section are used in later Chapters.

The photon density (ρ) in the laser cavity must satisfy the following equation:

$$\frac{d\rho}{dt} = \rho\, g(t) - \frac{\rho}{\tau_c} \qquad (2.13)$$

where τ_c is the lifetime of the radiation in the laser cavity and g(t) is the pulsed gain in appropriate units. The photon density will start to build up once the gain in the cavity exceeds the loss i.e.,once $g(t) > 1/\tau_c$. The time, measured from the peak of the current pulse, at which the increasing gain equals the cavity loss is defined as t_{th}.

$$g(t_{th}) = 1/\tau_c \tag{2.14}$$

At this time the laser intensity commences to build up rapidly from its initial value ρ_i to a subsequent value ρ_f which is intense enough to be detected. This buildup time is given by

$$\ell n\ (\rho_f/\rho_i) = \int_{t_{th}}^{t_f} [g(t) - 1/\tau_c]\ dt \tag{2.15}$$

where t_f is the time from the peak of the current pulse to the onset of lasing. The cavity loss and t_f can be measured experimentally, and ρ_f/ρ_i can easily be determined. However, the time-dependence and magnitude of $g(t)$ cannot be determined from a single relationship like (2.15).

This difficulty is easily overcome by measuring t_f as a function of rotational line over the entire 10.4 μ band, maintaining the cavity loss and ρ_f/ρ_i constant. Experimentally, this corresponds to replacing one mirror in the cavity with a grating, and tuning the grating to successive rotational transitions. Theoretically, if the gain on P(18) is given by $g(t)$, the gain on any other transition is given by $g(t)P(J)$ where $P(J)$ is the relative gain factor as plotted in Figure 3. Equations (2.14) and (2.15) become

$$g(t_{th})\ P(J) = 1/\tau_c \qquad (2.16)$$

and

$$\ell n\ (\rho_f/\rho_i) = \int_{t_{th}}^{t_f} [g(t)\ P(J) - \frac{1}{\tau_c}]\ dt \qquad (2.17)$$

If the time-delay, t_f, is measured for sufficient rotational lines, the time-dependence and the magnitude of the gain can easily be determined. This is a very useful property of the time-delays, but just as important is the fact that time-delay measurements provide a very accurate measurement of relative gain. If two transitions with similar time-dependent gains are compared, the transition with the larger gain will lase earlier in time. This property is used extensively in Chapter 4. The advantages of using time-delay measurements compared with direct gain measurements are detailed in References [70-72].

2.8 Summary

This Chapter has presented a review of CO_2 laser molecular dynamics. A knowledge of the background information discussed here will be assumed when particular aspects of the CO_2 laser or gain dynamics are discussed in the following sections.

CHAPTER 3

EXPERIMENTAL APPARATUS AND PRELIMINARY GAIN MEASUREMENTS

In this Chapter,a detailed description is given of the apparatus used for making small-signal gain measurements in a TE CO_2 amplifier. The direct measurement of small-signal gain is a very powerful method of investigating the dynamics of a laser system. The time-dependence of the pulsed gain in TE CO_2 lasers is a measure of the relevant collisional relaxation rates, while the magnitude of the gain determines the laser level populations. Furthermore, measurements of gain as a function of rotational line enable the temperature of the discharge gas to be determined. It is fortunate that gain measurements in TE lasers are relatively easy to make. Low pressure cw CO_2 lasers are ideal probes as they operate on the same transitions and wavelengths as the TE CO_2 lasers. The cw laser used for these measurements is described in detail, as is the TE pin-pin discharge system. The technique used to trigger the TE discharge, and the detection system are also discussed. Finally, some gain measurements are presented, and preliminary results for the variation of gain with discharge input energy are given. The problems involved in interpreting these results are discussed.

3.1 The Pin-Pin Discharge System

The first TEA CO_2 laser was developed by Beaulieu, who employed a linear pin-plane discharge system [6]. Subsequently, a number of techniques were used to obtain multiple transverse discharges distributed along a laser cavity [8]; for small volumes the resistive pin-pin system was very successful and found particular use in helical electrode arrangements [73]. The development of double-discharge systems and E-beam lasers [8] led to more efficient excitation of large discharge volumes. However, as detailed in the Introduction, the pin-pin discharge is to be preferred as a scientific tool for investigating the properties of TE lasers, and was used throughout this work.

The resistors used in any pin-pin discharge system must withstand repetitive, large current pulses for long periods of time. Several types of resistor were examined under extreme discharge conditions, and a wide variety of behaviour resulted. Many resistors failed after a few current pulses, but several types showed no deterioration after many hours. The best performance was obtained from Allen-Bradley carbon composite resistors, and these were employed for all subsequent experiments. Both 1 watt and ½ watt resistors were used with nominal values ranging from 56Ω to 1kΩ; no resistor deterioration has occurred even under conditions of large current pulses (∼ 40 amps/pin) at fast repetition rates. A further series of measurements confirmed that the Allen-Bradley resistors maintain constant resistance throughout the discharge current pulse.

Two different geometries were used for the pin-pin arrays; a linear array similar to that used by Robinson [74], and a double helical array of the type used by Fortin [73]. The helical array results in a gain medium with cylindrical symmetry and is useful for producing laser outputs in the fundamental TEM_{00} mode [73]. However, it is much easier to interpret measurements of spatial gain distributions made using linear pin-pin arrays, as the gain contributions from adjacent discharges are added in a straight-forward manner (see Chapter 5). Consequently linear arrays were generally used throughout this work. The resistors were epoxied into 3.75 cm I.D. Perspex tubes, with a fixed anode-cathode spacing of 2.5 cm. The individual resistor spacing was varied from 3.8 to 12 mm, and the total discharge length (L) from 23 cm to 92 cm.

The gas mixture to be excited flowed through the Perspex tube at a few litres/min (N.T.P.). High purity CO_2, He and N_2 gases were used (as supplied by Matheson), and the flow rate of each gas was monitored by individually calibrated flowmeters. The flowmeter calibrations were accurate to better than 2%. The gases were mixed by a series of baffles before they entered the discharge volume, and were pumped out by two oil-free Edwards ECB1 pumps. These pumps maintained an adequate gas flow at pressures from 20 torr to one atmosphere. The ends of the discharge tube were sealed by O-ring mounted NaCl Brewster windows. Vacuum fittings were used throughout the gas-handling system. Care was taken to minimise leaks into the discharge volume, resulting in a total leakage rate of less than 1 cc/min (N.T.P.).

The gas mixtures were excited by discharging a low inductance capacitor through the resistor array. The circuit used is typical of the simple circuits employed in high-voltage pulsed lasers [73]; it is shown schematically in Figure 6. The power supply (Universal Voltronics) is capable of delivering 100 mA current at a maximum voltage of 50 kV. The present circuit is limited to 38 kV by the hold-off capability of the spark-gap (EG and G, GP 14-B, oil-immersed). This spark-gap is fired by a high-voltage trigger module (EG and G TM11) which is triggered in turn by a pulse generator (Data-Pulse 100A). The capacitors used in the experiments were all rated to 50 kV, and ranged in value from 1 nF to 50 nF. All connections were made as short as possible, and thick copper braid was used to reduce the inductance of the discharge circuit.

This simple discharge circuit was found to give very stable operation over a wide range of gas mixture and pressure, with discharge energy inputs up to 400 J/ℓ-atm. (see Chapter 5). The discharge current and voltage pulses were routinely monitored using a Tektronix P6015 voltage probe and a Pearson Model 411 current probe. The length of the current pulse depends upon the value of the discharge capacitor and gas pressure; typical values range from 100 to 500 ns with pulse magnitudes up to a few kiloamperes. The time-dependence of the voltage pulse is similar to that of the current pulse, while its magnitude is proportional to the discharge gas pressure ($\sim$ 15 kV at one atmosphere). Typical current and voltage pulses are also shown in Figure 6.

FIGURE 6

Schematic diagram of the discharge circuit. Also shown are typical current and voltage pulses obtained when a 20 nF capacitor, charged to 20 kV, was discharged through a 3% CO_2: 97% He mixture at atmospheric pressure.

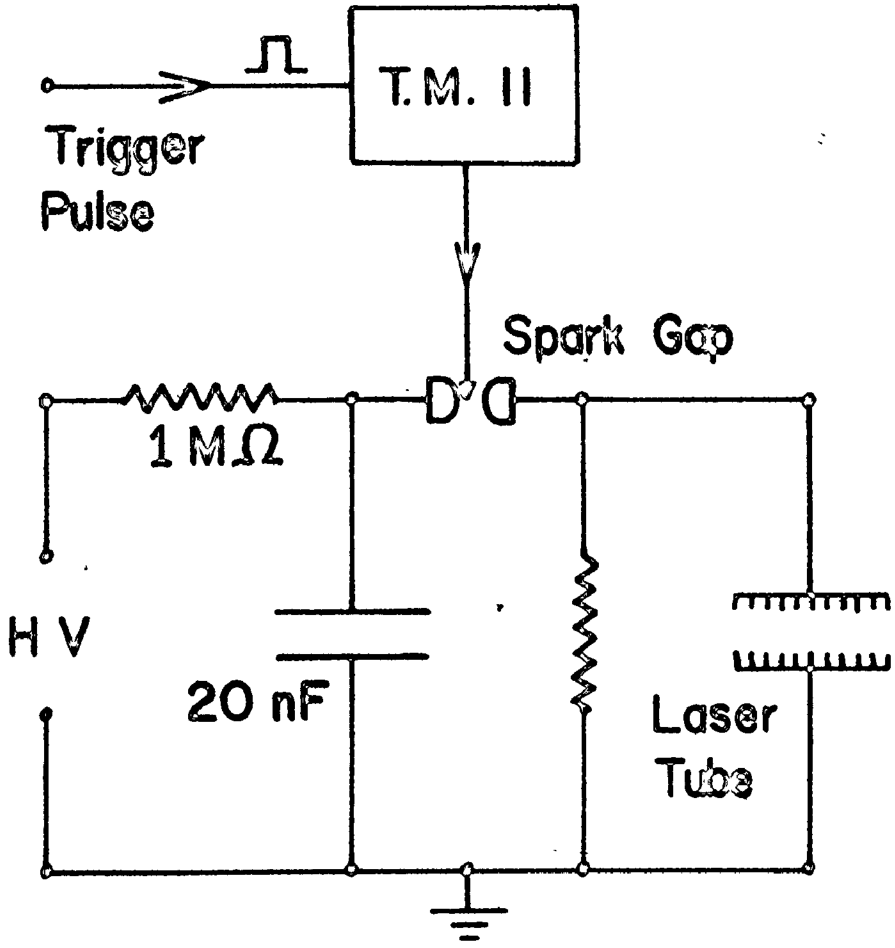
Trigger Pulse
T.M. II
Spark Gap
1 MΩ
H V
20 nF
Laser Tube

DISCHARGE CIRCUIT

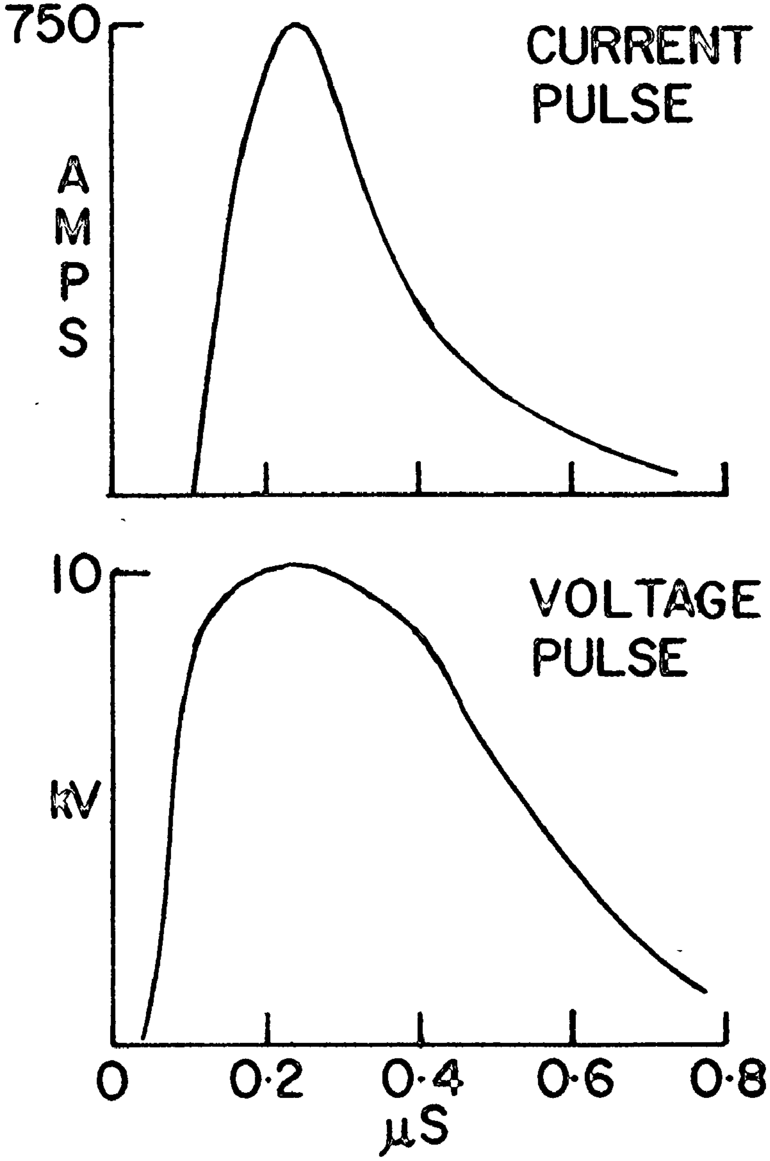

3.2 Gain Measurement Apparatus

The technique described here for measuring small-signal gain in a TE discharge is a modification of that used by Jacobs [75]. Figure 7 is a schematic diagram of the entire apparatus; the individual components are described in detail below.

(a) CO_2 Probe Laser

A stable, low pressure cw CO_2 laser was constructed for these measurements. A sealed-off gain tube containing a mixture of He, N_2 and CO_2 (4: 2: 1) at 10 torr total pressure was excited by a stabilised dc power supply. Currents of 4 to 6 mA were used with no special provision for cooling. The gain tube was mounted in a cavity consisting of a grating and a 10 m radius mirror separated by Invar rods. The grating and mirror supports were also made of Invar to ensure good thermal stability. The grating was a gold-coated replica (Oriel A-82-3533-1060), blazed at 10.6 μ, and provided a measured first order reflectivity of ∿ 92%. Laser output was obtained through the 2% transmitting mirror, (Oriel A-37-742-90). This mirror was mounted on a sensitive micrometer drive for fine tuning of the total cavity length. The laser operated in the fundamental TEM_{00} mode with an output power of approximately one watt. The internal grating allowed the output to be tuned over many lines in the P and R branches of the 10.4 μ band (P(6) - P(42) and R(8) - R(28)). Amplitude stability was better than 2% in the short term, but thermal

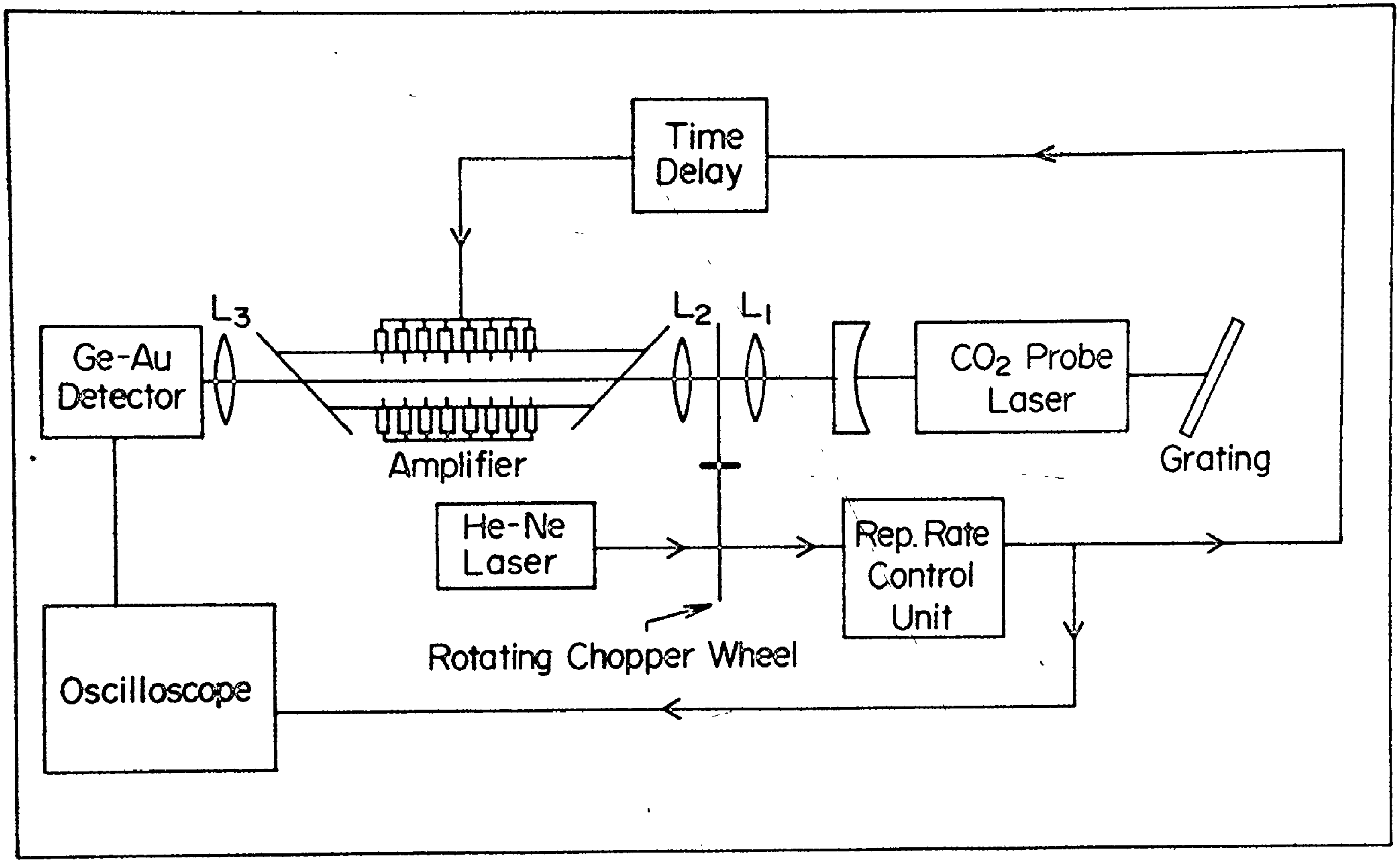
Time Delay
L$_3$
L$_2$
L$_1$
Ge-Au Detector
CO$_2$ Probe Laser
Amplifier
Grating
He-Ne Laser
Rep. Rate Control Unit
Rotating Chopper Wheel
Oscilloscope

Figure 7: Schematic diagram of the apparatus used for measuring small-signal gain.

effects caused the cavity length to drift off line centre over a period of hours. This was easily corrected by manually retuning the output mirror, an operation which took only a few seconds. The absence of water cooling made the laser extremely convenient to operate, but reduced the gain tube lifetime to a few hundred hours between gas refills. This cw laser proved to be an ideal probe for the measurement of gain in TE amplifiers.

(b) Chopper System

It is convenient to use a chopped probe beam, as opposed to a continuous beam, for this type of gain measurement. This enables ac detection methods to be employed, and the beam amplitude can easily be continuously monitored. By chopping with a low duty-cycle, the detector can be protected from overheating. The lenses used in the chopper system also served to focus the probe beam into the TE amplifier. The probe beam passed through two 1" focal length Ge lenses, L_1 and L_2, (Oriel A-11-741-11) spaced approximately 2" apart. The beam was chopped by a spinning disc at the common focus of the two lenses. This arrangement produces fast rise and fall-times in the probe pulse. One of the lenses was mounted on a micrometer driven X-Y-Z positioner. Adjustments in the X and Y direction enabled the probe beam to be deflected horizontally and vertically, and by carefully adjusting the separation of the lenses, the probe beam could be focussed at the centre of the TE amplifier. The effective beam diameter in the discharge was kept as small as possible, and the maximum spot size was generally less than 2 mm (1/e intensity) throughout the discharge region. This ensured that reasonably accurate measurements of spatial gain distributions could be made. A beam pulse repetition rate of approximately 100 p.p.s. was used. This was ideal for monitoring the amplitude of the probe beam, but was much too fast to serve as a trigger for the TE amplifier discharge.

The method used to trigger the amplifier discharge circuit is similar to that employed by Jacobs [75], modified to permit electronic control of the repetition rate of the amplifier. The rotating chopper wheel periodically admitted the cw probe beam and a 6328 Å He-Ne laser "trigger" beam through two separate small slots located 180° apart. The "trigger" beam fell upon a photodiode and the resulting train of pulses was fed to a repetition rate control unit. This reduced the pulse repetition rate to 2 or 3 p.p.s. while maintaining the time synchronisation. Figure 8 is a schematic diagram of the control unit. The output pulses of this unit, with a suitable time-delay, were used to trigger both the discharge and the monitoring oscilloscope. Figure 9 shows a typical gain signal superimposed upon the modulated probe laser signal. Note that this scheme yields a single oscilloscope trace of the probe beam amplitude prior to, during, and after amplification. The time-delay to the amplifier could be adjusted to locate the gain pulse anywhere on the probe signal. This enabled the time base to be expanded to determine risetimes, or compressed to examine the absorption after the amplifier pulse. Further advantages of this technique are

FIGURE 8

Schematic diagram of the repetition-rate control unit. The 4-bit binary counters perform simultaneous division of the pulse rate by factors of 2,4,8 and 16 at the A, B, C and D outputs.

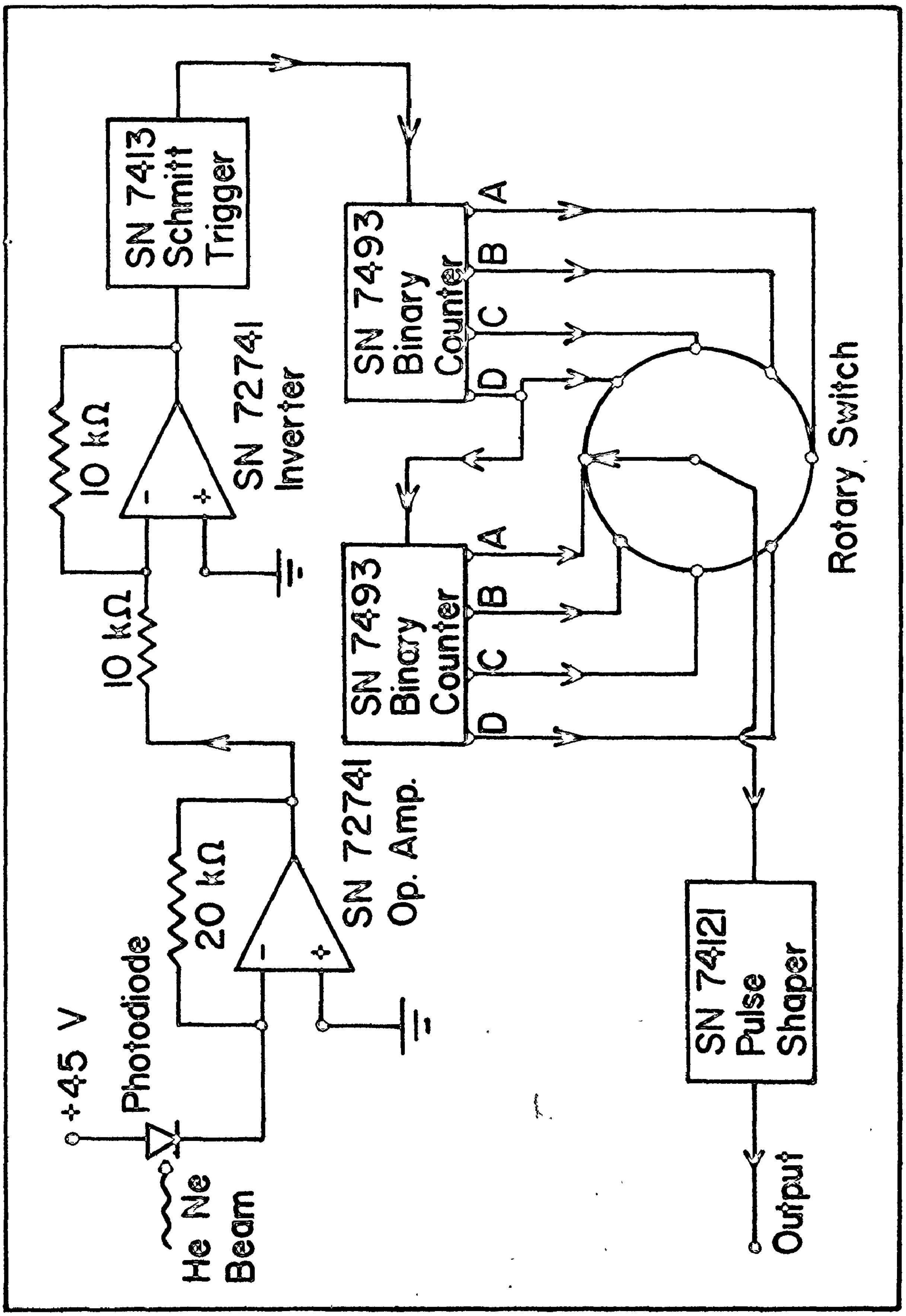
He Ne Beam
Photodiode
+45 V
20 kΩ
SN 72741 Op. Amp.
10 kΩ
10 kΩ
SN 72741 Inverter
SN 7413 Schmitt Trigger
SN 7493 Binary Counter
A
B
C
D
SN 7493 Binary Counter
A
B
C
D
Rotary Switch
SN 74121 Pulse Shaper
Output

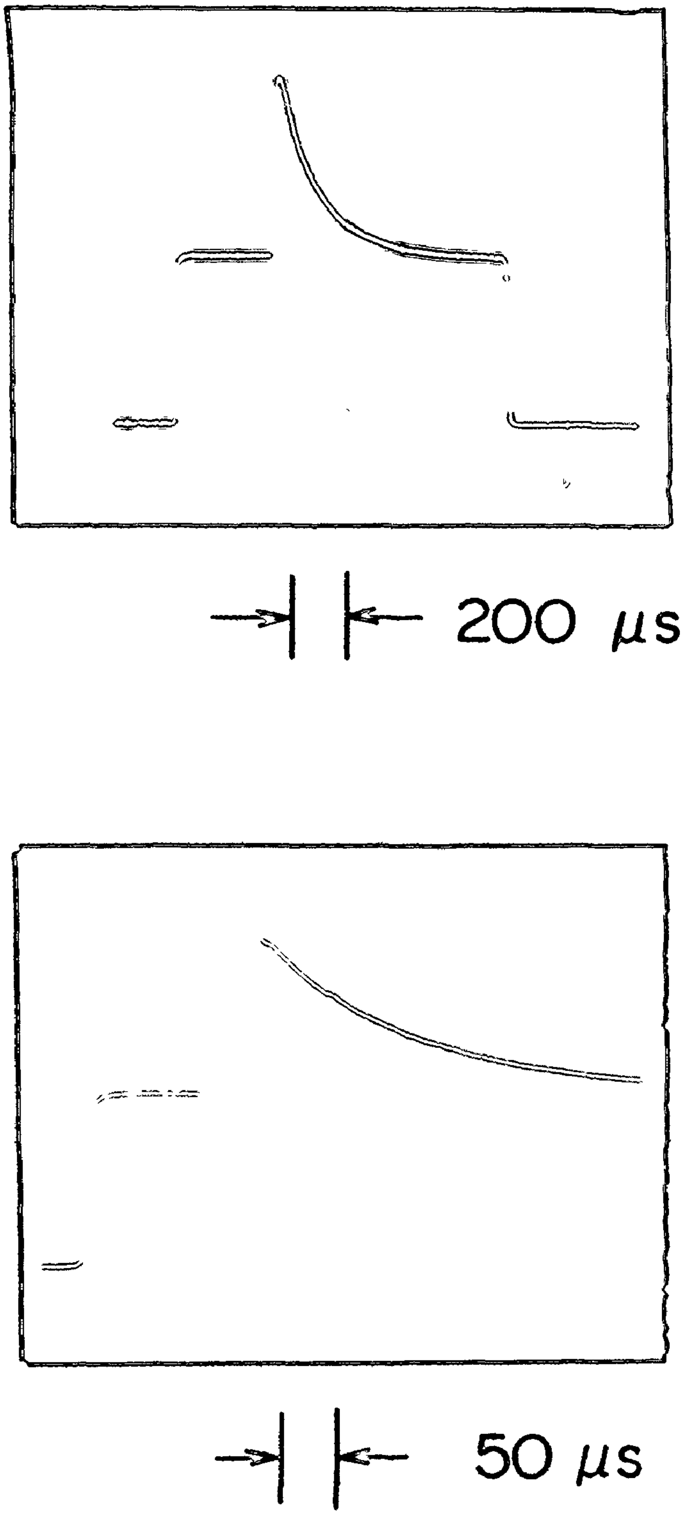

Figure 9: Typical gain signal superimposed upon the modulated probe laser beam. Gas mixture is 85% He: 5% N_2: 10% CO_2 at 80 torr, and amplifier length is 92 cm.

described by Jacobs [75].

(c) TE Amplifier

The amplifier tube used for the majority of the gain measurements consisted of a linear pin-pin array of Allen-Bradley ½ watt 56 Ω resistors. The individual resistors were spaced 3.8 mm apart, and the total discharge length could be adjusted from 23 cm to 92 cm. Further details are given in Section 3.1.

(d) Detection System

A Ge:Au detector (SBRC-40742) cooled with liquid nitrogen, was used in the gain measurements. This is a photo-conductive device with a risetime of 2 ns into a 50 Ω load. However, in order to increase the sensitivity of the detector, the load resistor was varied from 1 to 5 kΩ. The detector signal was amplified by a Tektronix 1A7A Plug-in unit (bandwidth 1 MHz) and displayed on a Type 556 dual-beam oscilloscope. The risetime of the entire detection system was ∿ 300 ns. This is fast enough for all the required measurements. After passing through the TE amplifier, the probe beam was directed onto the detector element by a 10" focal length Ge lens, L_3 (Coherent Radiation LS-05). A 90 volt bias was used in the detector circuit, and the resultant signals were ∿ 20 mV with less than 0.2 mV background noise.

3.3 Preliminary Gain Measurements

Before any accurate gain measurements were made, the system was checked for possible problems. The gains measured under all conditions remained constant when the probe signal was reduced by a factor of 10, confirming that the gain was measured in the small-signal region. With the probe beam switched off, the amplifier was fired and a check made to ensure that no significant radiation reached the detector. Finally, a series of measurements on the detector system ensured that its response was linear over the anticipated range of intensities. The entire apparatus was operated for a period of several months with no significant problems. With the TE amplifier operating in a region of good stability, gain peaks could be measured to an accuracy of 3%, with a similar error in the repeatability pulse-to-pulse and day-to-day.

When the TE amplifier was operated at very high input energies, a strong shock wave was produced in the discharge volume. The wave propagated across the amplifier tube at the velocity of sound and was reflected from the Perspex walls. This resulted in several small ripples on the measured gain profiles. The time between ripples was $\sim$ 40 μsec, corresponding to the time taken for the shock wave to cross the amplifier tube. The magnitude of the ripples was minimised by careful alignment of the lens L_3; they did not significantly interfere with measurements of gain peaks. The discharge plasma caused no other detectable changes in the probe beam, e.g., lensing effects in the amplifier were negligible [73,76].

At this stage, it is worthwhile discussing briefly the main features of the measured gain profiles, as an introduction to the detailed examination given in Chapters 4 and 5. Typical gain profiles are shown in Figure 9. Note that the risetime of the gain is much faster then the falltime. This falltime is exponential, while the behaviour of the risetime is a little more complicated (see Chapter 4). Both the risetime and the falltime are inversely proportional to the total pressure of the discharge gas. Experimentally, it is found that the risetime of the gain is determined by the partial pressure of helium in the discharge mixture; it is changed very little by variations in the CO_2 content. The falltime of the gain does depend somewhat on the gas mixture, exactly as expected from the behaviour of the lifetime of the upper laser level [11,70]. At 100 torr in a 10% CO_2: 90% He mixture, the time taken to reach the gain peak is ∿ 10 μs, and the falltime (1/e) is 85 μs. The behaviour of the lower laser level, and its effect on the risetime of the gain will be discussed in detail in Chapter 4.

The magnitude of the gain depends strongly upon the input energy to the discharge, and also upon the gas mixture. However, for all the gas mixtures and pressures investigated it was found that the gain ceased to increase with increasing discharge energy beyond a certain point. Initially, the small-signal gain increases rapidly with energy, but soon levels off and finally falls as very large values of discharge energy are reached. Figure 10

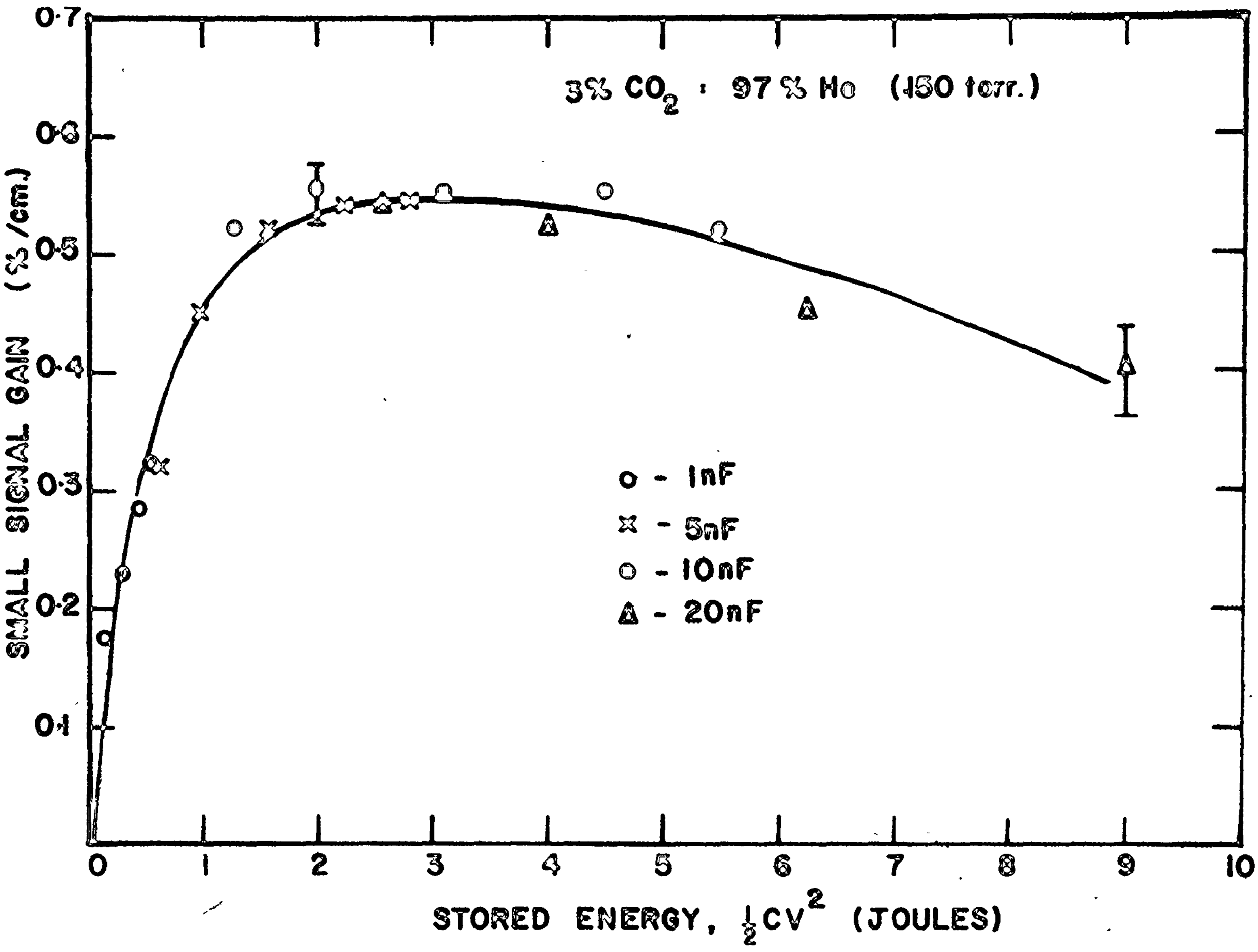

Figure 10: Small-signal gain as a function of stored energy.

is typical ~~of~~ the results obtained. The peak gain in %/cm on the P(18) transition is plotted as a function of the energy stored in the discharge capacitor for a 3% CO_2: 97% He mixture at 150 torr. This is not a mixture normally used in high pressure CO_2 lasers, but it very clearly demonstrates the occurrence of the gain saturation with increasing energy. The saturation value of the gain depends upon the gas mixture; it ranges from 0.6%/cm in 3% CO_2 mixtures to 1.5%/cm in 20% CO_2: 80% He mixtures, and 3.5%/cm in a variety of CO_2: N_2: He mixtures.

Gain saturation with increasing discharge energy has been observed in discrete electrode, double-discharge and E-beam systems [7,30-34]. It is very important to determine if the gain saturation is a fundamental property of the discharge, or is caused by effects of a secondary nature such as temperature increases. The optimisation of energy extraction from high power TE lasers requires a knowledge of the discharge pumping efficiencies at high input energies. However, at this stage, we cannot use the data of Figure 10 to draw conclusions about variations in the discharge efficiency with input energy. Firstly, some obvious candidates for causing the observed saturation effect must be considered and either eliminated or allowed for. For example, it must be ascertained that the culprit is neither discharge deterioration nor high gas temperatures at high input energies. Secondly, mainly for purposes of comparison with theoretical calculations of electron excitation, the stored energy must be related to the discharge input energy in J/ℓ-atm. Furthermore, the measured gain should be converted into an upper level population, which requires a knowledge of the gain mechanism and gas temperature. These issues will be examined in Chapters 4 and 5.

3.4 Summary

This Chapter contains a detailed description of the experimental apparatus employed in the measurement of small-signal gain. Preliminary results of these measurements are given, with emphasis on the variation of the gain profile with discharge mixture and pressure. The magnitude of the gain peak, and its dependence on input energy is also considered, and the problems involved in interpreting these results are discussed. The next two Chapters are devoted to resolving these problems, and developing an understanding of the gain mechanisms (particularly the risetime),and the gain saturation phenomena in TE CO_2 lasers.

CHAPTER 4

STUDIES OF THE INVERSION AND LOWER LEVEL RELAXATION IN PULSED TE CO_2 LASERS

The work described in this Chapter is aimed at identifying the gain mechanism in pulsed TE CO_2 lasers, particularly the behaviour of the lower level (10°0) during the risetime of the gain. As described in the Introduction, a knowledge of the lower level relaxation rate is required to accurately model both the gain and laser dynamics. In mixtures consisting solely of He and CO_2, the upper laser level (00°1) can only be pumped by direct electron excitation. (The discharge does produce some CO by dissociation of CO_2, but the fractional dissociation is much too small to constitute an effective pump of the upper laser level via vibrationally excited CO - see Chapter 5). Hence any increase in gain after the cessation of the current pulse must be caused by a relaxation of the bending and symmetric stretching modes. Two alternative models are developed to describe this relaxation and the consequent increase in gain. A series of measurements is described which enables us to unambiguously identify the correct model, and to determine the relaxation rate controlling the emptying of the lower laser level. Once the correct gain mechanism has been determined, the efficiency of the current pulse at pumping the bending and symmetric stretching (BS) modes can be calculated from measurements of the initial values of the gain. At low input energies this calculated efficiency is found to be in good agreement with theoretical estimates; further evidence that the chosen model for the gain mechanism is correct.

4.1 Introduction

It has generally been supposed that the rise and fall-times of the gain in pulsed CO_2 laser discharges reflect the effective lifetimes of the lower and upper laser levels [9,10]. Furthermore, the symmetric stretching vibrational mode of CO_2 (including the lower laser level, 10°0) is thought to be very strongly coupled to the bending mode. Consequently, the relaxation of the lower laser level is controlled by the energy decay in the bending mode, in particular the vibration-translation (V-T) relaxation of the 01'0 level. As thermal equilibrium is very rapidly established between the bending and symmetric stretching vibrational modes they can be assumed to have a common temperature (T_1) [77], which falls to a value close to the gas translational temperature by the time the peak value of the gain is attained. As a particular consequence of the model, no more than 5% of the total CO_2 molecules can be put into the lower laser level, whatever the value of T_1, and this population will have fallen to less than 1% at the gain peak (at which time $T_1 \simeq$ gas translational temperature). The inversion in pulsed CO_2 lasers is typically several percent of the available CO_2 molecules, and hence the ratio of the upper (N_u) to lower (N_ℓ) laser level populations should be a relatively large number (>6) at the gain peak.

Several measurements have been reported recently which cast doubt on the above interpretation of the gain dynamics. In the first place, some measurements of the lower level relaxation indicate that the coupling between the Fermi-Resonance levels (10°0, 02°0) and the rest of the bending mode may be much weaker than hitherto supposed [12,13]. Secondly, measurements of the gain on different rotational lines for the (00°1 → 10°0) transition in pulsed discharges have been employed to show that the population in the lower laser level exceeds 10% of the total number of CO_2 molecules [14]. Several investigators have reported low values for the ratio of the upper to the lower laser level populations at the peak of the gain [14,15]. These results are clearly not consistent with the conventional model of the pulsed gain dynamics, but they can be accounted for if the following alternate model is adopted. Suppose that, at the end of the current pulse, an inversion is produced between the laser levels, and considerable energy is stored in the bending mode. The risetime of the gain now simply corresponds to the emptying of the energy from the bending mode and the consequent decrease in the value of the partition function. (The partition function of CO_2, and its effect on the gain of the 10.4 μ band, is discussed in Appendix A). During this time, the lower laser level is supposed to be more or less decoupled from the bending mode, and so suffers little decay. The falltime of the gain corresponds, as before, to the decay of the upper laser level, but there may now also be a contribution from the lower level (presumably somewhat similar) decay time.

It is important to establish which of these two models correctly describes the laser gain dynamics. The pumping efficiencies into the upper level and the associated laser dynamical calculations are very different in the two models. Consequently, the approach to the problem of extracting more output energy per unit volume from CO_2 lasers depends greatly on which model is correct. The work described subsequently is aimed at discriminating unambiguously between the two possible dynamical models. The strategy employed is described briefly below.

Gain measurements of the conventional type allow the difference between N_u and N_ℓ to be monitored. This alone cannot distinguish between the two models. What is required is a means of measuring the ratio of the upper to the lower laser level populations during the dynamical changes in the gain. This can be done, in principle, by measuring the gain as a function of time on many lines in the P and R branches of the 10.4 μ band. The ratio of the maximum gain obtained in the R-branch to the maximum gain in the P-branch (R/P hereafter) is a measure of the ratio N_u/N_ℓ at the instant of time chosen, provided that the rotational temperature is known [1,78,79]. Measurements of gain, made in the conventional fashion employing the apparatus described in Chapter 3, are reported in Section 4.2. These results are analysed to determine a rotational temperature, and the accuracy with which a value for N_u/N_ℓ can be extracted is studied. It is concluded that this technique lacks sufficient precision for the task at hand. A new technique, having a much higher precision,is decribed in Section 4.3. This method employs in-cavity time-delays to accurately measure relative gains, as described in Section 2.7. This approach permits the ratio N_u/N_ℓ to be monitored from the end of the current pulse to the peak of the gain. The decay of the lower laser level during this time is clearly demonstrated. This behaviour is consistent with the model in which the BS modes are in thermal equilibrium, and the energy decay is controlled by the V-T relaxation of the 01'0 level. The alternate model, in which the 10°0 population decays much more slowly than the risetime of the gain, is ruled out. In Section 4.4, this issue is settled beyond doubt by some studies of the dynamics of lasing action on the hot band transition (01'1 → 11'0) at 11 μ. Finally, in Section 4.5, the temperature of the combined BS mode (T_1) is studied as a function of the discharge input energy.

4.2 Direct Laser Amplifier Gain Measurements

The apparatus described in Chapter 3 was used to make direct gain measurements in a pulsed TE amplifier. A discharge length of 46 cm was employed, and the probe laser beam was carefully aligned along the centre of the discharge volume. Figure 11 shows the measured peak gains obtained on the P and R branches of the

FIGURE 11

Measured peak gain for several R and P branch transitions in the 10.4 μ band. The fitted curve (using Equations 2.10 and 2.11) corresponds to T = 340°K and N_u/N_ℓ = 10. A 10% CO_2: 6% N_2: 84% He mixture at 80 torr total pressure was used, with an input energy of ∿100 J/ℓ-atm. The P(18) peak gain was 2%/cm. Some typical error bars are also indicated.

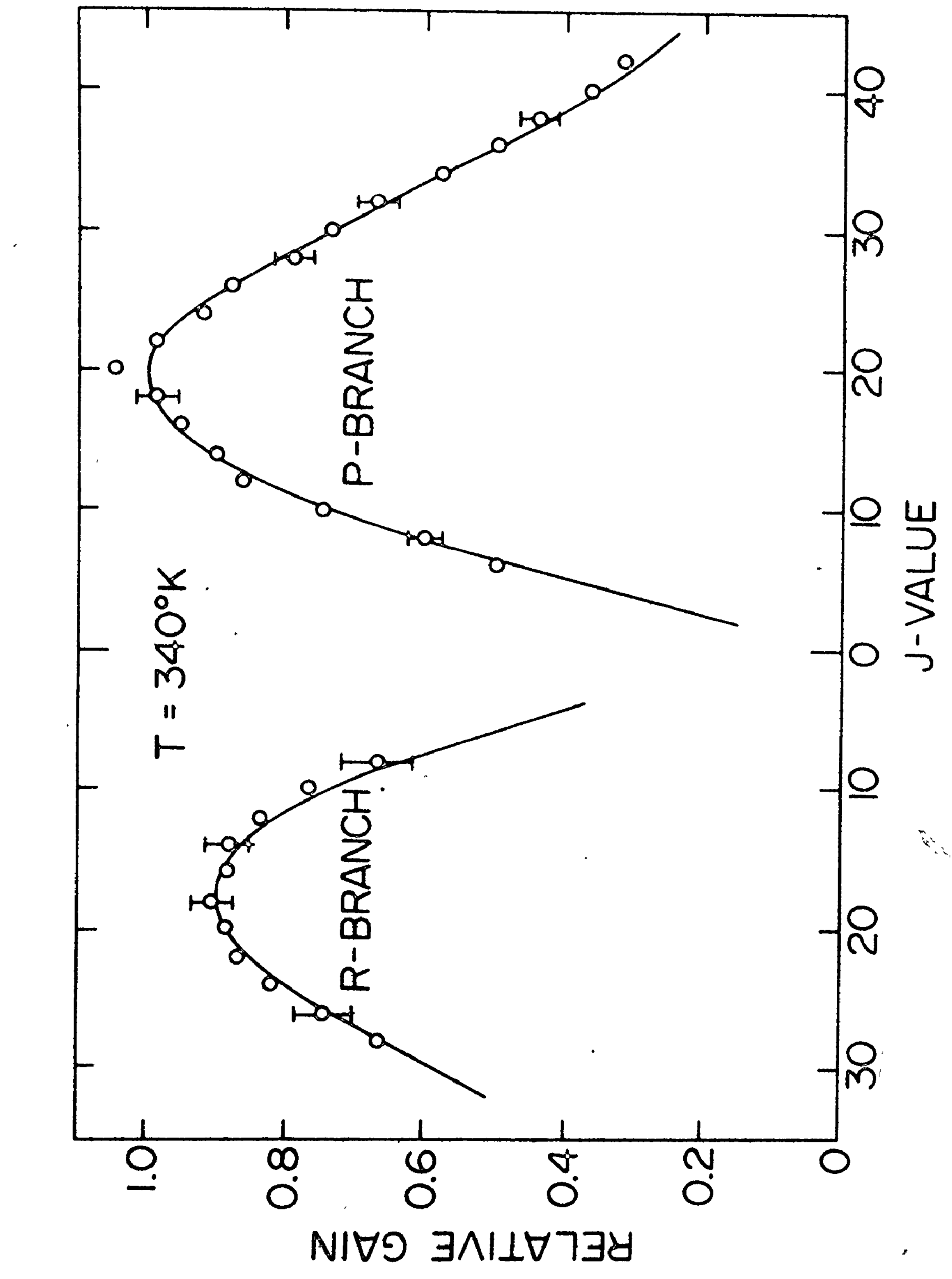
T = 340°K
R-BRANCH
P-BRANCH
RELATIVE GAIN
1.0
0.8
0.6
0.4
0.2
0
J-VALUE
30
20
10
0
10
20
30
40

10.4 μ band for all the wavelengths at which the cw laser probe could be operated. A moderately low total gas pressure of 80 torr was employed in the amplifier to ensure excellent stability and repeatability of the discharge. This is reflected in the small errors shown for the gain measurements. The gas mixture was 10% CO_2: 6% N_2: 84% He, and the energy input to the discharge was approximately 100 J/ℓ-atm. (The technique used for measuring discharge energies is explained in Chapter 5). The measured gain on P(18) was 2%/cm. In the work described here, we are only interested in the relative values of gain on different rotational transitions. Hence, Equations (2.10) and (2.11) can be simplified and written as

$$\alpha_P\ (J) = \frac{(\text{const.})N_\ell B_\ell.J.F_J}{\Delta\nu(J).\ \ \lambda(J)} \left[\frac{N_u B_u}{N_\ell B_\ell} \exp\left(-\ \frac{E_u(J-1)}{kT}\right) - \exp\left(-\ \frac{E_\ell(J)}{kT}\right) \right] \tag{4.1}$$

a similar expression holds for the R-branch, viz.,

$$\alpha_R\ (J) = \frac{(\text{const.}).N_\ell B_\ell.(J+1)F_J}{\lambda(J)\Delta\nu(J)} \left[\frac{N_u B_u}{N_\ell B_\ell} \exp\left(-\ \frac{E_u(J+1)}{kT}\right) - \exp\left(-\ \frac{E_\ell(J)}{kT}\right) \right] \tag{4.2}$$

In these two expressions, the constant contains all the factors which are not J-dependent; all other symbols are defined in Section 2.3 .

Careful examination of Equations (4.1) and (4.2) shows that the variation of gain with J depends strongly upon the value of the rotational temperature T. Observe that in Figure 11 the measured ratio of the gain maximum of the R-branch to that on the P-branch is 0.90. As we shall see, for a value as high as this, the variation in gain with J is insensitive to N_u/N_ℓ, and depends almost entirely on the rotational temperature. The lines fitted to the experimental points correspond to a value for T of 340°K to within a precision of ±15°K. This rather moderate increase above room temperature is in agreement with measurements reported elsewhere [78]. Observe that the gain on the P(20) line is anomalously high. Such an effect has been reported previously, and ascribed to the presence of a hot band gain line which overlaps P(20) [50,80]. Figure 12 shows results obtained with the same gas mixture and total pressure as employed previously, but with a considerably larger discharge input energy ($\sim$250 J/ℓ-atm). The rotational temperature which best fits the observations in this case is 410°K with an estimated precision of ±20°K. Observe that, once again, the gain on the P(20) line is anomalously high. In this figure, we have only shown the P-branch for convenience. The maximum gain on the R-branch, on the same arbitrary scale as the P-branch, is 0.90±0.02.

The fit obtained between theory and experiment for the J-dependence of the gain in the above experiments is excellent, and the precision of the data points is very high. The question now is, given this precision, how well can we determine N_u/N_ℓ? Figure 13

FIGURE 12

Measured peak gain for several P-branch transitions in the 10. 4 μ band. The fitted curve corresponds to T = 410°K and N_u/N_ℓ = 10. Gas mixture and pressure were the same as for Figure 11, but the discharge energy was increased to ∿250 J/ℓ-atm. This gave a peak gain of 1.5%/cm on P(18).

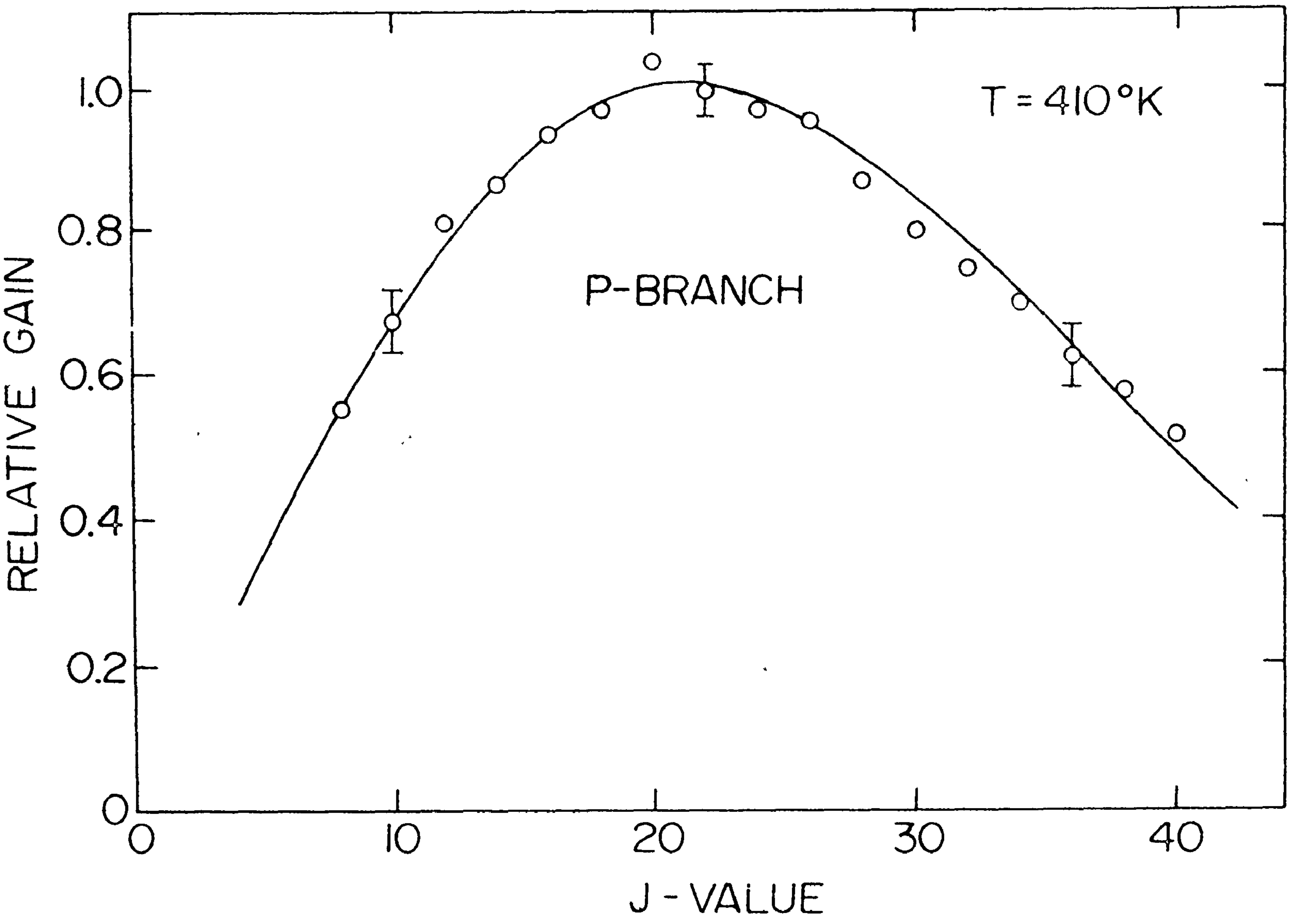
T = 410°K
P-BRANCH
RELATIVE GAIN
1.0
0.8
0.6
0.4
0.2
0
0
10
20
30
40
J - VALUE

displays the results of a computer calculation of the ratio (R/P) as a function of N_u/N_ℓ, for two rather different rotational temperatures. Evidently, R/P is extremely insensitive to the value of N_u/N_ℓ when $R/P > 0.85$.

It should be emphasised that when considering relative gains, the value of (R/P) is the only factor which is sensitive to N_u/N_ℓ. Patel gives a further demonstration of this for values of N_u/N_ℓ very close to 1.0 [1].

The experimental implications of this behaviour are illustrated by the error bar shown in the figure, which represents a precision of ±5% in the ratio (R/P). Evidently, either the precision of the gain measurements must be made much better than 5%, or this method of determining N_u/N_ℓ must be abandoned for values greater than 2. A precision of 5% is typical of results obtained with direct gain measurements and so the only recourse is to find a more accurate method. It is fortunate that it is only the ratio of the gains on the P and R branches, not the absolute values, which is required. In this case, a high precision technique for comparing the relative gains will do the trick. One approach to this problem is described in the next section.

4.3 In-Cavity Laser Gain Measurements

Section 2.7 describes an in-cavity time-delay technique which can be used for very accurate measurements of relative

FIGURE 13

The ratio of the maximum gain in the R-branch to the maximum gain in the P-branch (R/P) plotted as a function of N_u/N_ℓ, for two different rotational temperatures. Also displayed is a typical experimental error bar of ±5% in the value of R/P.

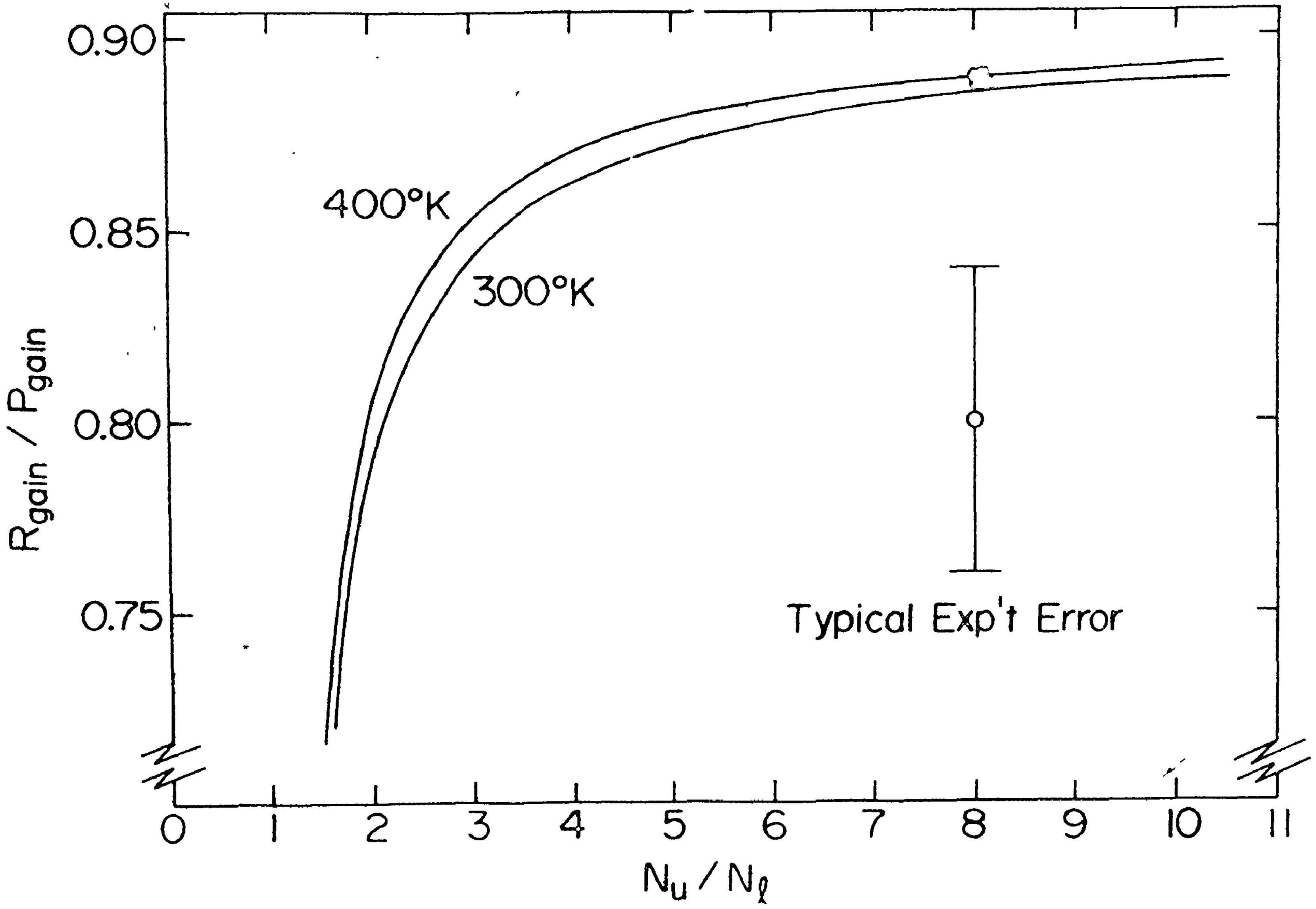
0.90
0.85
0.80
0.75
R_{gain} / P_{gain}
400°K
300°K
Typical Exp't Error
0
1
2
3
4
5
6
7
8
9
10
11
N_u / N_ℓ

gains [70-72]. The use of a diffraction grating within the laser cavity permits lasing on a wide variety of P and R branch lines in the 10.4 μ band. At a given discharge input energy, the time-delay to the onset of lasing is measured over these P and R branch lines. Now, the relative variation of the gain over the P and R branch lines is well known (see Equation 4.1 and 4.2); it depends on the rotational temperature and the J-value for the particular line. Consequently, for an assumed value of the rotational temperature the gain on each rotational line relative to that on P(18) can be predicted. The time-delay data is now treated as follows. Assume a value for the rotational temperature, and calculate the gains on all the relevant P and R branch lines relative to P(18), which is assigned an arbitrary value of 1.0. For each rotational line, plot the calculated relative gain against the observed time-delay. Now, increasing the rotational temperature has the effect of increasing the relative gain on high J-value lines and reducing that on the low J-value lines (see Figure 14). Accordingly, only if we made the correct choice of initial temperature will the high J and low J-value points lie on the same curve. This is illustrated in Figure 15. The high and low J-value points are indicated by crosses and circles respectively. The anomalous point indicated by a square corresponds to the P(20) line. (It is of interest to note that anomalous gain is found on P(20) at discharge pressures as low as 25 torr. This suggests either a very close coincidence between P(20) in the (00°1 → 10°0) band and

FIGURE 14

Relative gains on the P-branch transitions of the 10.4 μ band for two different rotational temperatures, calculated using Equation 2.10.

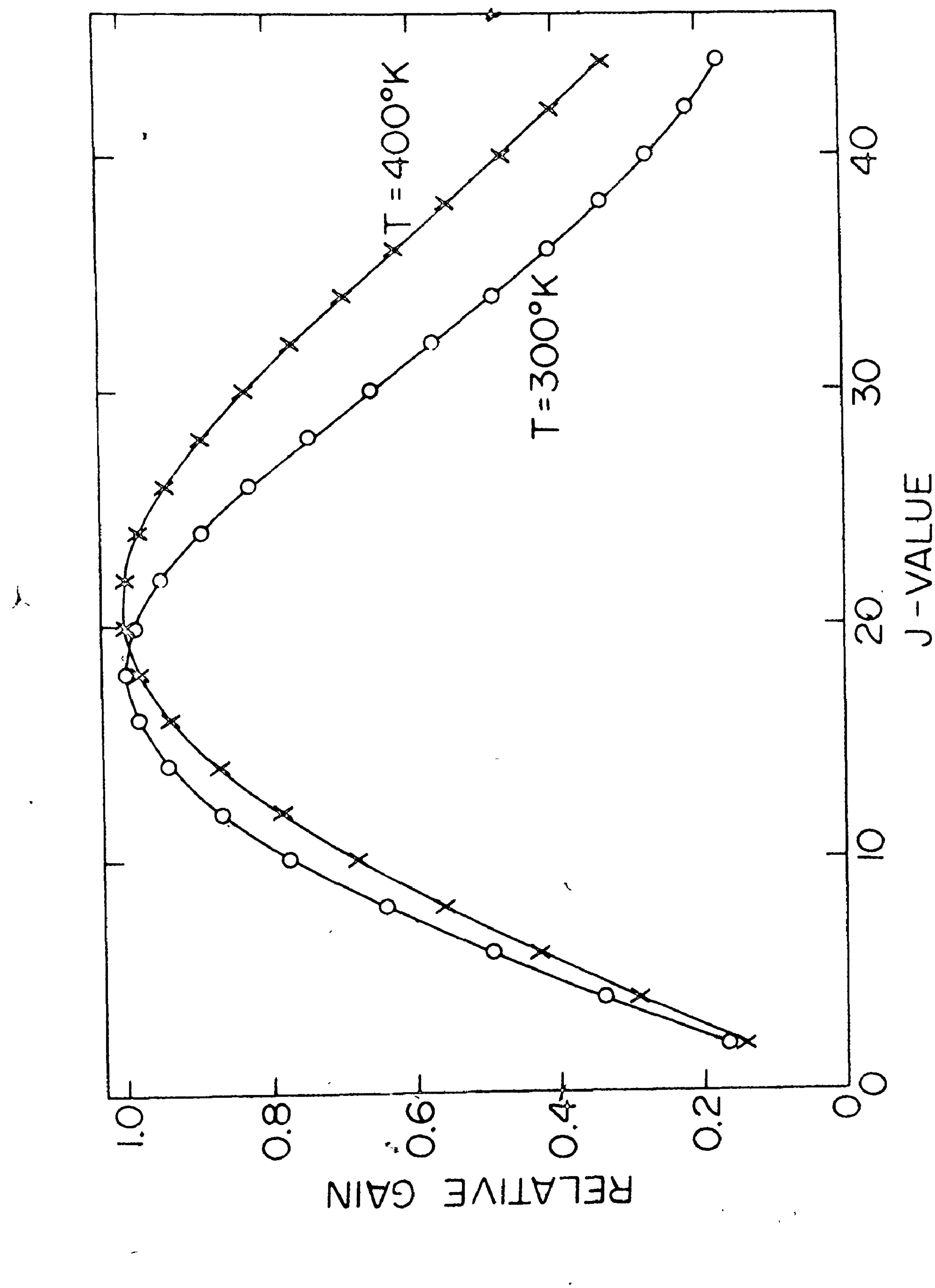
RELATIVE GAIN
1.0
0.8
0.6
0.4
0.2
0
J-VALUE
0
10
20
30
40
T = 400°K
T=300°K

FIGURE 15

Time-delay to lasing as a function of relative gain for transitions P(6) to P(38) and R(6) to R(34). Transitions with J-values greater than 20 are represented by X, those with J-values less than 20 by ○. P(20) is represented by □. The time-delay curve is plotted for two different rotational temperatures, 330°K and 360°K. (N_u/N_ℓ was taken as 10 in each case). The data for 360°K has been shifted 5 μs to the right. Discharge mixture is 10% CO_2: 90% He at 75 torr total pressure, with an input energy ∿90 J/ℓ-atm.

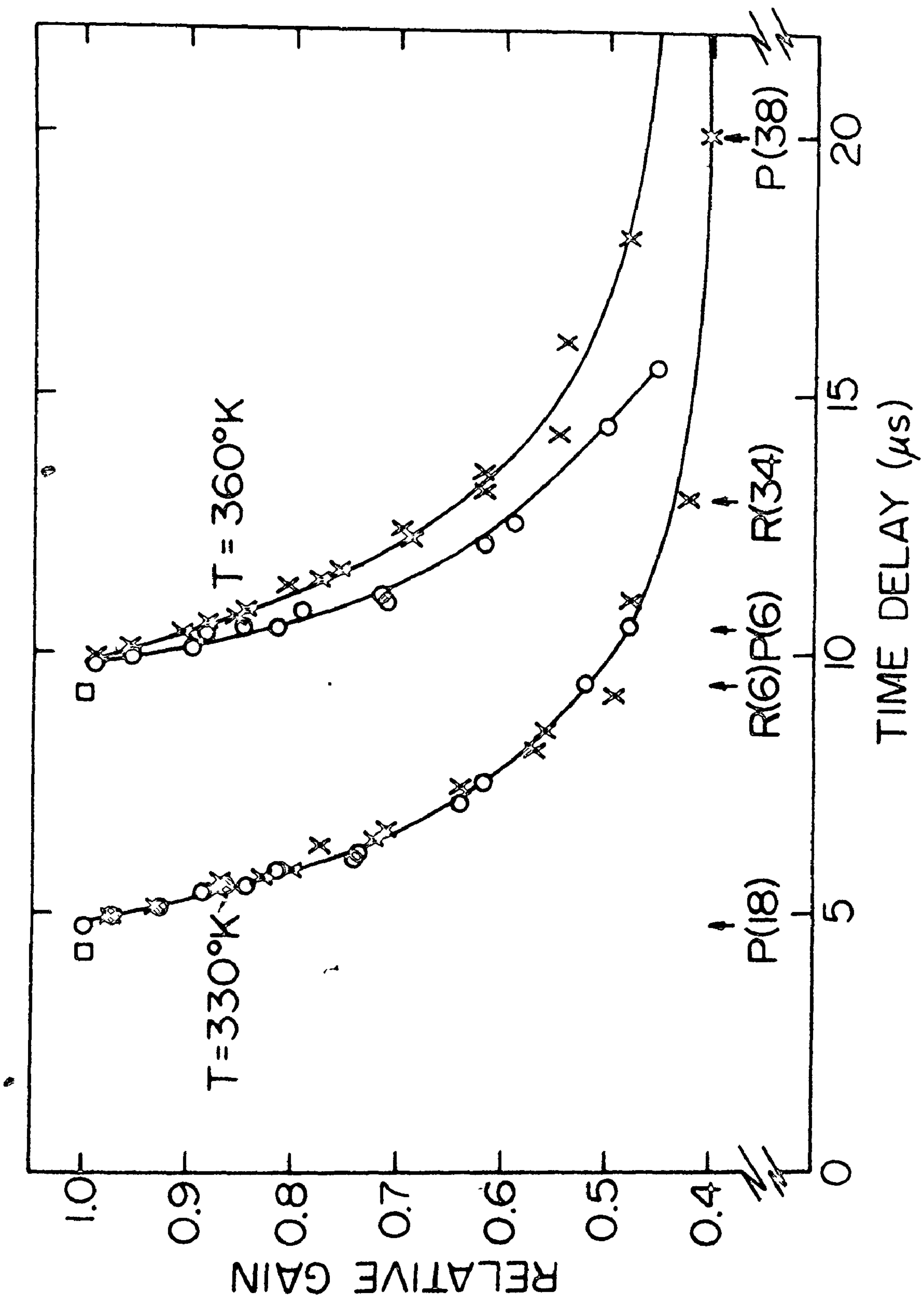
RELATIVE GAIN
1.0
0.9
0.8
0.7
0.6
0.5
0.4
TIME DELAY (μs)
0
5
10
15
20
T=330°K
T = 360°K
P(18)
R(6)P(6)
R(34)
P(38)

P(23) in the (01'1 → 11'0) band, or an unexpectedly narrow linewidth for the P(20) transition [50,80]). Two choices of rotational temperature are shown. The value of 360°K is obviously a wrong choice in that the low and high J-value points are clearly separated. A reduction of only 30°K is sufficient to bring the two sets of points into agreement. This serves to indicate the precision with which the rotational temperature can be determined. The gas mixture and other relevant experimental parameters are given in the figure caption. There is a complication which has been ignored thus far. From Section 4.2 it is known that the relative gain variation amongst the rotational levels depends on N_u/N_ℓ. Consequently, it follows that to fit a rotational temperature requires a value for N_u/N_ℓ. Although this is certainly true, the value chosen is of little consequence provided that it is greater than four. Furthermore, the values of T and N_u/N_ℓ can, if necessary, be simultaneously determined. Variations in N_u/N_ℓ serve mainly to change the ratio of the peak gain in the R-branch to that in the P-branch. The following strategy can now be applied. Select a value of N_u/N_ℓ, and separately fit a rotational temperature to the P-branch and R-branch data, employing the method indicated in Figure 15. Repeat for different values of N_u/N_ℓ. In general, the rotational temperatures obtained for the P and R branches will be different. Only when N_u/N_ℓ has the right value will the two temperatures agree. Typical results are displayed in Figure 16. Evidently, for the experimental situation analysed (which is the same as for Figure 15) the value of N_u/N_ℓ is

FIGURE 16

Determination of N_u/N_ℓ using the data of Figure 15. As N_u/N_ℓ is varied, the P and R branch temperatures are fitted separately, using Equations 2.10 and 2.11. The error bars represent fitting errors.

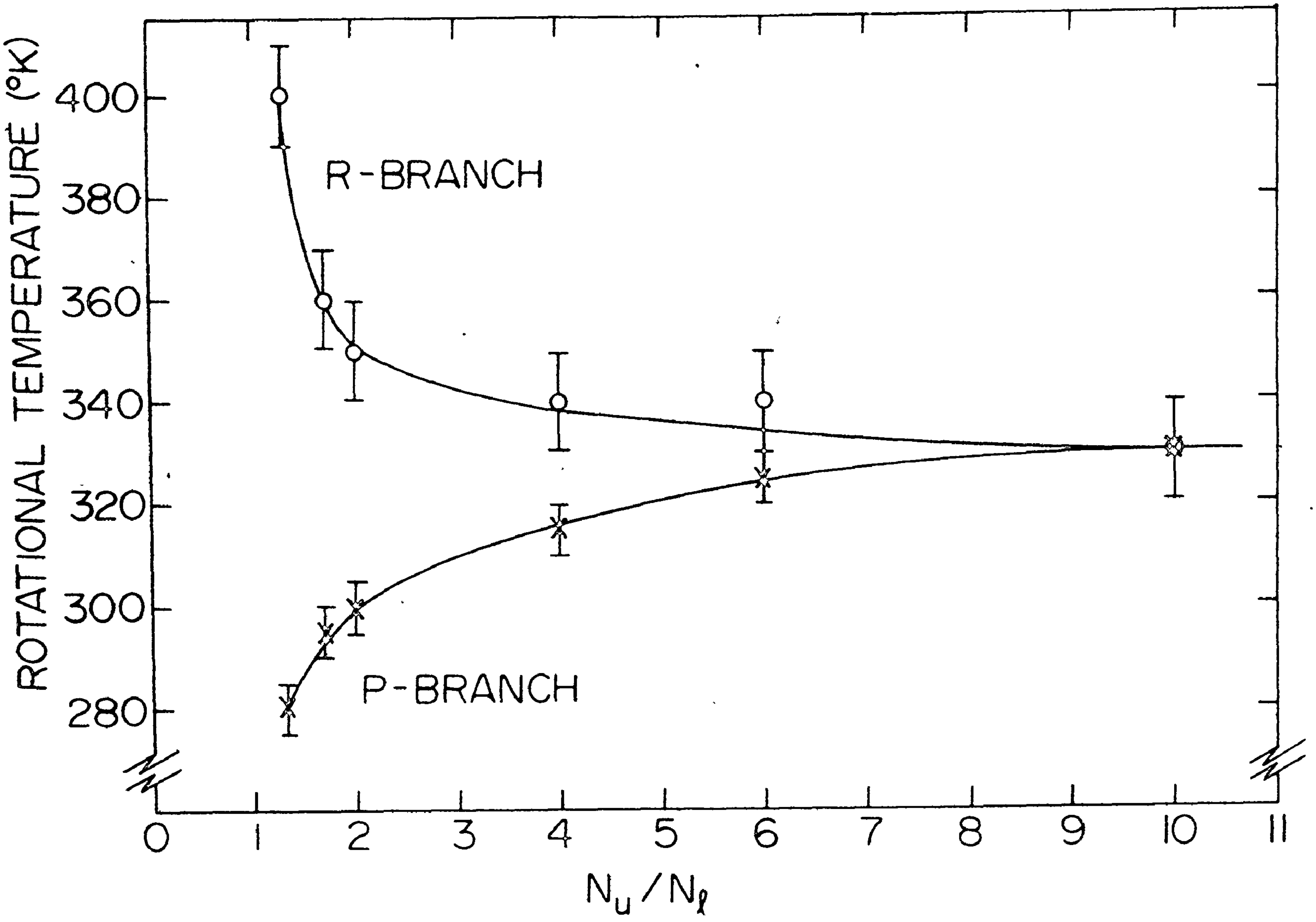
ROTATIONAL TEMPERATURE (°K)
400
380
360
340
320
300
280
R-BRANCH
P-BRANCH
0
1
2
3
4
5
6
7
8
9
10
11
N_u/N_ℓ

≥ 6 and T is 330°K. As indicated earlier, it is actually only necessary to carry out this procedure when N_u/N_ℓ is less than four. In making measurements over the wide wavelength range required for this method, it is important to take precautions that the resonator loss is not significantly wavelength dependent.

When an appropriate determination of the values of T and N_u/N_ℓ has been made according to the above prescription, the resulting time-delay curve is an accurate plot of laser pulse time-delay against relative gain. This is all we need to compare the gain on the P and R-branches of the 10.4 μ band. It is of interest to observe that we can employ the technique described in Section 2.7 to determine the temporal variation of the gain once the plot of relative gain against time-delay is known. Furthermore, if the cavity loss is known to fair precision, the actual magnitude of the peak gain (on P(18) say) can be determined. Figure 17 shows the time-variation and magnitude of the gain on P(18) deduced in this way for a 10% CO_2: 90% He gas mixture at 75 torr total pressure. Also shown is the result of a direct measurement of the gain on the same line using a probe laser. The small discrepencies between the two curves are well within the range of experimental error.

A method has now been established for determining an accurate plot of relative gain against observed time-delay in the laser resonator. Clearly, the maximum gain on the R-branch will correspond to that line which lases with the shortest time-delay. It is only

FIGURE 17

Time variation of the gain on P(18) as measured directly with a cw probe laser (solid line) and as deduced from the time - delay data of Figure 15 (dashed line). Discharge conditions are given in the caption of Figure 15. Zero time corresponds to the peak of the discharge current pulse.

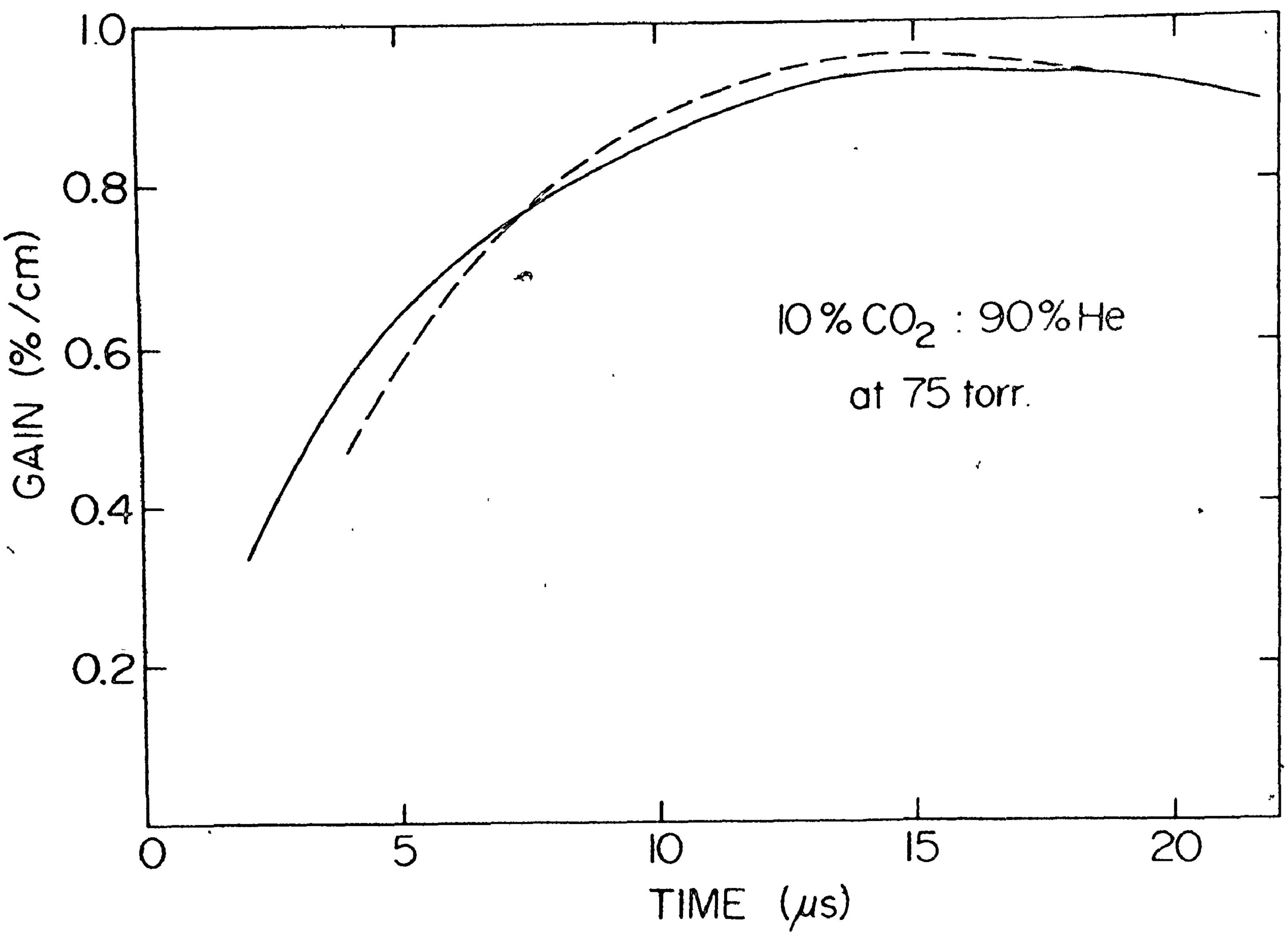
1.0
0.8
0.6
0.4
0.2
GAIN (%/cm)
0
5
10
15
20
TIME (μs)
10% CO2 : 90% He
at 75 torr.

necessary to locate this time-delay on the curve of relative gain against time-delay in order to establish the R/P ratio. This technique can be employed to measure the R/P ratio as a function of time, by changing either the laser cavity loss or gain on P(18). As a matter of fact, this R/P ratio is an average over the time to the onset of lasing from the instant the gain exceeds the loss. Operation at relatively low pressure ensures that this time is short compared with the risetime of the gain. (i.e., $t_{th} \gg (t_f - t_{th})$ using the nomenclature of Section 2.7). Figure 18 shows the results of such an experiment carried out with a 10% CO_2: 90% He gas mixture at a total pressure of 35 torr. The different curves were generated by changing the gain and loss in the laser resonator. The horizontal error bar displayed on each curve represents the maximum variation in the time-delay of that R-branch line with the highest gain. As a measure of the precision of the technique, the data points employed in obtaining one of the time-delay curves are also displayed. The values of the N_u/N_ℓ ratios appropriate to each of the error bars are shown in the figure. Since the value of N_u is falling during this time, these observations can only be accounted for if the lower laser level itself is emptying during the risetime of the gain. In the next section, we present further independent evidence that this indeed must be the case.

4.4 Hot Band Lasing Observations

It is known that there is a hot band transition (01'1 → 11'0)

FIGURE 18

Variation of the ratio N_u/N_ℓ during the risetime of the gain. The four time-delay curves are generated by varying the excitation conditions and cavity loss for a 10% CO_2: 90% He mixture at 35 torr total pressure. The horizontal bars on each curve represent the maximum variation in the time-delay of the R-branch line with the highest gain. Also indicated is the corresponding range of N_u/N_ℓ. The gain peak occurs approximately 27 μs after the peak of the current pulse (0 μs).

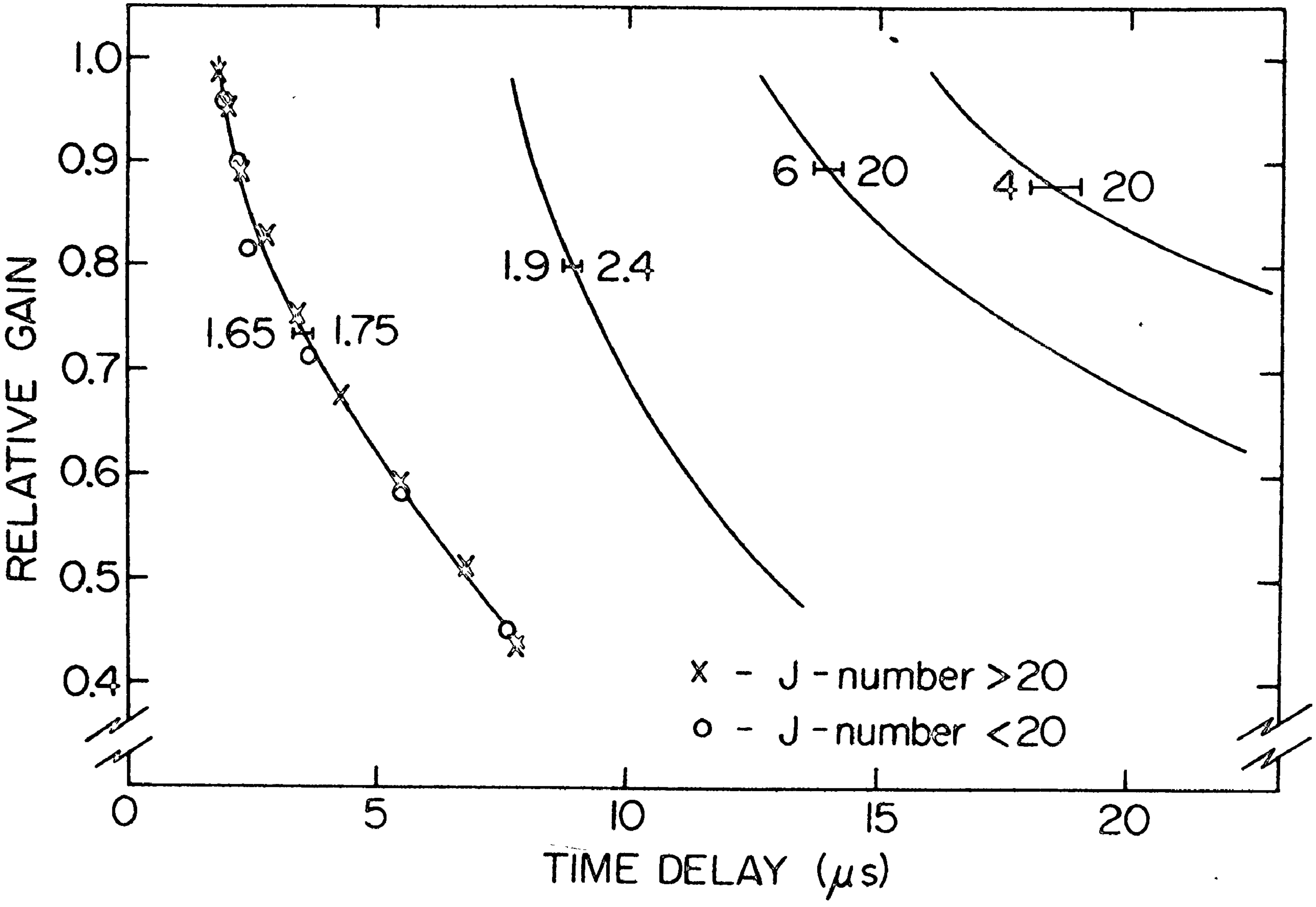
1.0
0.9
0.8
0.7
0.6
0.5
0.4
RELATIVE GAIN
0
5
10
15
20
TIME DELAY (μs)
1.65
1.75
1.9
2.4
6
20
4
20
x - J-number >20
o - J-number <20

which has maximum gain in the region of 11 μ. The inversion which obtains for this band is related to that of the 10.4 μ band by the ratio of the 01'0 to the 00°0 populations (see Section 2.4). Evidently, the ratio of the gain in the hot band to that of P(18) in the 10.4 μ band is a measure of the bending mode temperature. Consequently, time-delay measurements of the type described in Section 4.3 can be employed to determine the bending mode temperature. Figure 19 shows plots of relative gain against time-delay obtained in the fashion described in Section 4.3. The gas mixture was 10% CO_2: 90% He at a total pressure of 35 torr. The limits of the time-delay obtained for the peak of the hot band are indicated by the horizontal error bars on the time-delay curves. The two different curves were obtained by varying the resonator loss. By this method, it was determined that the gain on the hot band was 26% of that on P(18) during the initial portion of the gain risetime. This determination was checked by measuring the time delay obtained on P(18) for one fourth of the gain (see arrow in the figure). The measured gain ratio corresponds to a bending mode temperature of 700°K. At the later time, the measured gain ratio of 0.155 corresponds to a bending mode temperature of 515°K. This confirms that the bending mode does not attain very high vibrational temperatures (∿1300°K) such as would be required if the rise of the gain corresponded only to the change in partition function as the bending mode cools (see Appendix A). The time-delay measurements on the hot band were made

FIGURE 19

Variation of the bending mode temperature, T_1, during the risetime of the gain. The two time-delay curves are generated by varying the cavity loss for a 10% CO_2: 90% He mixture at 35 torr total pressure. The horizontal bars on each curve represent the maximum variation in the time-delay of the P(20) transition of the hot band. The arrow indicates the time-delay obtained on P(18) of the 10.4 μ band when the total gain in the amplifier has been reduced by a factor of 4. The gain peak occurs approximately 27 μs after the peak of the current pulse (0 μs).

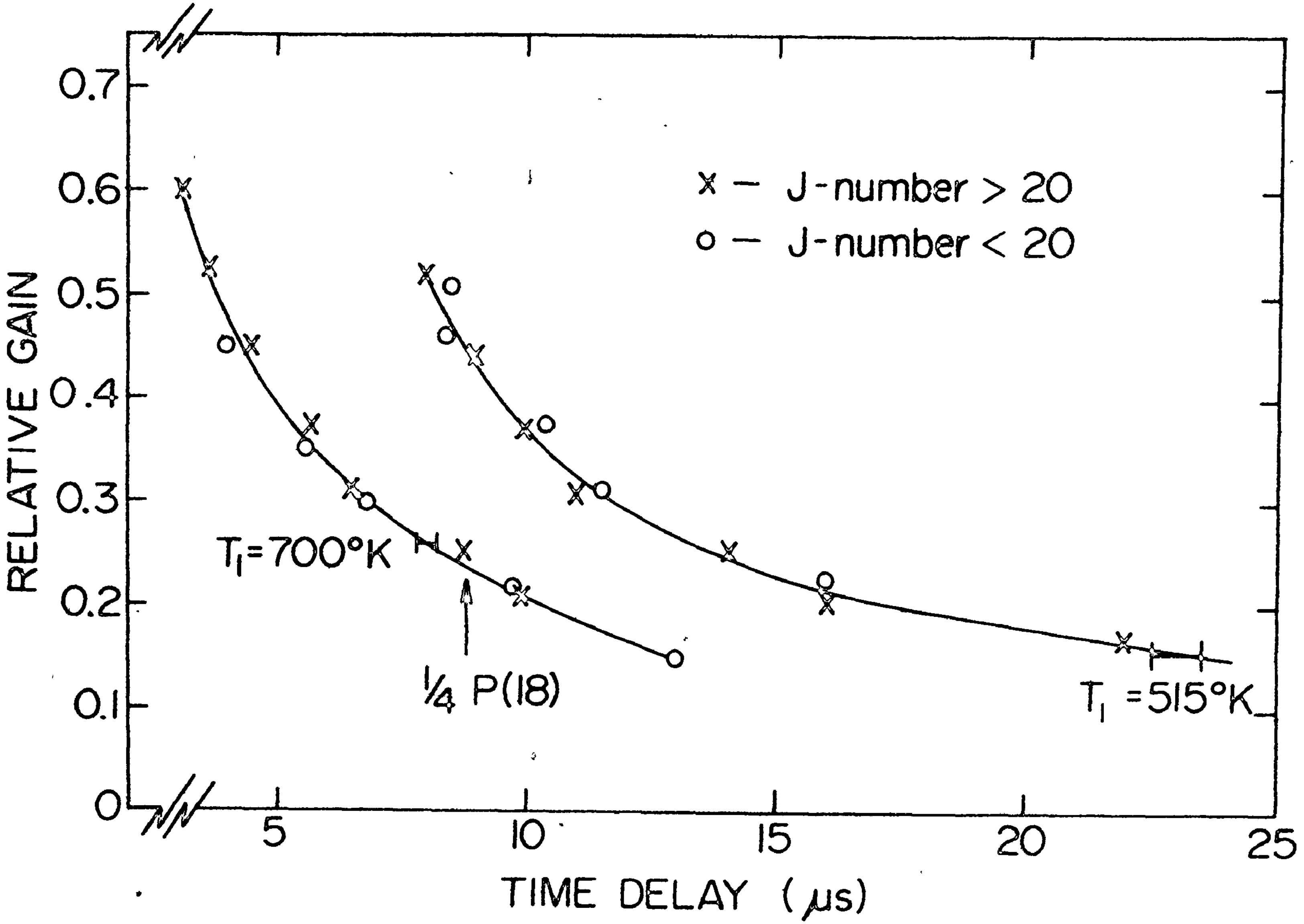
x — J-number > 20
o — J-number < 20
RELATIVE GAIN
0
0.1
0.2
0.3
0.4
0.5
0.6
0.7
TIME DELAY (μs)
5
10
15
20
25
T_1=700°K
T_1 =515°K
1/4 P(18)

using the P(20) line at 10.99 μ. There is a stronger transition at 11.02 μ, corresponding to the overlap of the P(56) line in the 10.4 μ band with the P(23) line in the hot band [81]. This transition was avoided in the present work.

4.5 Direct Measurements of the Bending Mode Temperature

The results of the previous sections have enabled us to establish that the lower laser level is strongly coupled to the bending mode levels, and that the population of the lower level decays during the risetime of the gain. As thermal equilibrium is rapidly established between the BS modes, they can be assumed to have a common temperature, T_1. Since the correct model for the risetime of the gain has been ascertained, direct gain measurements can be used to determine the value of T_1 immediately after the current pulse. The calculated relaxation of T_1 via the 01'0 V-T collisions can also be compared with the experimental gain risetime.

The laser level populations after the discharge current pulse will depend upon the electronic pumping rates during the discharge. The models of discharges in CO_2 laser media described in Section 2.5 permit the excitation efficiency of the various vibrational modes in CO_2 to be calculated. In the case of pulsed discharges, one general consequence of these models is that immediately after the current pulse there should be an initial inversion between the upper and lower laser levels in the 10.4 μ band. It is very difficult to observe the presence of such an initial inversion in TE CO_2 lasers because, under normal operating conditions, the risetime of the gain is commensurate with the current pulse length. Also, typical TE laser discharges contain nitrogen which is efficiently pumped by direct electron excitation into excited vibrational states. The excited nitrogen subsequently transfers energy to the upper laser level in CO_2, on a time-scale similar to the risetime of the gain. This effect further tends to obscure the presence of an initial inversion. Both problems can be circumvented by operating a TE CO_2 laser at a sufficiently low pressure that the risetime of the gain greatly exceeds the current pulse length, using gas mixtures containing only CO_2 and He. It is of great intrinsic interest to observe the initial inversion in such discharges, and it also provides a new comparison between the above theories and experiment.

In what follows, it is shown that, by a proper choice of discharge conditions, the predicted initial inversion can indeed be observed. Furthermore, the magnitude of this initial inversion has been studied as a function of discharge input energy and used to determine the behaviour of the initial lower laser level population and bending mode vibrational temperature.

(a) Experimental Observations

The apparatus described in Chapter 3 was employed to make direct measurements of the risetime of the gain in a pulsed TE amplifier. The maximum available discharge length (92 cm) was used to give as large a signal as possible. In addition, the load resistor in the detector system was adjusted to give the minimum detector risetime of 300 ns. Care was taken to minimise the noise in the detector circuit caused by the powerful discharge current pulse. Figure 20 shows the time-variations of the gain for three different input energies to the discharge. This data was transcribed directly from oscilloscope trace photographs. The gas mixture employed was 10% CO_2: 90% He, at a total gas pressure of 35 torr. The traces shown in the figure clearly indicate the presence of an initial step in the gain. The two upper traces were obtained with low input energies to the discharge; observe that there is little subsequent increase in the gain. The lowest trace corresponds to a somewhat higher discharge energy; both the initial "step" and the subsequent increase to a gain peak are clearly apparent. To analyse these observations in terms of gain medium populations, it is appropriate to transform the measured gain per pass into a gain per unit length. Figure 21 shows the gain in %/cm plotted as a function of time, obtained from trace 3 of Figure 20. Also plotted in Figure 21 is a dashed curve which represents the gain calculated according to the model in which the combined BS modes decay via the V-T relaxation of the 01'0 level. The calculated gain curve is determined using the V-T rate for helium given by Taylor and Bitterman [11] (10 μs for this mixture and pressure). Evidently, this model is an excellent representation of the gain dynamics. As the inversion at the peak of the gain

FIGURE 20

Gain curves for three different excitation energies in a 10% CO_2: 90% He mixture at 35 torr total pressure. The curves are normalised to a constant initial gain "step". Zero time corresponds to the end of the current pulse. Curves A, B and C correspond to discharge input energies of 8, 16 and 110 J/ℓ-atm respectively, giving peak gains of 0.13, 0.28 and 1.0%/cm.

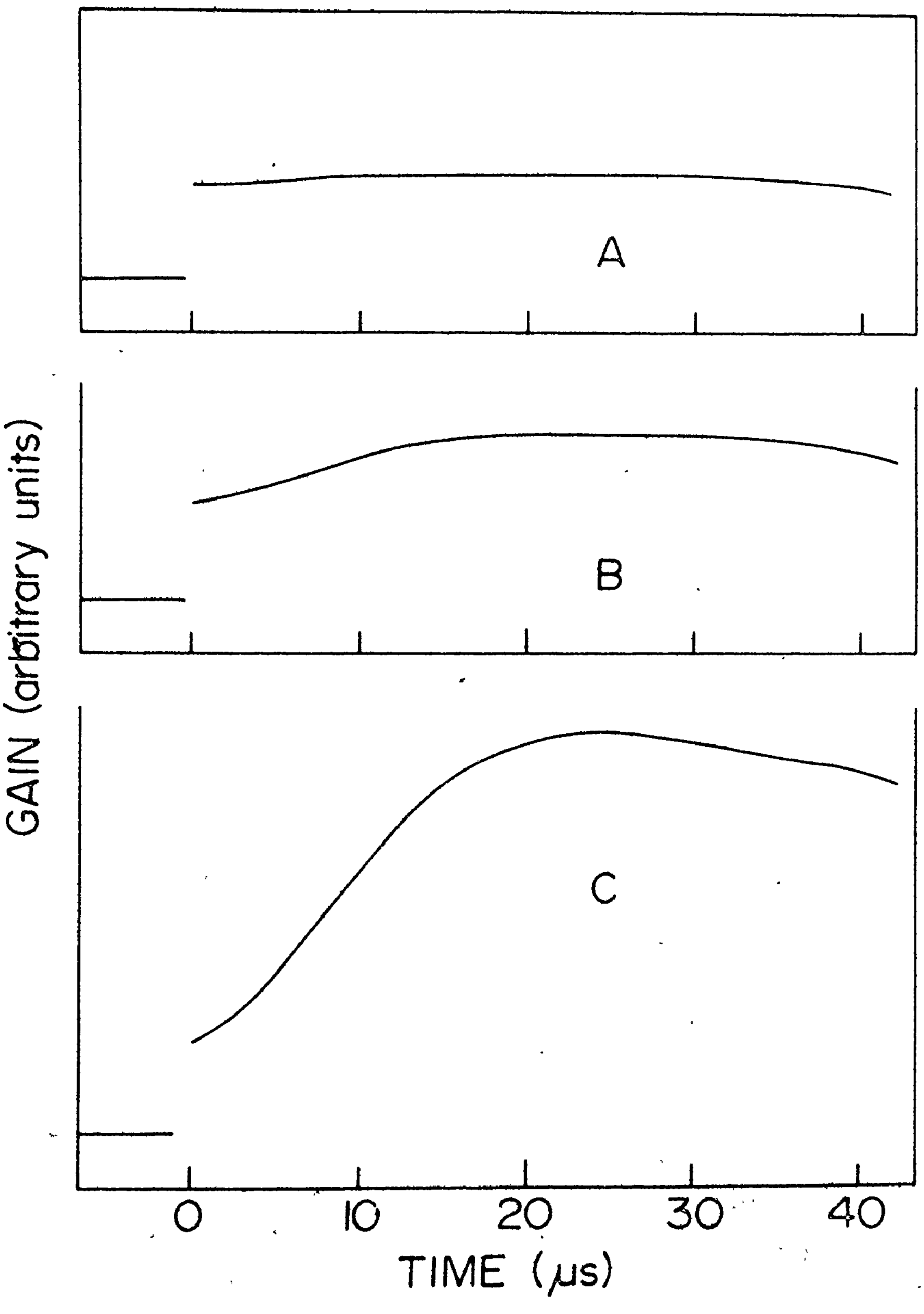
A
B
C
GAIN (arbitrary units)
0
10
20
30
40
TIME (μs)

FIGURE 21

Comparison of measured and calculated gain curves for 10% CO_2: 90% He at 35 torr total pressure. The dashed line is the calculated gain curve using a V-T relaxation time of 10 μs, and an initial value for T_1 of 630°K. The solid line is the gain curve obtained directly from oscilloscope photographs.

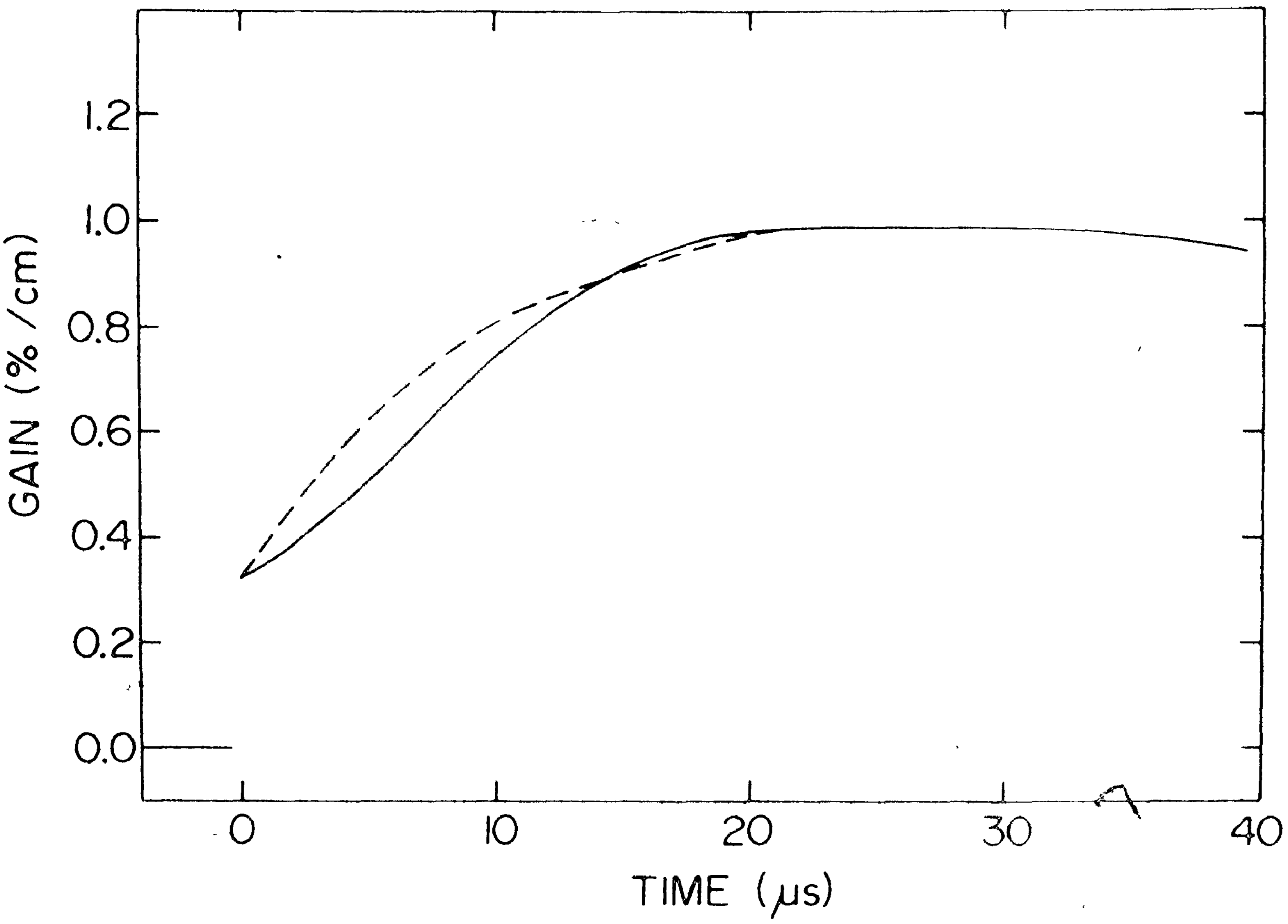
GAIN (% /cm)
1.2
1.0
0.8
0.6
0.4
0.2
0.0
0
10
20
30
40
TIME (μs)

corresponds primarily to the upper level population (the lower level having emptied), and as the decay time of the upper level is known (given simply by the falltime of the gain), we can calculate the initial population in the upper level. From this value, and the measured initial gain, the initial value of T_1 can be determined. Increasing T_1 not only reduces the calculated gain by populating the lower laser level, but also reduces the effective inversion by increasing the partition function (Appendix A). Hence, the dynamics of the gain risetime provide a very sensitive method of determining T_1 immediately after the excitation pulse. The initial value of T_1 employed in Figure 21 is 630°K, which is in reasonably good agreement with the value of 700°K determined by an entirely different method in Section 4.4 (the discharge conditions were the same in each case).

Figure 22 shows the variation of T_1, determined according to the above prescription, as a function of the input energy to the discharge. Initially, the mode temperature increases rapidly with increasing discharge input energy, then begins to level off and finally saturates at high input energy to the discharge. This behaviour implies that, at the higher input energies, the discharge is becoming less and less effective at pumping energy into the combined BS modes. A very similar saturation effect for the upper laser level is reported in Chapter 5. In that Chapter, it is shown that the effect is not due to discharge deterioration, and the same conditions apply to the present work.

FIGURE 22

A plot of the initial value of the temperature of the combined bending and symmetric stretch modes (T_1) as a function of discharge energy. The gas mixture was 10% CO_2: 90% He at 50 torr total pressure. These results are typical of those observed over a range of CO_2: He gas mixtures.

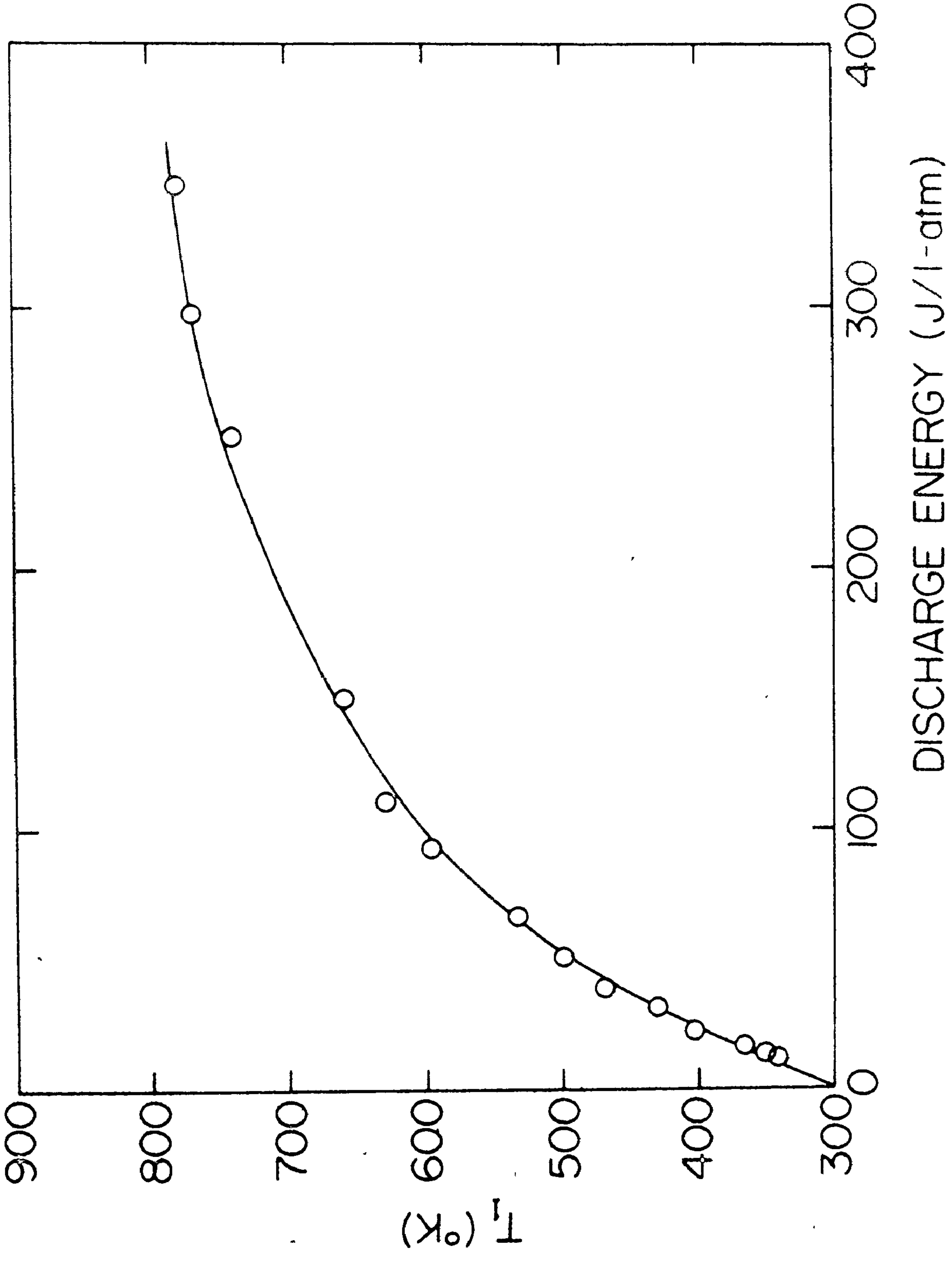
T_1 (°K)
900
800
700
600
500
400
300
0
100
200
300
400
DISCHARGE ENERGY (J/l-atm)

The data presented in Figures 20-22 is taken at gas pressures of 35 and 50 torr. The results obtained are independent of pressure in the range 35 torr to 150 torr, i.e., the absolute values of the gain step and peak gain remain constant while the risetime is inversely proportional to pressure. Above 150 torr, the risetime of the gain is so fast that accurate determinations of the gain step become very difficult. Similar variations of T_1 with discharge energy were obtained with other He: CO_2 gas mixtures.

4.6 Discussion and Conclusions

As was indicated in the introduction to this Chapter, there are two models which can account for the gross features of the gain evolution in pulsed CO_2 lasers. In one model, the risetime of the gain is a reflection of the decay of the population of the lower laser level. In the other model, this risetime corresponds only to the cooling of the bending mode, and both the upper and the lower laser level populations remain relatively unchanged. The key difference between these two models from an observational point of view lies in the behaviour of the ratio N_u/N_ℓ. For the former model, this ratio will be large at the gain peak, regardless of initial conditions, and will be monotonically increasing in value during the buildup of the gain. For the latter model, however, the ratio will be constant during the evolution of the gain. In this Chapter, we have reported experiments aimed at the determination of

N_u/N_ℓ at the peak of the gain, and for selected times during the gain buildup.

The conclusion reached as a result of these measurements, namely that the lower laser level undoubtedly empties during the risetime of the gain, is reinforced by some measurements concerning the gain on the hot band (01'1 → 11'0).

In Section 4.2, results are reported of the direct measurement of the peak gain on a number of rotational lines in the P and R branches of the 10.4 μ band. It is shown that these results can be analysed to obtain values for both the rotational temperature and the ratio N_u/N_ℓ. This ratio is found to be large at the peak of the gain for several discharge input energies. The precision with which values of N_u/N_ℓ can be obtained from experimental data is analysed.

It is shown that, although some indication of the size of N_u/N_ℓ can be obtained, it is too inaccurate in general to be employed for a study of changes in this ratio as the gain evolves. Accordingly, we have devised an alternative scheme which has the necessary accuracy.

A technique is described in Section 4.3 for comparing the gains on the P and R branches of the 10.4 μ band to a high precision. This is basically all that is required to obtain a value for N_u/N_ℓ. This method involves a comparison of the time-delays to the onset of lasing from the current pulse, for a number of P and R branch gain lines. This approach is used to determine the value of N_u/N_ℓ and the rotational temperature for selected times during the risetime of the gain. It is clearly demonstrated that N_u/N_ℓ changes from a value less than two at a time shortly after the end of the current pulse, to a value greater than six near the peak of the gain pulse. This constitutes clear evidence that the model of the gain dynamics in which the bending and symmetric stretch vibrational modes of Co_2 are strongly coupled is correct. The energy in these modes decays at a rate equal to the V-T relaxation rate of the 01'0 level. The coupling between the bending and symmetric stretch modes must be faster than this rate, which is determined by the partial pressure of the He in the gas mixture. For sufficiently high CO_2 content mixtures, the coupling between the 10°0 level and the bending mode is determined by the effectiveness of CO_2-CO_2 collisons [18]. In the particular case of a 10% CO_2: 90% He mixture, it follows that the relaxation rate of the 10°0 level into the bending mode must be greater than 3×10^4 $\text{torr}^{-1}\text{s}^{-1}$. This value is in good agreement with the calculations of Seeber [19] and Sharma [20], and the experimental results of Stark [18]. However, it exceeds the rate deduced in Reference 13 by an order of magnitude, and is significantly faster than that obtained in Reference 12.

Section 4.4 gives a brief account of some measurements made on the lasing behaviour of the hot band transition (01'1 → 11'0). The important characteristic of this transition is that the ratio of the hot band gain to the gain in the 10.4 μ band is a measure of the 01'0 population. We have applied this, using an experimental method much like that employed in Section 4.3, to show that the bending mode temperatures during the risetime of the gain are much too small to permit the gain increase after the current pulse to be accounted for in terms of a decrease in the partition function of the bending mode. This provides an independent confirmation of the above conclusions concerning the two possible models of the gain dynamics.

Finally, in Section 4.5, the correct model of the gain dynamics is used in a comparison between calculated and experimental gain risetimes. Very good agreement is obtained, and from the measured gain "step", the initial value of the combined BS mode temperature, T_1, can be determined. The variation of T_1 with discharge input energy shown in Figure 22 can be employed to determine the relative efficiency of the discharge in pumping this coupled mode system. In particular, the slope of the curve close to the origin can be used to determine how much of the discharge input energy goes directly into the combined mode. It is found in this way that 39% of the discharge energy is deposited in the two modes, which is in very good agreement with a value of 32% determined by a calculation using the computer program of Section 2.5, with the appropriate experimental conditions. If the alternative model for the risetime is used (in which the rise in gain simply measures the change in the partition function), much higher values of T_1 are required to account for the experimental gain profile. In fact, the required temperature increases are so large that they account for more than 100% of the discharge input energy! We believe this to be clear evidence in favour of the model adopted here for the emptying of the lower laser level.

It is apparent that the net electron excitation of the BS modes of CO_2 saturates with increasing discharge energy. A very similar saturation effect in the electron excitation of the upper laser level is reported in Chapter 5. The source of these saturation effects is not clear, although it is possibly to be found in de-excitation processes in the discharges such as might be produced by slow electrons. For both the upper laser level, and at least some levels within the BS modes, this requires electron de-excitation cross-sections an order of magnitude greater than the effective excitation cross-sections. This possibility will be discussed in greater detail in Chapter 5.

All the data presented in this Chapter was taken at gas pressures below 150 torr. However, relaxation rates in CO_2 lasers are collisionally controlled, and the results can be scaled directly to higher pressures. The duration of the gain pulse will, of course, be inversely proportional to the gas pressure. Even at atmospheric pressure, the lower laser level will be almost empty at the time of the gain peak, providing that short excitation current pulses are used.

It is also pertinent to observe that, although the conditions in low pressure dc excited CO_2 lasers are very different from those existing in pulsed lasers, several recent measurements have determined that the population of the lower laser level is close to equilibrium with the gas temperature [82-84]. Once again, this confirms the existence of very strong coupling between the bending and symmetric stretching modes.

4.7 Summary

The principle concern of this Chapter was to determine the behaviour of the lower laser level during the risetime of the gain. Several different methods were used, and they all lead to the unmistakable conclusion that the lower laser level is strongly coupled to the rest of the symmetric stretching and bending vibrational levels, and that the lower level empties during the risetime of the gain. This conclusion is of fundamental importance in the understanding of both the gain mechanism and lasing dynamics in TE CO_2 lasers.

Now that the risetime mechanism is ascertained, we are in a position to convert measured peak gains into laser level populations. This also requires a knowledge of the gas temperature, which can be accurately determined by the methods described in this Chapter. Hence we are now in a position to interpret the gain saturation effect illustrated in Figure 10 of Chapter 3. This is the subject of the next Chapter.

CHAPTER 5

REDUCTION OF THE PUMPING EFFICIENCY IN CO_2 LASERS AT HIGH DISCHARGE ENERGY

This Chapter concerns the variation of small-signal gain as a function of discharge input energy in TE CO_2 lasers. By converting measured gains to laser level populations, the pumping efficiency of the upper laser level can be determined over a range of input energies. This pumping efficiency is found to fall drastically at high input energies, with important consequences for the design of high power lasers. Section 5.2 of the Chapter describes the experimental technique; results are given in Section 5.3. Included in 5.3 is a detailed account of the steps involved in converting measured gain into laser level populations, and in obtaining the true discharge energy from the initial stored energy. The significance of these results is considered in Section 5.4, and the relationship of the present work to that reported by other authors is discussed.

5.1 Introduction

A number of studies of the parametric variations of small-signal gain in high pressure CO_2 lasers have been published [7,30-34]. Despite the large variety of methods used to pre-ionize the discharge medium (double-discharge systems, u.v. pre-ionization, electron beam pumping), it has invariably been found that the gain ceases to increase with increasing discharge energy beyond a certain point. This effect has been variously ascribed to a deterioration of the discharge quality, an increase in the discharge temperature, progressive shortening of the upper laser level lifetime,or a combination of all three. We have investigated this saturation effect to determine if it can be accounted for by the above-mentioned factors.

The experimental conditions are carefully chosen so that the onset of discharge deterioration can be clearly separated from the region of gain saturation*. Gas mixtures and pressures are chosen to make the effects of increasing temperature on the gain both moderate and measureable. Figure 10 of Chapter 3 is typical of the results obtained under such conditions. Initially, the small signal gain increases rapidly with increasing energy, but soon levels off and then remains constant as the energy is increased by a factor of 3. Finally, at very high input energies, thermal effects cause the gain to decrease. Measurements are made of the gas temperature and the lifetimes of the laser levels, and the effective pumping efficiency of the discharge is calculated. It transpires that thermal effects convincingly account for the fall in gain at high input energies, but gain saturation is now even more clearly demonstrated (Figures 23,31 and 33). In general, it is found that the pumping efficiency of the upper laser level decreases rapidly above 50 J/ℓ-atm., and complete saturation occurs around 200 J/ℓ-atm. This saturation appears to be a fundamental property of the discharge and places a limitation on the energy/ℓ which can be extracted from high pressure CO_2 lasers. Calculations [85] scaling the present generation of CO_2 lasers to higher and higher discharge energies must be modified to allow for decreasing pumping efficiency.

---

*Gain saturation is used throughout this Chapter to denote the saturation of the small-signal gain with increasing discharge energy.

5.2 Experimental Technique

The apparatus described in Chapter 3 was used to make small-signal gain measurements. A variety of TE amplifiers were examined, but most of the measurements were made on a resistor-pin type linear amplifier employing Allen-Bradley 56 Ω, ½ watt resistors, spaced 3.8 mm apart. The total discharge length (L) was varied from 23 cm to 92 cm. Typical resistive pin discharges use 1 kΩ resistors, resulting in serious energy losses in the resistors [30]. We found that 56 Ω resistors were sufficient to maintain discharge stability under our operating conditions, and resistive energy losses were minimised. The simple discharge system described in Chapter 3 was found to give very stable operation over a wide range of gas mixture and pressure, with energy inputs up to 400 J/ℓ-atm. Glow discharges were obtained under all conditions in low pressure

(<200 torr), high helium content (>80%) mixtures. At higher pressures some discharge deterioration was apparent with high energy input, but these regions could easily be determined (see below), and were carefully avoided in the present work. The pin-pin type of excitation gives good glow discharges without any pre-ionization,provided that the current pulse length is shorter than the time for a glow-to-arc transition [86]. Low pressure gas mixtures with a high helium content have sufficiently long glow-to-arc transition times. Gain was generally measured on the P(18) line of the 10.4 μ band to avoid complications associated with the P(20) line [50,80]. All other experimental details, and typical gain profiles, are given in Chapter 3.

5.3 Results and Analysis

Figure 10 presents observations typical of the variation of small-signal gain with stored energy [$E_c = \frac{1}{2} CV^2$]. The gas mixture used is 3% CO_2: 97% He at a pressure of 150 torr. This is not a mixture normally used in high pressure CO_2 lasers, but it is chosen here to display a very clear example of gain saturation. It should be noted that the gain depends only upon E_c, and not upon the individual values of capacitor or charging voltage. The charging voltage was varied over the range 16 kV to 32 kV.

It is very evident from Figure 10 that the gain not only fails to increase beyond a certain value of the stored energy, but actually begins to fall off at the higher energies. However, at this stage, we cannot use this to draw conclusions about variations in the discharge efficiency with input energy. As detailed in Section 3.3, we must first consider effects such as temperature increases and discharge deterioration which could be responsible for the observed gain saturation. The measured gains must then be converted into upper level populations,and the stored energy related to discharge input energy in J/ℓ-atm. This will enable us to make comparisons with theoretical calculations of electron excitation. In the following sections, all these issues are treated, and it is shown that the results are valid at and beyond atmospheric pressure.

The analysis of the data in Figure 10, as described in the following sections, is a rather lengthy process, and it seems worthwhile at this stage to anticipate the results. Figure 23 indicates the results typically obtained when the above factors are accounted for. The data is now presented in a form which can be compared directly with other work, both experimentaland theoretical. The dashed line is the population of the upper laser level, obtained by correcting the gain for thermal effects. The fall in gain at high energies is entirely caused by these effects. The corrected curve now demonstrates very clearly the occurrenceof a large loss in pumping effectiveness with increasing input energy. These results are typical of those obtained with other gas mixtures, leading to the conclusion that gain saturation is a fundamental property of CO_2 discharges.

FIGURE 23

Gain saturation characteristics of a 3% CO_2: 97% He mixture at 150 torr. The solid curve is the measured gain; representative error bars are given for two points. The dashed curve shows the population of the upper laser level as a percentage of the total number of CO_2 molecules present (N_{tot}). Excitation efficiency at low energies is indicated by the straight line.

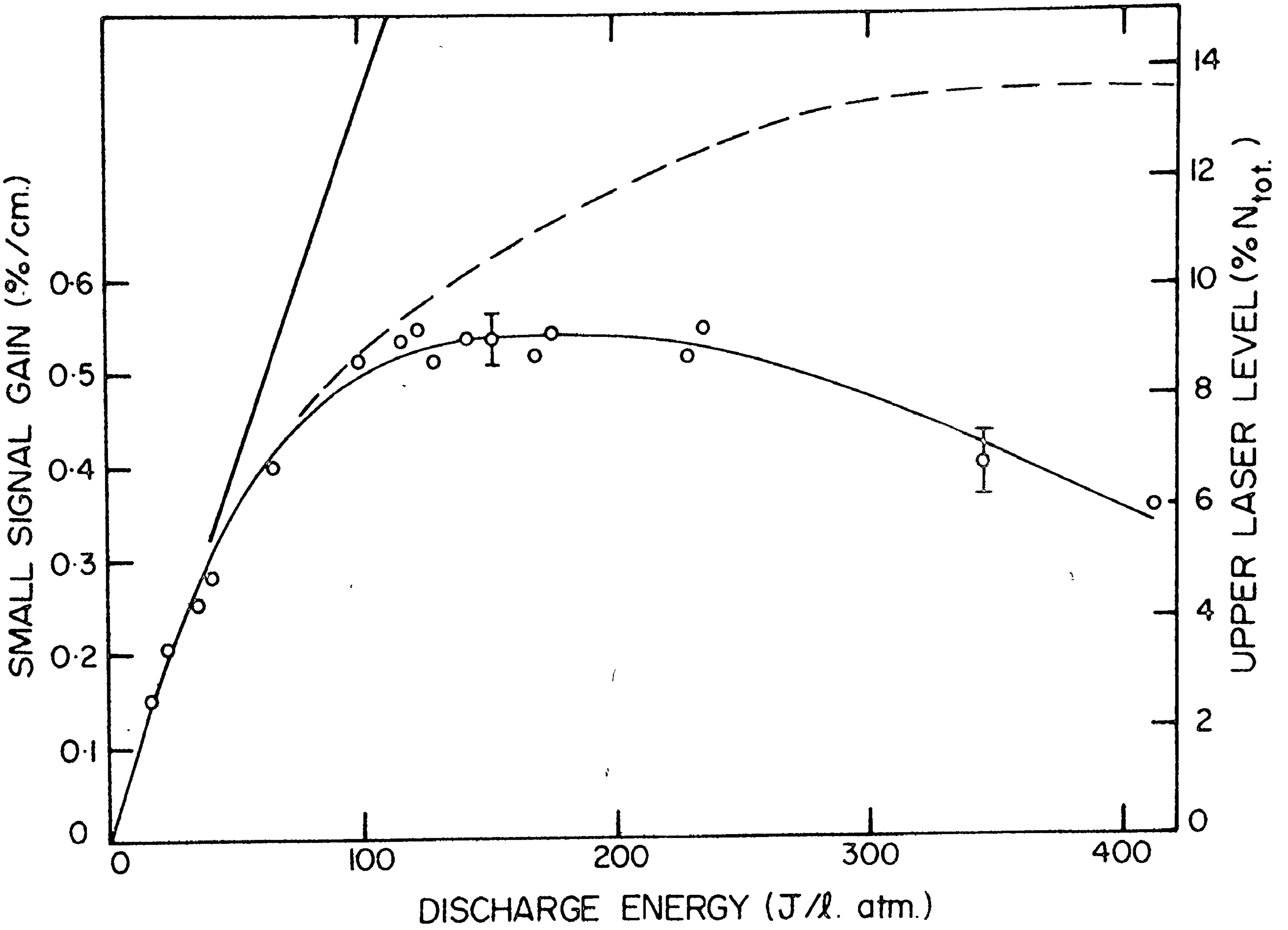
SMALL SIGNAL GAIN (%/cm.)
0
0·1
0·2
0·3
0·4
0·5
0·6
UPPER LASER LEVEL (% N$_{tot.}$)
0
2
4
6
8
10
12
14
DISCHARGE ENERGY (J/ℓ. atm.)
0
100
200
300
400

(a) Pressure Scaling and Discharge Quality

With a fixed gas mixture and pressure, the discharge voltage was monitored while the discharge capacitor and charging voltage were varied. The voltage drop across the discharge was found to be independent of the applied charging voltage. The voltage varied slowly at the time of the current pulse peak [87], and the value at this time was used to calculate E/N (discharge electric field/ particle density). The discharge voltage was directly proportional to gas pressure, i.e., E/N is constant. This is characteristic of self-sustained discharges, in which E/N is determined by the condition that the rates of ionisation and attachment must be equal [58]. Measurements were made of E/N for several mixtures, and the results compared with theoretical values obtained from calculations similar to those of Denes and Lowke [58]. Experimental results for a 10% CO_2: 90% He mixture are shown in Figure 24. The linear relationship between discharge voltage and pressure confirms that E/N is constant. The experimental values of E/N were found to be about 25% higher than the theoretical values, but the effects of impurities were not included in the calculations. The agreement between experiment and theory is satisfactory, and the experimental values of E/N are used in later calculations.

As E/N remains constant, the pumping efficiency of the discharge should be independent of pressure [21,22]. This was tested by measuring saturated gain (i.e., maximum gain obtainable

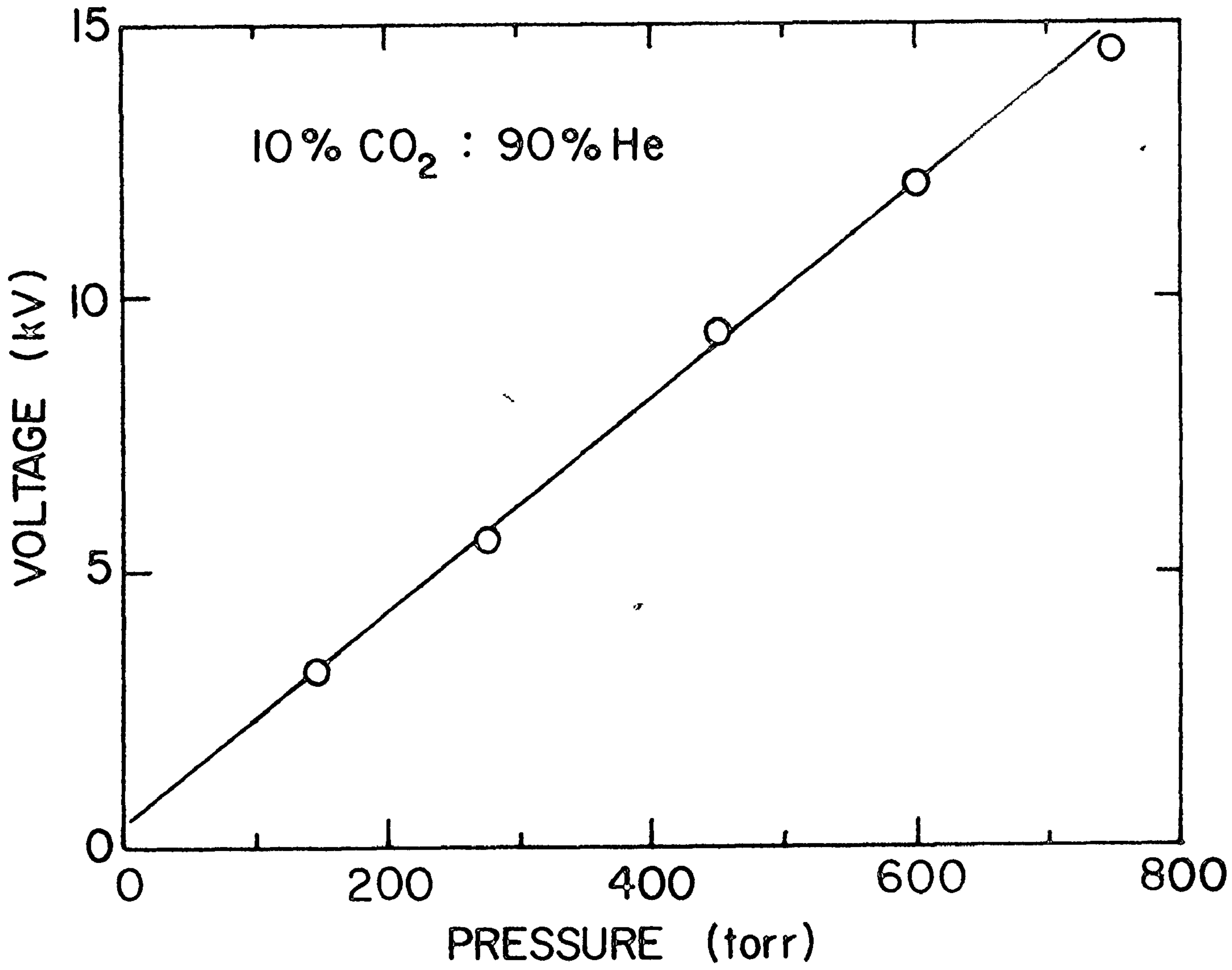

Figure 24: The variation of discharge voltage with gas pressure. The voltage was measured at the time of the current pulse peak, and was independent of storage capacitor and charging voltage.

as the input energy is varied) as a function of pressure. The results are shown in Figure 25. Observe that for a short discharge length (L = 23 cm) in 3% CO_2: 97% He, the saturated gain is indeed constant from <50 torr to atmospheric pressure. As L is increased, the gain falls off slightly at high pressure. This is even more apparent in the 10% CO_2: 90% He mixture. However, the saturated gain is still constant at low pressure, and remains constant to 400 torr for a 23 cm discharge.

The most appropriate conditions for producing good glow discharges are low pressure, high helium content mixtures, and very short current pulses [86]. It is under exactly these conditions that the saturated gain is independent of pressure. Very short current pulses can be used to saturate the 23 cm discharge length; longer discharges require more energy, and hence a longer current pulse. It seems probable that discharge deterioration is responsible for the poorer performance at high pressures. Glow-to-arc transitions must eventually take place in the discharge, leading to the appearance of filaments and bright arcs. Such visible deterioration of the discharge only occurs at or beyond the range of pressures employed in obtaining Figure 25. Nevertheless, data of the type shown in Figure 25 allows us to avoid the regions where discharge deterioration may affect the outcome of subsequently described experiments. Discharge deterioration is not the only reason for the poorer performance of the longer discharge tubes; it is more difficult to evenly distribute the energy from a single capacitor.

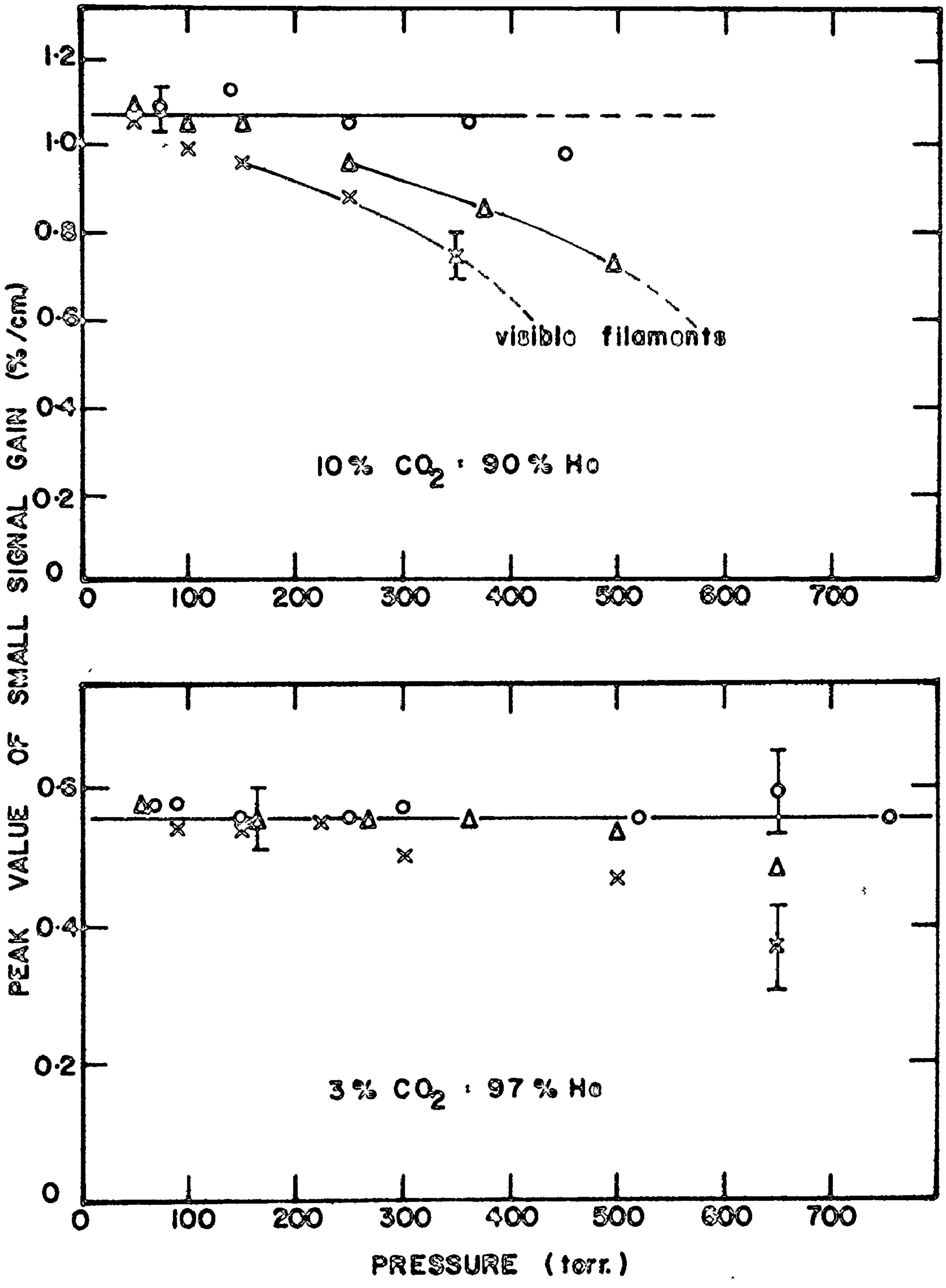

Figure 25: Peak gains as a function of pressure and discharge length. o , Δ, X correspond to lengths of 23 cm, 46 cm, and 92 cm, respectively.

The quality of the discharge, and the pressure scaling properties of gain saturation may also be tested in the following way. Measure the small-signal gain as a function of stored energy for the same He: CO_2 mixture at several different pressures. Plot the resulting gains as a function of stored energy scaled by the pressure. If all the points lie on the same curve then, over the range tested, the discharge quality has not deteriorated and the results obtained at one pressure can be scaled to any other pressure. Figure 26 shows the results of such a test for a 10% CO_2: 90% He gas mixture. Some deviations from a universal curve are apparent at high energy and pressure, precisely as expected from the results presented in Figure 25.

(b) Discharge Energy and Circuit Losses

As gain saturation occurs in an identical manner irrespective of pressure, we are free to choose an optimum pressure for further measurements. The ideal operating conditions for very stable discharges are pressures of $\sim$50 torr and very short discharge lengths. However, accurate gain measurements require a reasonable discharge length. In addition, higher pressures are required to ensure most of the stored energy enters the discharge gas, and is not used in heating the stabilising resistors [30]. A pressure of 150 torr and discharge length of 46 cm represents a suitable compromise, and is well within the "good discharge" region as defined

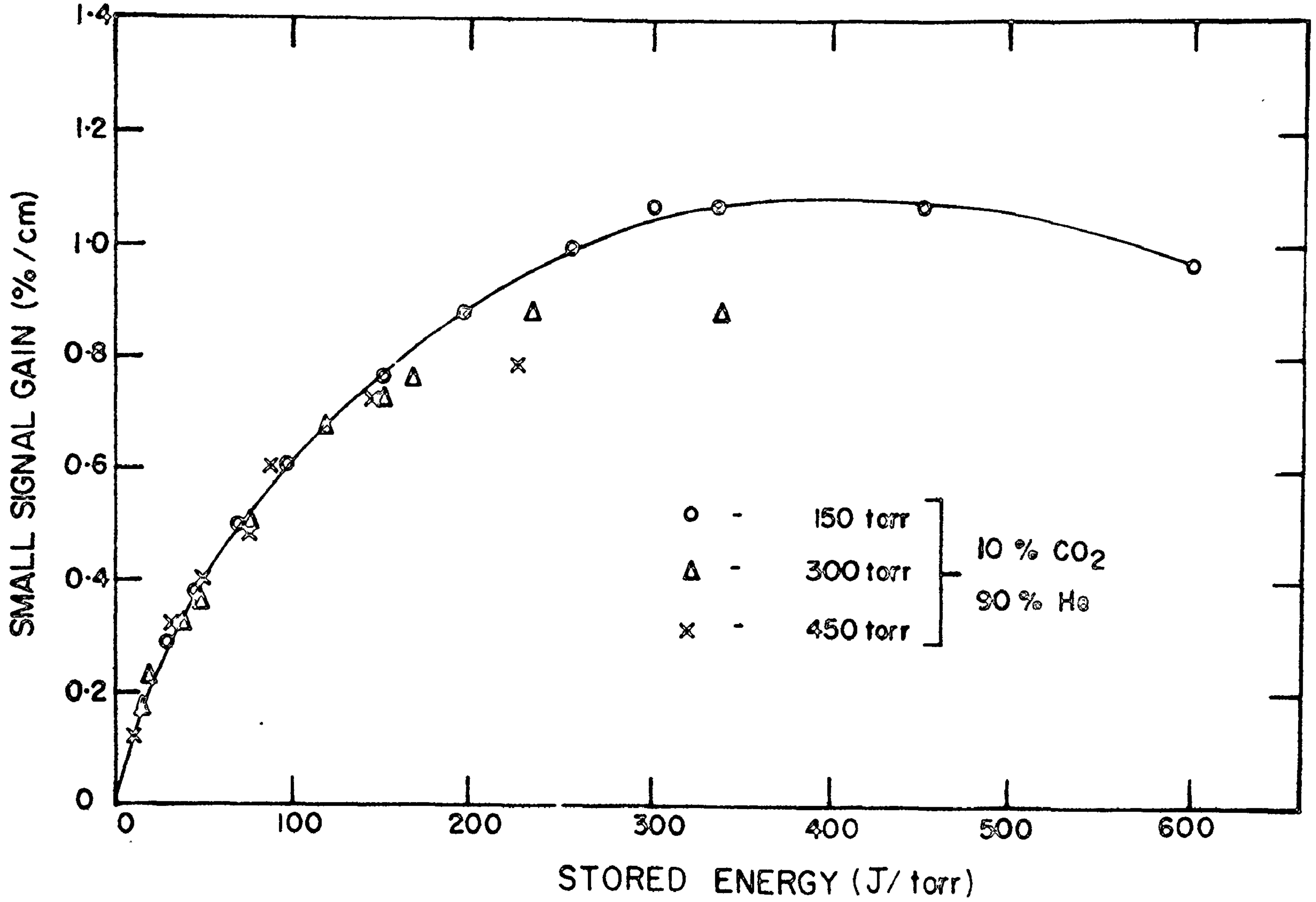

Figure 26: Small-signal gain of a 10% CO_2: 90% He mixture at various pressures. The energy axis has been scaled by pressure; see text for details.

by Figure 25. It now remains to determine the fraction of stored energy, E_c, that enters the gas. To relate the energy, E_g, deposited into the gas to E_c, the energy, E_r, dissipated in the resistors was computed by graphical integration of the measured I^2R drop across the resistors. The operating conditions are chosen such that E_r is always less than 30% of E_c. The energy losses in the spark gap (E_{sg}) and capacitor are expected to be small [30], and a high-voltage probe was used to verify that the capacitor was completely discharged. The energy absorbed by the spark gap was measured calorimetrically, and even for the most extreme conditions it was less than 20% of E_c. Finally, E_g is set equal to $E_c - (E_r + E_{sg})$. In some cases E_g was measured directly by graphical integration of IV, where V is the voltage drop across the gas only. These two methods were in good agreement, ensuring that all energy losses are accounted for.

(c) Discharge Volume

The next step in the analysis of the data is to obtain a value for the effective discharge volume and, more importantly, to determine how it changes with input energy. The spatial gain distribution can be measured by scanning across the discharge with the cw probe beam. However, it is only at very low energies that the gain distribution can be simply interpreted in terms of the spatial energy distribution. Once gain saturation begins, the gain distribution no longer reflects the spatial energy distribution.

This can be seen very clearly in Figure 27, which is a plot of spatial gain (longitudinally averaged) in a mixture of 10% N_2: 3% CO_2: 87% He at 100 torr. Curve 1 corresponds to an input energy just sufficient to saturate the gain at the centre. Curve 2 corresponds to 3 times that input energy, and the effects of increasing temperature on the gain can be clearly seen in the central hole. Note also that the gain in the wings reaches the usual saturation level. It is obvious that care must be taken in relating spatial gain distributions to the associated spatial distribution of the input energy at high values of the total input energy.

The next step, therefore, is to relate the observed spatial gain distribution to the underlying distribution of input energy to the discharge. Evidently, from Figure 27, the width of the gain distribution measured at the half maximum points increases with increasing input energy. However, this does not necessarily imply an increase in the width of the spatial energy distribution. Accordingly, we make the simple proposition that this spatial energy distribution is independent of input energy. This idea can be subjected to test in the following fashion. At low discharge input energies, the spatial distribution of the gain reflects the underlying energy distribution. Now suppose that, as the energy input is varied, this distribution remains unchanged and has a peak value which scales with the input energy. Consequently, since the gain is known as a function of input energy, the spatial distribution of the gain for energies well

FIGURE 27

Spatial variation of gain for a 3% CO_2: 10% N_2: 87% He mixture at 100 torr. Two gain distributions are shown, the one on the left (curve 1) corresponds to an input energy of 120 J/ℓ-atm. The other gain distribution (curve 2) corresponds to an input energy of 350 J/ℓ-atm. Representative gas temperatures are also shown.

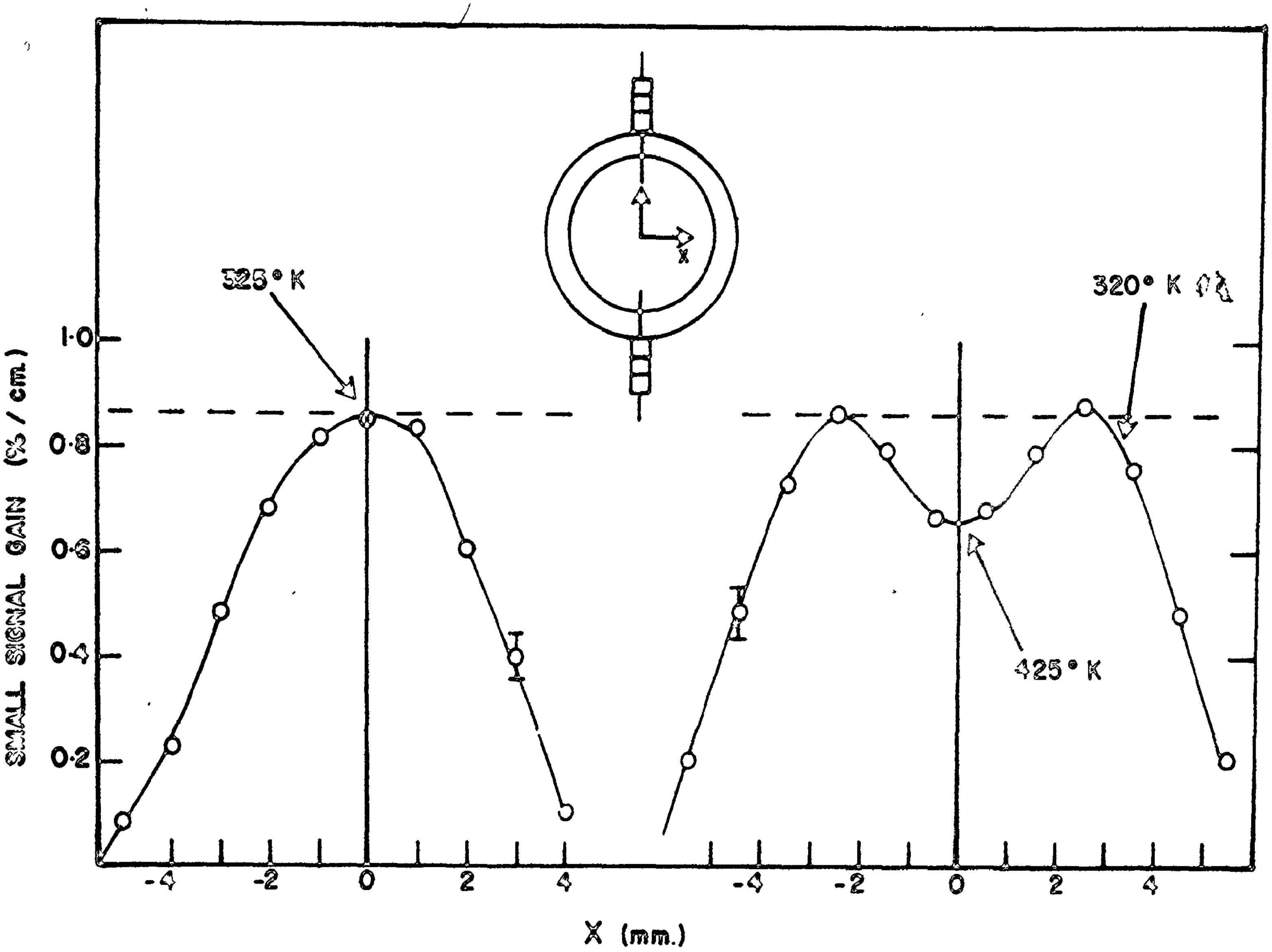
325° K
320° K
425° K
x
1·0
0·8
0·6
0·4
0·2
SMALL SIGNAL GAIN (% / cm.)
-4
-2
0
2
4
-4
-2
0
2
4
X (mm.)

into the saturation region can be predicted and compared with experimental observation. The results of such a test are shown in Figure 28; the discharge energy at the centre of the distribution is twice the saturation value. The solid curve is the calculated gain distribution, with the maximum gain occurring at the half energy points. The measured values of gain are indicated in the figure, and good agreement is obtained. All gain measurements are made with an effective beam diameter of $\sim$1.5 mm, and no deconvolution has been attempted. The good agreement between experiment and calculation confirms that no significant volume change occurs in the discharge. Very similar behaviour of the spatial energy distribution was obtained for all gas mixtures and pressures. The widths of the gain region reported here are consistent with those obtained by other authors [36,74,88].

The measurement was repeated at various distances from the anode and cathode pins, and the effective discharge cross-section was determined to be 1.2 cm^2. The individual resistors controlling the discharge are only 3.8 mm apart (compared to an energy distribution with a FWHM of 5.5 mm), and so the longitudinal energy distribution is expected to be approximately uniform. This was confirmed by doubling the resistor spacing and observing that the gain still saturates at the same level. Even with the double spacing, no gaps appear in the discharge. We are now in a position to convert the discharge energy, E_g, into J/ℓ-atm. With L = 46 cm, the discharge

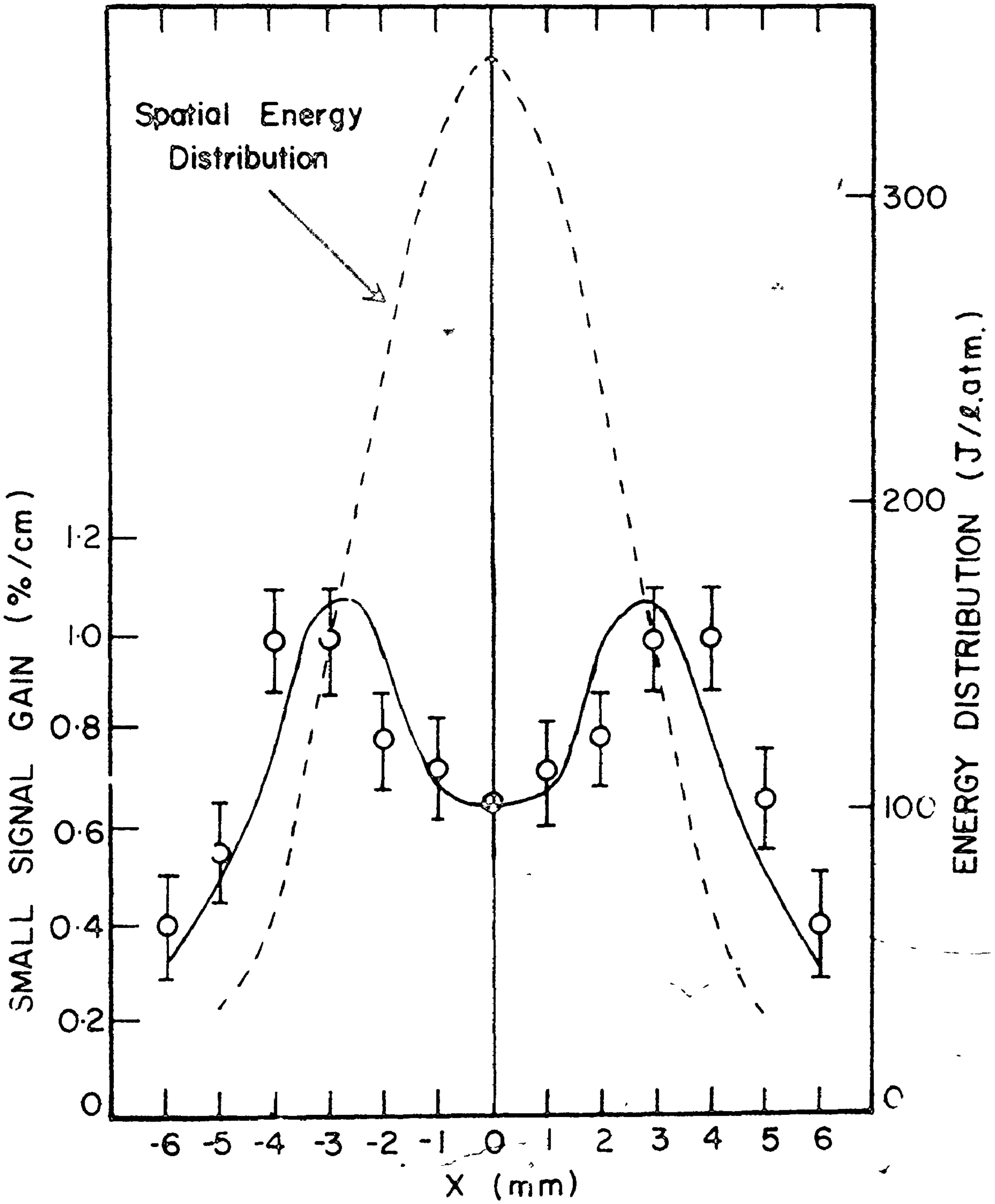

Figure 28: Spatial variation of gain for a 10% CO_2: 90% He mixture at 150 torr. The solid curve is the gain variation calculated using the indicated spatial energy distribution. Experimental points are also displayed.

volume is 55 cc , and the data of Figure 10 can be replotted as shown in Figure 23.

(d) Carbon Monoxide Production

A further experiment was carried out to provide an independent check on the values of E_g determined as indicated above. A carbon monoxide gas sampler (Bacharach model 19-7016) was used to measure the CO produced under typical discharge conditions. Calculations have been made by Nigham [21] and Lowke et al. [22] to determine the electron energy distributions in CO_2 discharges. They find that there are sufficient high energy electrons (>7 eV) present to cause significant dissociation of CO_2 into CO and oxygen [89,90]. As E/N is constant, the total CO produced per discharge pulse should be proportional to E_g.

Figure 29 shows the results obtained for the amount of CO produced as a function of the input energy to the discharge. The measured CO production was converted into the energy required to dissociate CO_2, supposing that 7 eV is used per molecule in this process. Both axes have the energy expressed in J/ℓ-atm. This is primarily to facilitate comparison with the other figures in this Chapter; the same discharge volume is employed in scaling each axis and the results are independent of the value of the volume employed. The CO production is directly proportional to the discharge energy, measured according to the methods described

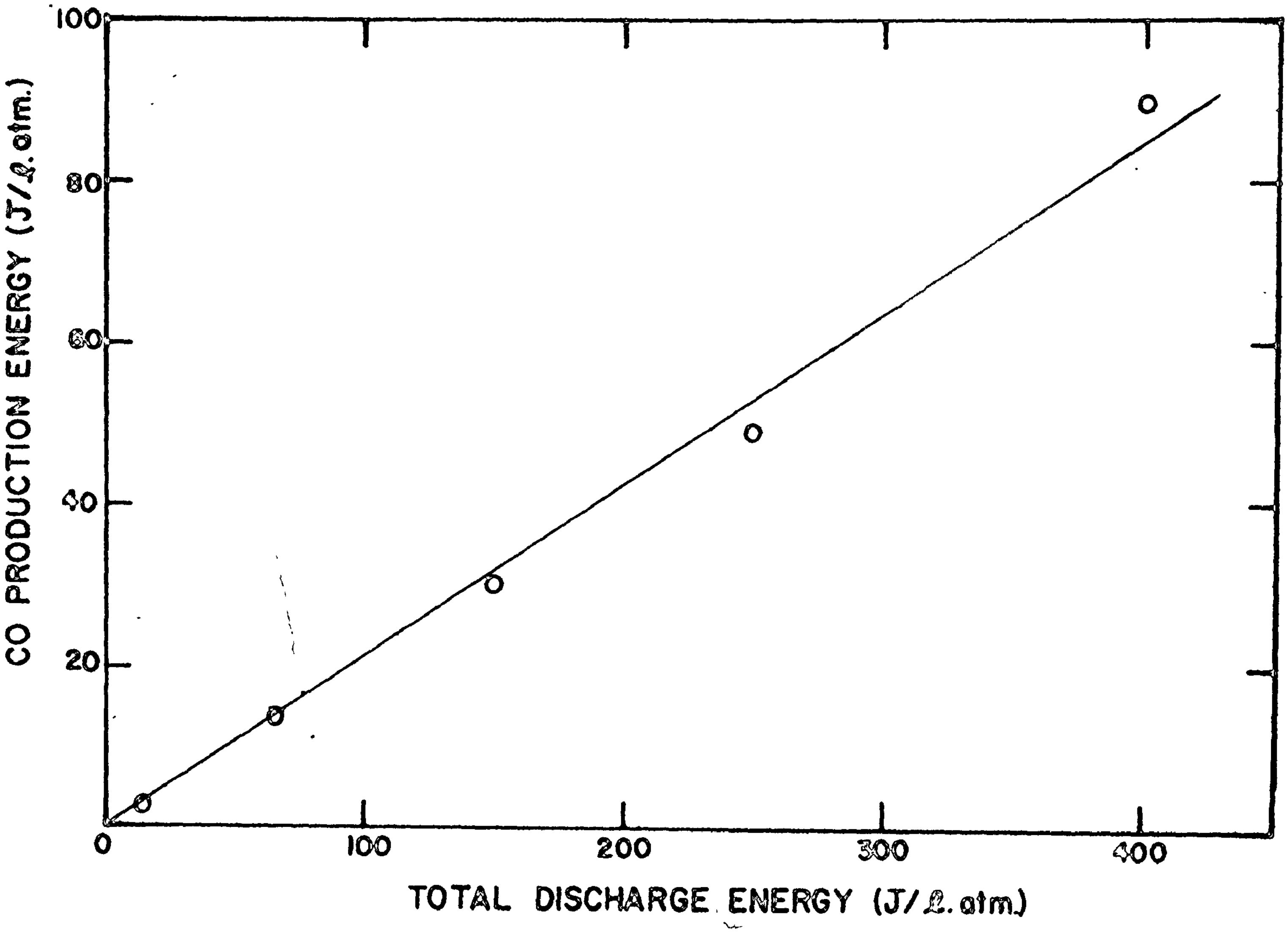

Figure 29: Carbon monoxide production in a 10% CO_2: 90% He mixture at 150 torr.

in section 5.3b, which lends an extra degree of confidence to those determinations. In addition, as will be seen subsequently, the fraction of the discharge input energy which produces dissociation is in good agreement with theoretical estimates. It is to be emphasised that the amount of CO within a discharge volume is always very much less than the CO_2 content.

(e) Temperature Measurements

For the purposes of subsequent comparison with theory, it is important that the measured gains (in %/cm) should be converted into an inversion, and thereby into an upper laser level population. Before this can be attempted, the temperature of the discharge gas must be known. Two methods were used to measure the translational temperature, T, of the gas mixture. (1) After the gain pulse, the cw probe beam experiences an increase in absorption. This is caused by a thermally-induced increase in the population of the lower laser level, and is maintained over a time of a few ms. [30]. The absorption can be measured and the population of the 10°0 level determined. After the gain pulse, all the modes of CO_2 will be in equilibrium with the translational temperature, which can be calculated directly from the 10°0 level population. This method can only be used when the temperature of the gas has increased sufficiently to cause appreciable absorption. (2) The gain on several rotational lines is measured, and the rotational temperature at the gain peak is determined. There is ample time for the rotational and translational temperature of the CO_2 to come into equilibrium, and so this technique constitutes a method of measuring the latter. This method is fully described in Chapter 4. However, it should be emphasised that the gain on lines near P(20) is relatively insensitive to temperature changes (see Figure 14). Consequently, it is appropriate to place more emphasis on the variations of the gain on lines such as P(34), P(36) and P(38),which are much more sensitive to temperature variations. This strategy was adopted for the measurements reported here.

Both methods are used and give good agreement. The in-cavity method of Section4.3 canonly be used under conditions of low discharge energy as it measures a temperature averaged over the mode volume. Once a "hole" is present in the spatial gain (see Figures 27 and 28) this average no longer approximates the true discharge temperature. However, when the measurements are limited to low discharge energies, the in-cavity method is in good agreement with the direct rotational gain method . Typical results are shown in Figure 30 for a 10% CO_2: 90% He mixture. A linear dependence of temperature on energy is obtained, with an increase in temperature of 200°K at 400 J/ℓ-atm. Also shown in Figure 30 is a plot of small-signal gain against discharge energy. Once again saturation occurs, but at high input energies the gain falls to less than half its peak value. It will be shown that this reduction in gain is entirely due to thermal effects.

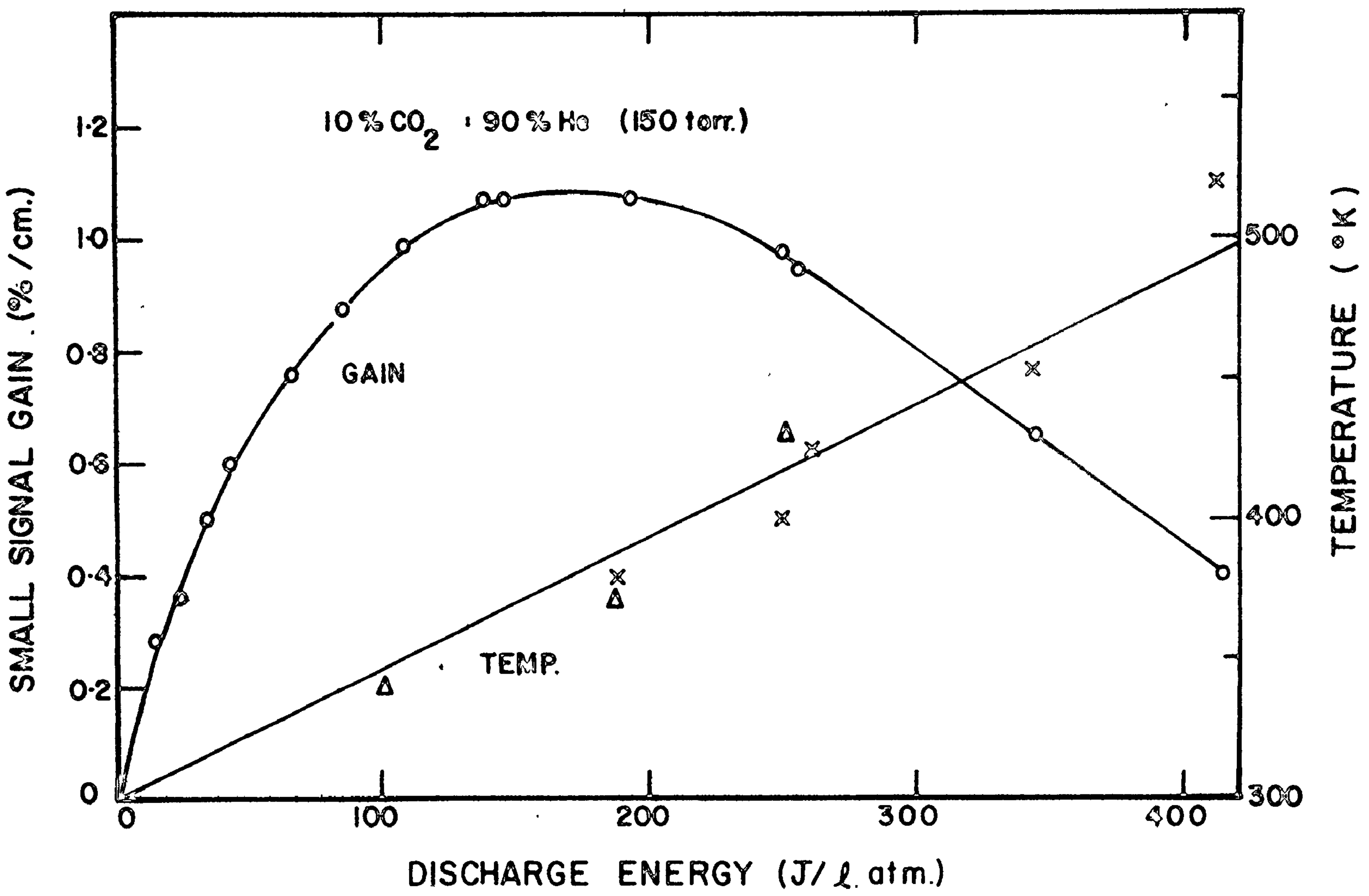

Figure 30: Small-signal gain and gas temperature as a function of energy. Temperatures measured by the absorption method (X) and rotational gain method (Δ) are both indicated. (see Section 5.3e).

(f) Thermal Effects and Gain

We are now in a position to convert small signal gain into inversion. The gain on the P-branch of the 10.4 μ band, α_P, is related to the laser level population by Equation 2.10, reproduced below

$$\alpha_P(J) = \frac{7.13\mathrm{x}10^{-19}\ J\ \{N_u B_u[\exp(-E_u(J-1)/kT)] - N_\ell B_\ell[\exp(-E_\ell(J)/kT)]\}}{\left(P_c + \frac{P_h}{1.69} + \frac{P_n}{1.33}\right)(3.42 - 0.0234J)\ \lambda(J)\ T^{\frac{1}{2}}} \qquad (2.10)$$

It is assumed that no significant expansion takes place during the risetime of the gain pulse, and so conditions of constant particle density prevail, i.e., P_c, P_h and P_n are all proportional to T.

All the terms in Equation 2.10 are known except N_u and N_ℓ. N_ℓ is the population in the 10°0 level at the gain peak. It has been shown in Chapter 4 that the lower level empties during the risetime of the gain, and that at the gain peak the population of the lower level is close to equilibrium with the gas temperature. Hence N_ℓ is taken to be the equilibrium value of the 10°0 population at a temperature T. N_u can now be determined from Equation 2.10, and is always much larger than N_ℓ.

The measured gain enables us to determine the population in the 00°1 level at the gain peak. However, we are interested in the pumping efficiency of the discharge into the entire asymmetric mode.

Consequently, we must include combination levels such as (01'1), which do not contribute to the gain on P(18), but may contain an appreciable fraction of N_u, particularly at high T. All the combination levels can be accounted for by multiplying N_u by the partition function of CO_2, Q(T), as given by Gray and Selvidge [91]. In fact, only the partition function for the bending and symmetric modes is required, but for $T < 500°K$, the asymmetric mode makes a negligible contribution to Q, and no error is introduced by using the total partition function (for further details, see Appendix A).

One further correction must be made before the excitation efficiency of the asymmetric mode during the excitation pulse can be determined. The value of N_u Q at the gain peak must be extrapolated back to the time of the current pulse. The falltime of the gain (t_2) is measured, and used to extrapolate this population value back to that which existed at the end of the current pulse. In the mixtures used throughout this work, the falltime of the gain is much longer than the risetime. This ensures that the extrapolation factor is always small. It is expected that the falltime of the gain will vary with discharge temperature and thereby with input energy. Consequently, t_2 is measured as a function of input energy for all mixtures, and a significant decrease at high energy is observed. In general, t_2 is halved once the discharge gas temperature reaches 450°K. This is consistent with the measured temperature dependence of the relaxation rate of the 00°1 level [11]. The falltime of the gain is still much longer than the risetime, and even in the most extreme case, the 00°1 population at the gain peak has only fallen to 70% of the initial population. Typically, the 00°1 population only falls by 10% during the risetime of the gain; a direct consequence of using mixtures with a high helium content. Helium is much more efficient at relaxing the lower laser level than the upper laser level [11].

(g) He: CO_2 Mixtures

Small-signal gains are converted to upper laser level populations as detailed in the previous section. The dashed line in Figure 31 is a plot of the upper laser level population as a function of energy, for a 10% CO_2: 90% He mixture. The population has been corrected for partition functions and extrapolated to the time of the current pulse, using measured rise and fall-times. It is plotted as a percentage of the total CO_2 molecules present (N_{tot}). Figure 23 is a similar plot for the 3% CO_2: 97% He mixture. Once again, correction for thermal effects removes the fall in gain at very high energy, and clearly reveals the underlying loss of pumping efficiency. In each case, the pumping efficiency rapidly decreases above 50 J/ℓ-atm. and total saturation is achieved around 250 J/ℓ-atm. These results are consistent with those obtained by other authors. For example, Richardson et al. [7] and Figuiera [32] both apparently observe the onset of gain saturation at discharge energies above 150 J/ℓ-atm.,

FIGURE 31

Gain saturation characteristics of a 10% CO_2: 90% He mixture at 150 torr. The solid curve is the measured gain; representative error bars are given for two points. The dashed curve shows the population of the upper laser level as a percentage of the total number of CO_2 molecules present (N_{tot}). Excitation efficiency at low energies is indicated by the straight line.

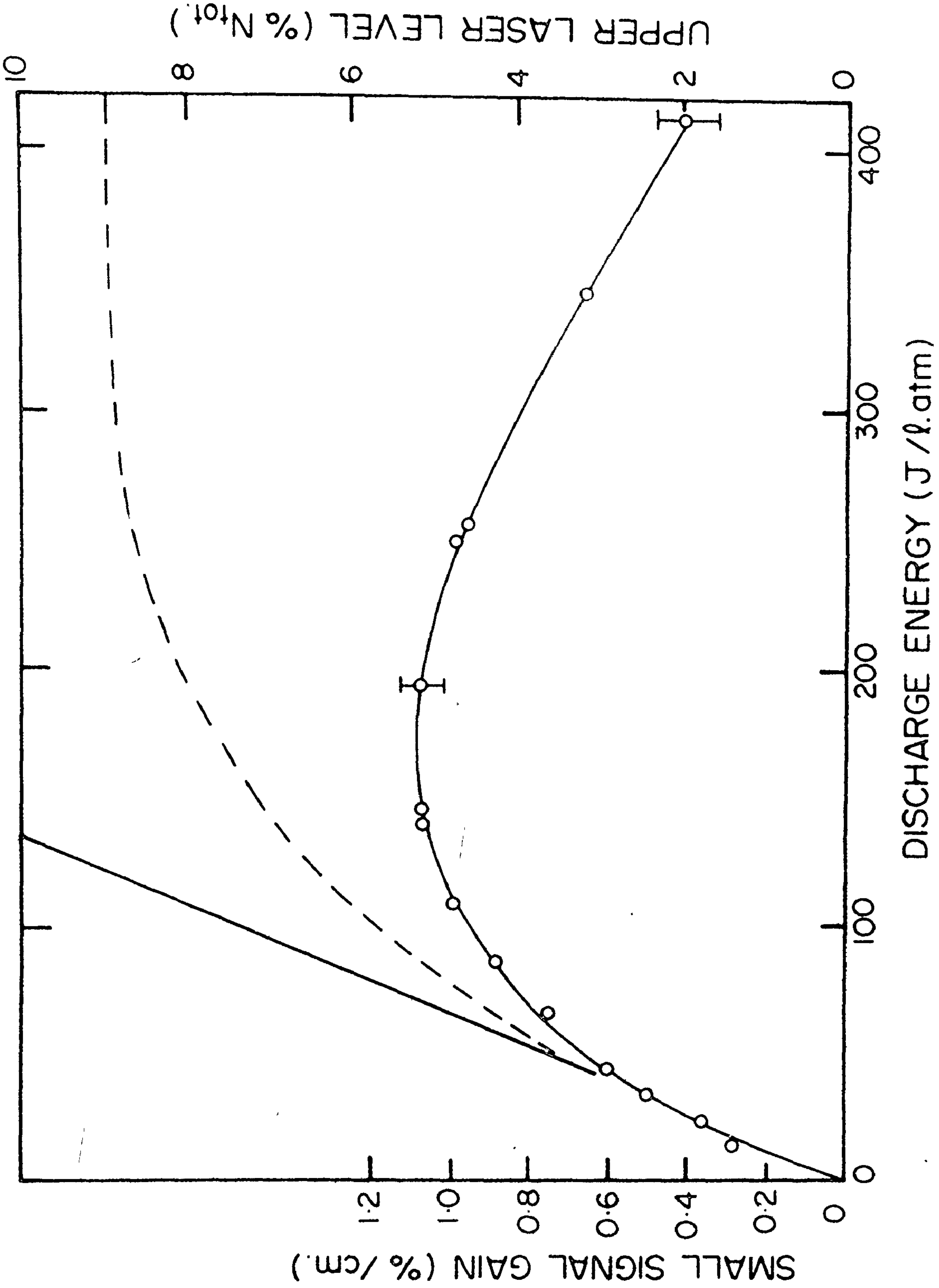
UPPER LASER LEVEL (% N$_{tot.}$)
10
8
6
4
2
0
SMALL SIGNAL GAIN (%/cm.)
1.2
1.0
0.8
0.6
0.4
0.2
0
DISCHARGE ENERGY (J/ℓ.atm)
0
100
200
300
400

although no attempt was made to correct for temperature effects. Lachambre et al. [31] also observed a non-linear relationship between gain and pump energy beyond 75 J/ℓ-atm.

It is apparent that proper allowance for the various effects produced by a rise in gas temperature effectively eliminates the fall in gain at high discharge energies. Nevertheless, the sum total of these effects is entirely inadequate to account for the observed gain saturation. However, at the highest input energies, the temperature correction is moderately large and it seems appropriate to detail the methods employed in making the corrections. There are several contributions to the temperature-induced degradation of the gain: (1) The inversion is distributed over more and more rotational lines as the temperature increases (2) The linewidth of the transition broadens as $T^{1/2}$ under the constant density conditions of the discharge (3) The population of the lower laser level is increased, (4) More and more combination states (e.g. 01'1) reducing the effective inversion are formed (5) The lifetime of the upper laser level shortens. All these effects can be simply accounted for once a temperature is known. Item (2), however, is deserving of a little further discussion. There is some uncertainty concerning the temperature dependence of the linewidth, $\Delta\nu$, of the 10.4 μ band transitions. Simple physical considerations indicate the $\Delta\nu$ should broaden as $T^{1/2}$ under conditions of constant particle density. However, measurements made by Ely and McCubbin [50] in pure CO_2 indicate that $\Delta\nu$ is temperature independent in the range 300 - 400°K. (Ely and McCubbin find that $\Delta\nu \propto T^{-1}$ at constant pressure. This is equivalent to temperature independence under conditions of constant particle density). Our conclusions are not sensitive to the behaviour of $\Delta\nu$. This can be seen in Figure 32. The pumping efficiency of the upper laser level is plotted against discharge energy; both linewidth formulations are used. In each case a drastic reduction in pumping efficiency occurs at high energy. In all the gas mixtures examined, the measured pumping efficiency at high input energies is $\sim$4 times smaller than that at low energies. We generally use the formulation $\Delta\nu \propto T^{1/2}$, which gives the larger correction at high temperatures.

(h) Relative Excitation Efficiencies

In this section, we compare the theoretically calculated discharge excitation efficiencies with those observed experimentally at very low values of the input energy. The agreement obtained confirms that such calculations provide a good description of the discharge at low input energies. Several authors [21,22,28,29,67] have calculated the electron energy distribution functions and relative pumping efficiencies in CO_2 laser mixtures. As described in Section 2.5, we have carried out similar calculations for the mixtures used in this thesis. Relative pumping efficiencies are strongly dependent upon the value of E/N; in all cases experimental

FIGURE 32

Excitation efficiency in the 10% CO_2: 90% He mixture as a function of discharge energy. The results of using the two possible dependences of linewidth ($\Delta\nu$) on temperature are shown.

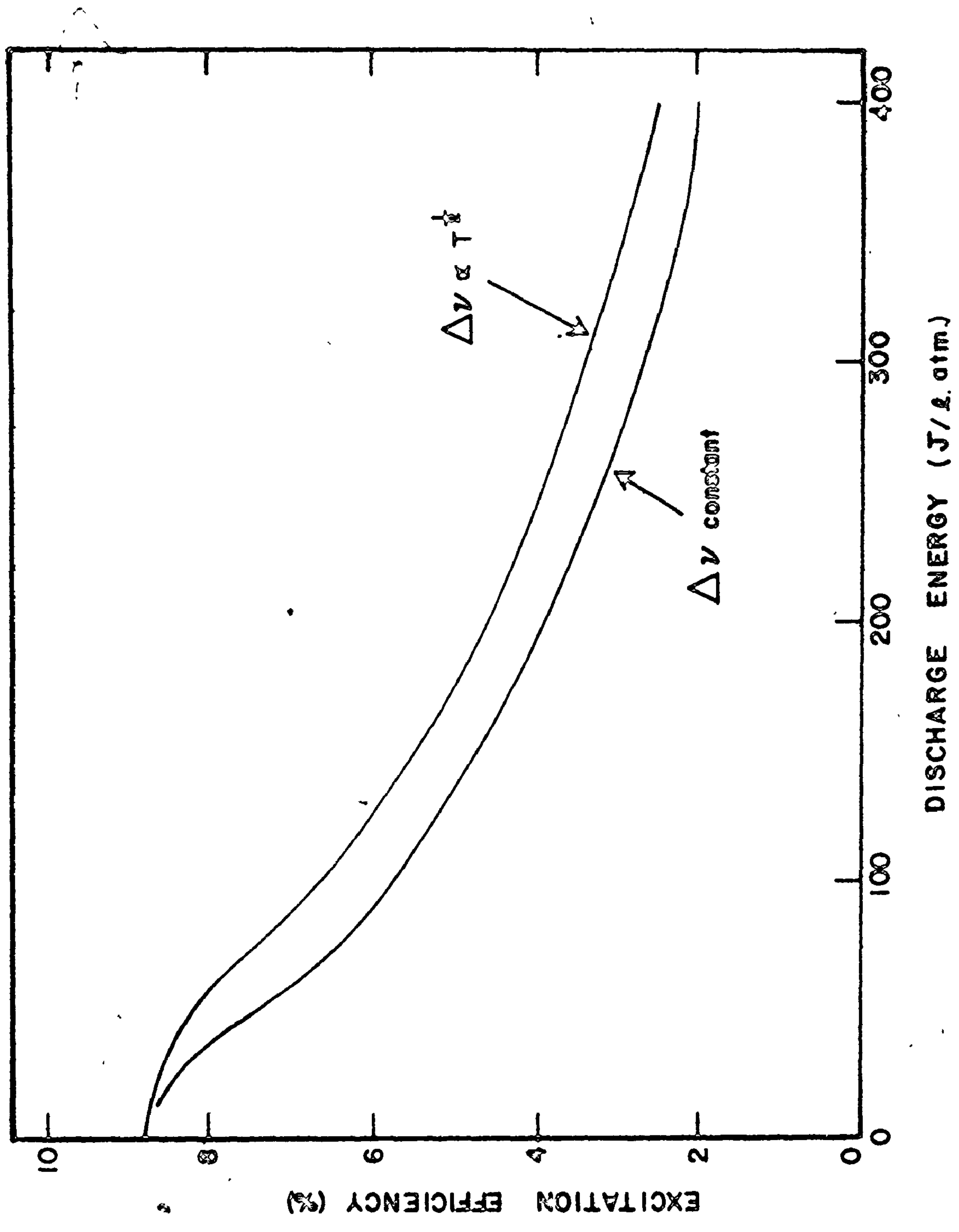
EXCITATION EFFICIENCY (%)
DISCHARGE ENERGY (J/ℓ atm)
0
2
4
6
8
10
0
100
200
300
400
Δν ∝ T^½
Δν constant

values of E/N were used. The pumping efficiency of the asymmetric mode in CO_2 is of particular interest. We obtained good agreement between the experimental results at low energies and the theoretical calculations. In the 3% CO_2: 97% He mixture, the electrical pumping efficiency at low input energy (straight line in Figure 23) is measured as 4.8%, in excellent agreement with the theoretical value of 4.6%. In the case of the 10% CO_2: 90% He mixture, the experimental efficiency at low energies is 8.5%, also in good agreement with the theoretical value of 9.8%. The calculations based on the work of Nigham [21] and Lowke et al. [22] agree with experiment at low discharge energies. However, these calculations do not predict any gain saturation at high discharge energy; the pumping efficiency is assumed to remain constant.

Further comparisons between theory and experiment were made for the 10% CO_2 mixture. The relative efficiency of CO production can be determined from Figure 29. This experimental value is 23%. A theoretical value can be obtained by integrating over the cross-section for CO_2 dissociation [22,90] using the calculated electron energy distribution. Once again a production energy of 7 eV per CO molecules is assumed. The calculated value is 28%, in very good agreement, considering the uncertainties in the cross-section data. It is also of some interest to note that we are now in a position to check on the energy balance, in that the input energy which results in gas heating can be calculated and compared with that from measured heating. This input energy is taken to include all the bending and symmetric stretching modes of CO_2, as they rapidly relax into the helium thermal bath. The calculated value is 37% of the input energy and the experimental percentage is 32 (obtained from the straight line in Figure 30). Once again, good agreement is obtained. Table 2 summarises these results. The overall agreement between experiment and calculation at low energy is very satisfactory.

(i) $He:N_2:CO_2$ Mixtures

The gain saturation phenomenon is not confined to $He: CO_2$ mixtures. Very similar results are obtained in $He:N_2:CO_2$. A mixture containing 10% N_2 and 3% CO_2 (just sufficient CO_2 to monitor the population of the N_2^* level) was used to obtain the results shown in Figure 33. Once again the small-signal gain saturates and then decreases at high input energy. The dashed line represents the upper laser level, after thermal effects have been taken into account. At the time of the gain peak, the asymmetric mode of CO_2 is in equilibrium with the vibrationally excited N_2 [11]. Hence the dashed line in Figure 33 is also representative of the population of the $\nu = 1$ level of the nitrogen in the mixture. Note that saturation occurs when 16% of the total nitrogen molecules are excited to the $\nu = 1$ level. This corresponds to a vibrational temperature of 2100°K, and significant energy is stored in the higher vibrational levels of N_2. However, the total vibrational energy will remain constant from 200 J/ℓ-atm. to 400 J/ℓ-atm. Experimentally, it is found that all $He: N_2$ mixtures containing up to one-third N_2, saturate when the

TABLE 2

Relative Excitation Efficiencies

Mixture is 10% CO_2: 90% He with E/N = 2.4×10^{-16} V cm^2

Process	Calculated Energy Input %	Measured Energy Input %
Asymmetric Mode Excitation	9.8	8.5 (at low energies)
CO Production	28.	23.
Gas Heating	37.	32.
Electronic Excitation and Ionisation	25.	not measured

FIGURE 33

Gain saturation characteristics of a 3% CO_2: 10% N_2: 87% He mixture at 100 torr. The solid curve is the measured gain; representative error bars are given for two points. The dashed curve shows the population of the upper laser level as a percentage of the total number of CO_2 molecules present (N_{tot}). Excitation efficiency at low energies is indicated by the straight line.

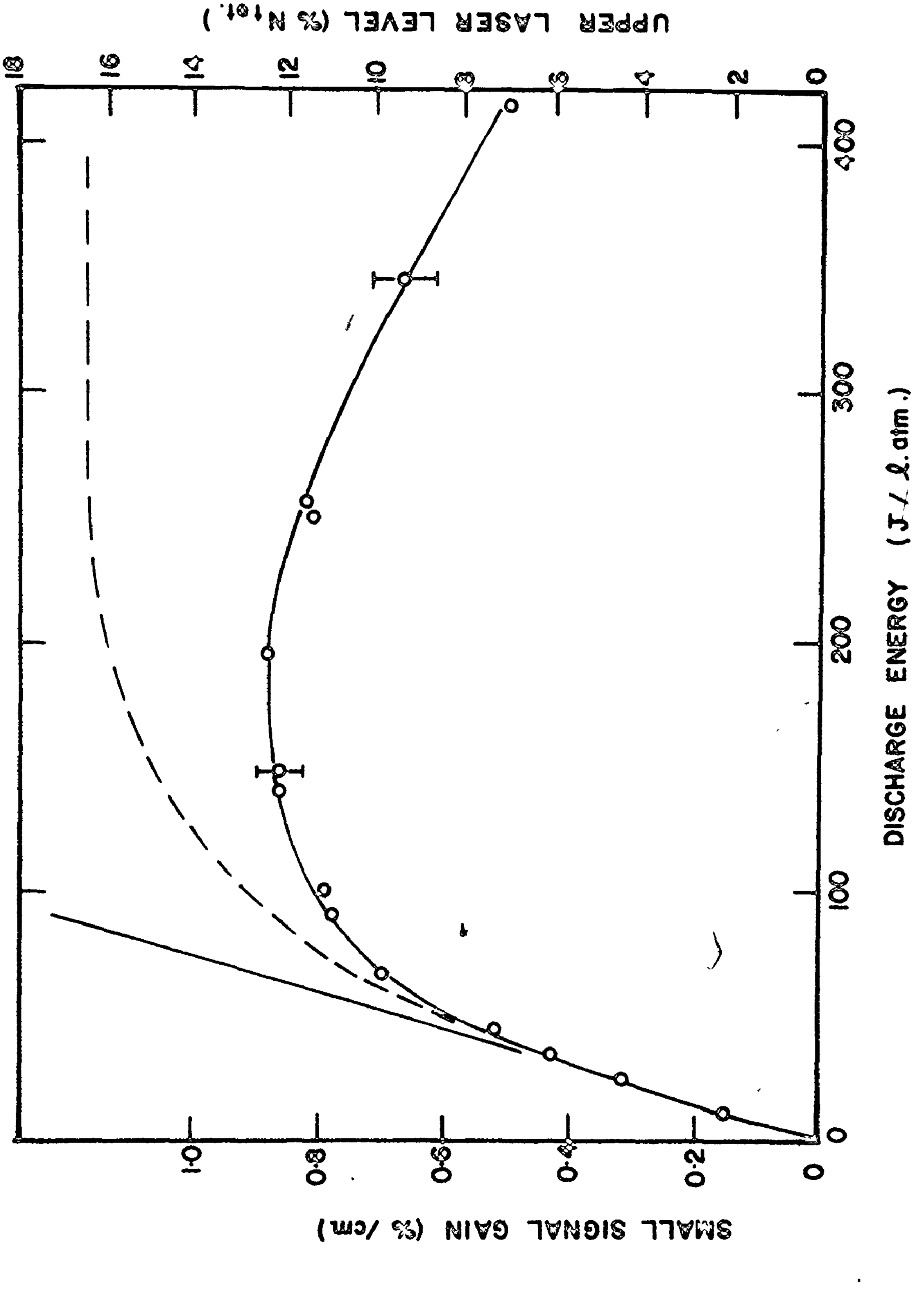
UPPER LASER LEVEL (% N$_{tot.}$)
18
16
14
12
10
8
6
4
2
0
SMALL SIGNAL GAIN (%/cm)
1·0
0·8
0·6
0·4
0·2
0
DISCHARGE ENERGY (J/ℓ.atm.)
0
100
200
300
400

$\nu = 1$ level has a population of 16% of the total nitrogen molecules. (A trace of CO_2 is added to these mixtures to give a measurable gain). This relatively high saturation level, plus the high pumping efficiency of N_2 mixtures, makes nitrogen a particularly important constituent of CO_2 lasers.

He:CO_2 mixtures behave somewhat differently; the saturated population of the upper laser level is 14% of the available CO_2 molecules at low CO_2 concentrations, and falls to only 5% when the He:CO_2 ratio is 4:1. Typical He:N_2:CO_2 laser mixtures containing at least 50% He were also examined. Gain saturation with increasing energy was evident in all mixtures. Peak gains of 3.5%/cm (P(20), 10.4 μ band), were easily obtained, in agreement with other reported results [7,31,32].

5.4 Discussion and Conclusions

Clear evidence of saturation in the net electron excitation of CO_2 (00°1) and also of N_2^* has been presented. This result is independent of gas pressure and applies at and above atmospheric pressure. Furthermore, the peak values of the gain coefficient observed in the saturation region are in excellent agreement with those observed for optimally pumped systems of all the presently reported types. Evidently this dramatic loss of pumping efficiency with increasing input energy is a generally observed effect. The peak gain obtainable with the present system agrees directly with measurements made on double discharge and u.v. pre-ionized systems, which also operate with short current pulses and values of E/N appropriate to self-sustained discharges [58,67].

The E-beam pumped laser amplifier deserves special comment. These discharges operate over a range of externally controlled values of E/N. Long current pulses can also be employed which enable the lower laser level to empty during the current pulse. This factor alone increases the short pulse maximum gain of 3.5%/cm to approximately 5%/cm. The peak gains typically achieved in electron-beam pumped lasers are in fact 5%/cm, and gain saturation with increasing discharge energy is routinely observed [33,34].

The source of the gain saturation effect reported in this Chapter is not clear.It is possible that its origin is to be found in de-excitation processes in discharges such as might be produced by slow electrons. The existence of processes of this type has received some support from work on low pressure CO_2 laser amplifiers. Investigations of the relaxation of the upper laser level in low pressure dc excited CO_2 lasers have been carried out, in an attempt to measure the effectiveness of discharge electrons at de-exciting the 00°1 level of CO_2 [92,93]. Large cross-sections are measured for this process, generally an order of magnitude greater than the effective excitation cross-section. These results cannot be accounted for using standard calculations of de-excitation by collisions of the second kind, and averaging over the calculated electron distribution functions [93]. However, if the assumption is made that gain saturation occurs when the rate of 00°1 de-excitation becomes equal to the pumping rate, an effective de-excitation cross-section approximately 8 times the effective excitation cross-section is obtained in the He:CO_2 mixtures. This value is in reasonable agreement with the values obtained in the low pressure amplifier investigations [92,93]. The dashed lines in Figures 23,31 and 33 exponentially approach the final saturation level; this is the expected behaviour if de-excitation becomes progressively more important with the increasing population in the upper laser level. In Section 4.5 a similar saturation effect was observed in the pumping of the BS modes, suggesting that de-excitation processes may also be important for some of these levels. Large cross-sections for electron de-excitation of the lower laser level were measured by Gower and Carswell [92]. It is evident that further investigation is required of the role of electrons in de-exciting vibrationally excited molecules in CO_2 lasers, both during and after the discharge.

Several authors have calculated the efficiency of pumping the laser mode in CO_2 laser mixtures [21,22,28,67]. At low input energies, our results are in good agreement with these calculations. However, it is clear that, at the present level of sophistication, the excitation models of discharge operation will produce incorrect results at all but the most modest of input energies.

5.5 Summary

This Chapter had dealt with the electronic pumping efficiency of the upper laser level in CO_2. To determine the pumping efficiency from measurements of small-signal gain, a rather involved procedure was followed, and much attention was paid to eliminating effects of a secondary nature. The end result of these investigations is the conclusion that the pumping efficiency of the upper laser level falls drastically at high discharge energies. This clearly has important consequences for all high energy TE CO_2 lasers.

Chapters 4 and 5 have been concerned with measurements and theories of small-signal gain. The next Chapter deals with the dynamics of the laser pulses in TE CO_2 lasers. The knowledge gained to this point enables us to accurately determine the conditions in the gain medium prior to lasing. We are therefore in a much better position than previous authors [35-38] to compare theoretical laser models with experiment. Hence, we are able to determine the effect of rotational coupling upon the laser dynamics, and obtain detailed information concerning the relaxation of the lower laser level during lasing.

CHAPTER 6

STUDIES OF ROTATIONAL COUPLING AND LOWER LEVEL RELAXATION RATES DURING Q-SWITCHED TE CO_2 LASER PULSES

The previous Chapters have been concerned with the small-signal gain in TE CO_2 lasers. The magnitude of the gain, and its time-dependence, have been investigated, and particular emphasis has been placed upon the behaviour of the lower laser level (10°0) during the gain risetime. In Section 2.6, a model is presented where it is postulated that the relaxation of the 10°0 population is controlled by two different rates; (1) A fast relaxation into the bending mode levels (Rate 1) and (2) A slower relaxation of the bending mode energy via V-T collisions from the 01'0 level. This model is consistent with the results of Chapter 4, where it is shown that Rate 1 is at least as fast as the V-T rate.

We have determined the relaxation rates which control the time-dependence of the small-signal gain (see Figure 21 for an example). However, very rapid population changes are caused by stimulated emission during an intense laser pulse. The population changes take place on a timescale of ∿ 100 ns, and consequently different relaxation processes influence the development of the laser pulse. To optimise the performance of TE CO_2 lasers, it is of fundamental importance to determine these rates. It is the object of this Chapter to determine the relevant relaxation rates by comparing experimental laser pulses with the predictions of various theoretical models. It is shown that rotational relaxation processes dominate the laser dynamics in moderately low pressure TE CO_2 lasers. The inclusion of rotational coupling in the model of the laser dynamics represents a significant improvement over previous models [35-38], and accounts for most of the difficulties obtained with these models. We also investigate the lower laser level relaxation rates in detail, and values are determined for both Rate 1 and the V-T rate. These relaxation rates are measured under conditions relevant to the laser dynamics, and the results lead to a better understanding of the lower laser level relaxation processes.

6.1 Introduction

Several authors have published models of gain-switched laser pulses in TE CO_2 cavities [35-38]. These models are very similar in their treatment of the behaviour of the vibrational levels in CO_2, and they generally suppose that the rotational sublevels within the upper and lower laser level remain in thermal equilibrium throughout the laser pulse. At first sight, this seems very reasonable since the laser pulse is typically 200 ns long, and the rotational sublevels exchange energy on a subnanosecond time-scale in atmospheric pressure gas mixtures. However, the degree to which the rotational level population distribution is disturbed from its equilibrium value can be determined only by a comparison between the net rate of stimulated emission and the rate at which the rotational distribution is restored to equilibrium. It will be shown that, even at atmospheric pressure, the intense gain-switched laser pulse causes the rotational population distribution to deviate considerably from thermal equilibrium. We shall demonstrate that rotational coupling dominates the laser pulse dynamics in moderately low pressure TE CO_2 lasers.

In order to demonstrate the importance of rotational coupling, it is important to make accurate comparisons between theory and experiment. In particular, we wish to compare experimentally observed pulses with the pulses predicted by models which either include or exclude rotational coupling. To make these comparisons with any degree of success, it is essential that all experimental parameters are known, and that the only variables in the theory are the relaxation rates under consideration.

The experimental apparatus described in Section 6.2 is designed to allow the laser level populations at the onset of lasing to be determined. We use the simple and accurate method of directly measuring the small-signal gain in the laser cavity. The laser level populations at any instant of time can then be calculated as in Chapters 4 and 5. Furthermore, control over the time of lasing, and hence the initial level populations, is obtained by including a Q-switch in the cavity. This Q-switch also enables the laser pulse to be delayed until the influence of all extraneous discharge products has disappeared. The experimental technique enables us to carefully characterise the experimental conditions, which represents a considerable advantage over previous researchers [35-38]. In general, these authors estimated laser level populations by modelling the complex excitation processes occurring during the discharge pulse, following the procedure of Section 2.5. In addition, the time of lasing obtained experimentally could not be controlled; it was determined solely by the cavity build-up time (see Section 2.7). (Lyons [38] did employ a rotating mirror Q-switch, but this produces a continuously changing cavity loss). These factors introducean extraneous complexity into the fit between theory and experiment, in that the theoretical electron excitation parameters must be chosen to give the observed time-delay to lasing. We have designed our experiments to circumvent such difficulties, and directly determined the laser level populations at the onset of lasing. In comparing theory and experiment, Gilbert et al. [36], Vlases and Moeny [35], and Lyons, all found that the experimental pulses had much longer fall-times than those predicted by the theory. It will be shown that this is a direct consequence of the failure to include rotational coupling in the theoretical model.

The rotational energy exchange rate is pressure dependent, and reveals itself most strongly through laser operation at moderately low gas pressures. For this reason, the experimental work described subsequently was carried out for pressures in the range 30 - 150 torr. The observed laser pulses consisted of intense gain-switched spikes followed by slowly decaying "tails". The shape of the initial gain-switched spike is sensitive to the rotational relaxation rate in CO_2, whereas it will be shown that the behaviour of the laser pulse "tail" is determined by the various relaxation rates controlling the decay of the lower laser level population. All these relaxation rates can be determined by comparing theoretical and experimental laser pulses over a wide range of pressure. It is extremely important that rotational level coupling be properly incorporated into the theoretical model before a careful study is made of the laser pulse tails. This ensures that the appropriate conditions of inversion and radiation density at the outset of the output pulse tail can be reproduced. These correct starting conditions are essential for subsequent comparisons between the theoretical and experimental behaviour of the tails.

Section 6.3 details the theoretical model, and Section 6.4 demonstrates the effect of rotational coupling. Section 6.5 deals with the laser pulse tails, and relaxation rates for the lower laser level are determined. Finally, in Section 6.6, the importance of this work is discussed, and the results are related to the work of others.

6.2 Experimental Technique

Figure 34 is a schematic diagram of the apparatus used to observe the laser pulses. The laser cavity contains the linear pin-pin resistor type discharge tube (Allen-Bradley 56 Ω, spaced 3.8 mm apart) used in Chapters 4 and 5. Also present in the cavity are two 1" focal

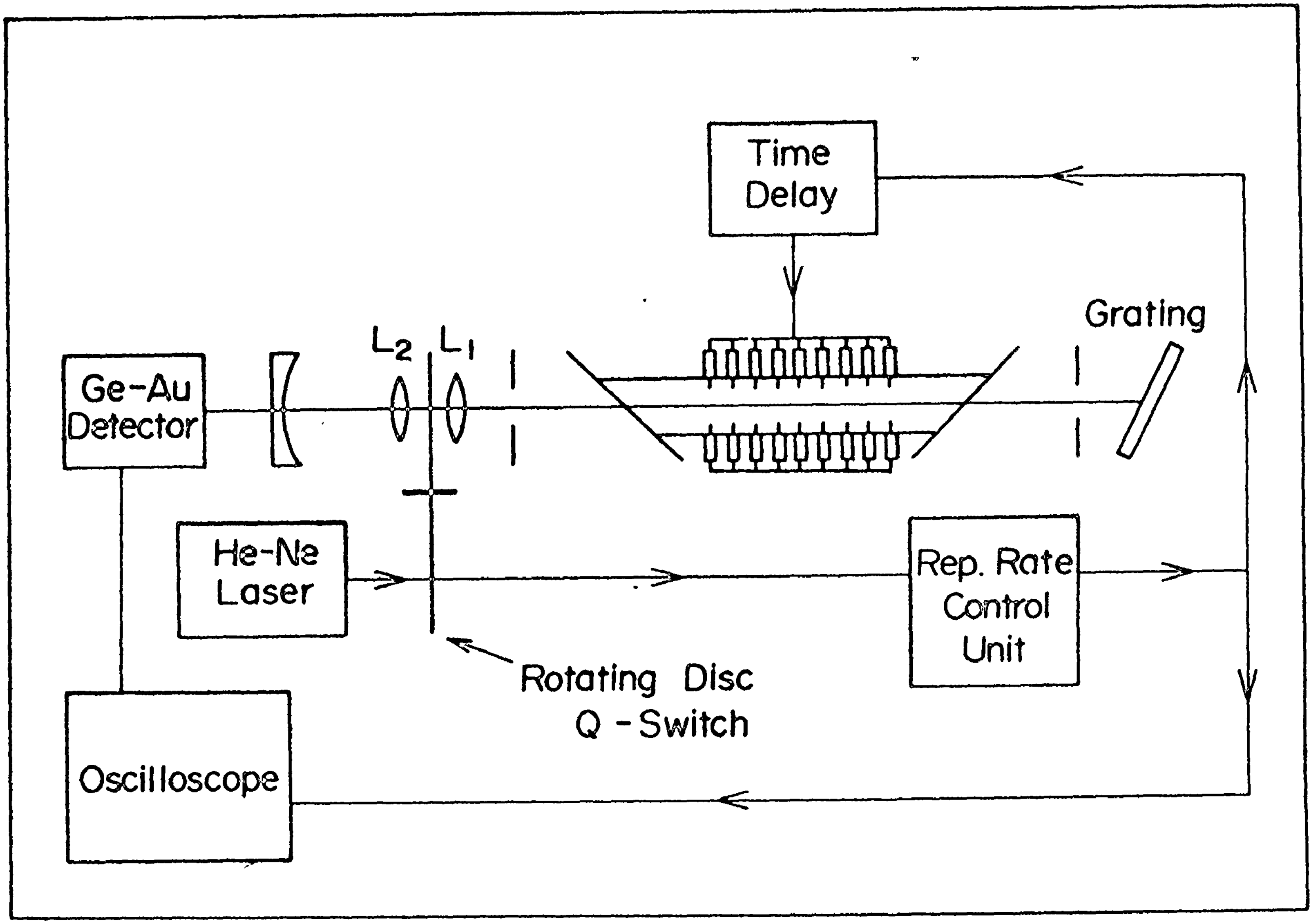
Time
Delay
Grating
Ge-Au
Detector
L_2
L_1
He-Ne
Laser
Rep. Rate
Control
Unit
Rotating Disc
Q -Switch
Oscilloscope

Figure 34: Schematic diagram of the apparatus used to observe Q-switched laser pulses.

length, antireflection-coated Ge lenses. A diffraction grating acts as one mirror of the resonator, and permits the laser wavelength to be selected from a range of rotational lines. The cavity can be Q-switched by means of a rapidly-rotating slotted disc, positioned to intersect the cavity at the common focus of the two lenses. The speed of the rotating disc can be varied up to a maximum of 30,000 rpm. At this speed the edge of the disc crosses the focal spot ($\sim$10 μ radius) in <200 ns. The corresponding cavity switch-on time is < 100 ns (50% loss to zero loss). This activation time of the Q-switch is considerably faster than the buildup time of the laser pulse; consequently no additional losses are introduced into the cavity during lasing. The timing of the Q-switching relative to the firing of the gain tube is controlled using a 6328 Å He-Ne laser "trigger" beam, in an identical manner to that described in Section 3.2. The time-delay controlling the firing of the laser discharge can be adjusted so that the laser pulse is located at any interval during the time-dependent gain. Two apertures were positioned in the cavity to ensure that lasing occurred in the TEM_{00} mode, and that no higher order transverse modes were present. The Ge:Au detector described in Section 3.2 was used; the detection system risetime was set initially at 2 ns. Lasing generally occurred on several longitudinal modes, as evidenced by nanosecond spiking structure in the pulse. It was experimentally determined that the laser pulse envelope did not depend upon the details of this structure. Consequently,the detector system response time was subsequently adjusted to display only the pulse envelope.

The magnitude and time-dependence of the small-signal gain in the discharge tube can be accurately determined by the methods described in the previous Chapters. The total cavity loss can be determined by two different methods; (1) Comparison with a cavity of known loss formed by two mirrors with known reflectivities,and (2) Directly measuring the small-signal gain in the cavity at threshold. These two methods gave results which were in good agreement. The total cavity length was 200 cm, and the cavity losses were such that the cavity decay time was 33 ns. The shape of the laser output pulse was studied at various stages during the time-development of the laser gain. Figure 35 illustrates the laser pulses observed prior to, and just after, the peak of the gain. In each pulse, the falltime of the initial gain-switched spike is much longer than the cavity decay time of 33 ns. This is a consequence of the finite coupling time between the rotational sublevels. The subsequent slower decay is controlled by the emptying of the lower laser level population. Notice particularly the relatively large and very long pulse tails which occur for laser operation at times well before the gain maximum. The pulse tails which occur for times at, and beyond, the gain peak are well-defined but relatively smaller in magnitude. Furthermore, the tails in this region decay away at a rate roughly an order of magnitude faster than those observed during the risetime of the gain. The great differences observed in the pulses which occur before or after the gain peak arise in the following manner.

FIGURE 35

Two experimentally observed laser pulses together with the small-signal gain profile. A 10% CO_2: 90% He gas mixture was employed, at a total pressure of 36 torr. Pulse 1 is obtained whenno Q-switch is used; lasing occurs early in the risetime of the gain. Pulse 2 is typical of the pulses obtained when lasing is arranged to take place at, or just beyond, the peak of the gain. Note that an expanded time-scale is employed in plotting Pulse 2. The peak intensity of Pulse 2 is 5 times that of Pulse 1.

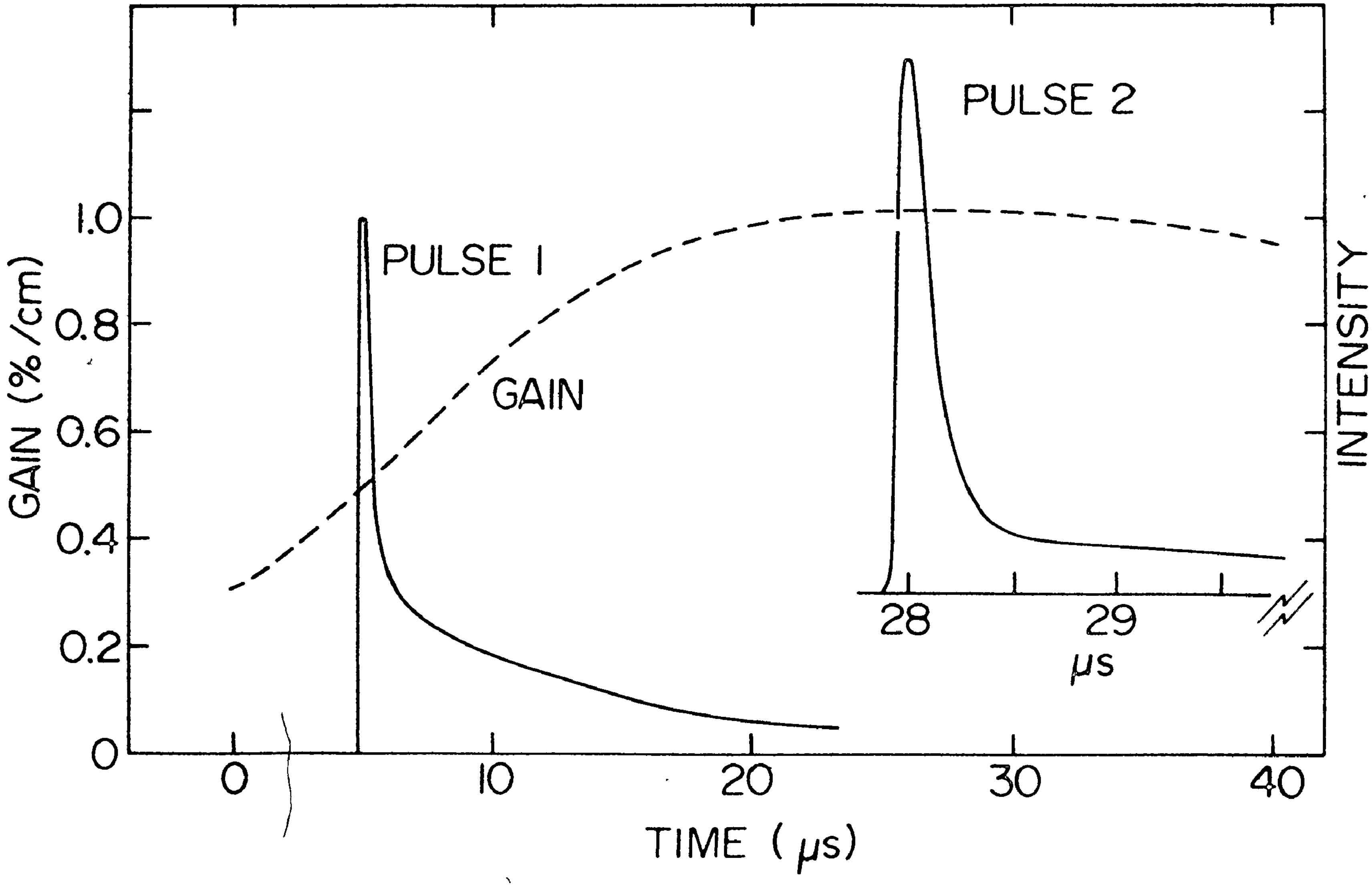
PULSE 1
PULSE 2
GAIN
GAIN (%/cm)
1.0
0.8
0.6
0.4
0.2
0
INTENSITY
0
10
20
30
40
TIME (μs)
28
29
μs

During the early part of the gain risetime, there is a large population in both the upper and lower laser levels. The gain increases as the population decays away from the lower laser level. The bending and symmetric stretching (BS) modes are in thermal equilibrium during this decay, which arises through V-T transitions from the 01'0 level. If lasing occurs during the early part of this decay, then there is a large population remaining in the lower laser level after the peak of the laser pulse. This population is near equilibrium with the rest of the BS modes. It decays away at the V-T rate and so serves to pump the inversion on the same time-scale. This pumping thereby controls the decay time of the laser pulse tail. When lasing occurs after the peak of the gain pulse, the situation is very different. In this case, the initial energy pumped into the BS modes has decayed away, and these modes are near equilibrium with the translational degree of freedom. As a consequence,the lower level is almost empty just prior to the onset of lasing. The population transferred to the lower laser level during the main laser pulse can now relax to the rest of the BS mode at Rate 1. Again, this produces a pumping of the inversion which serves to control the decay rate of the laser pulse tail. The time-scale is naturally much shorter in this case than when the decay is controlled by the V-T rate.

Evidently, we can qualitatively explain the behaviour of the laser pulse in the two different operating regimes. We must now develop a quantitative theory which includes all the features discussed above, i.e., rotational coupling, a fast relaxation of the lower laser level into the bending mode, and the V-T relaxation of the bending mode. If sufficiently good agreement is obtained between the laser model predictions and the experimental observations, values can be determined for the relevant molecular relaxation rates. In Sections 6.4 and 6.5 it will be shown that the agreement between theory and observation is excellent. This is particularly satisfying as it has not required the judicious use of a many variable-parameter fit.

6.3 Theoretical Model

The laser model employed here is similar to that used by Manes and Seguin [37]; but with the major difference that it has been extended to allow explicitly for the effects of rotational level coupling. The excess population in the lower laser level relaxes to the combined BS mode with a time constant τ_1. The BS mode thereafter loses energy at the V-T rate. We have simplified the model by considering all relaxation rates to be constant throughout the laser pulse. This assumption is reasonable when, as in the case here, all mode temperatures remain small during the pulse [37,94].

The differential equations governing the system are as follows:

$$\frac{dN_u}{dt} = -g_\alpha c(n^u_{J-1} - n^\ell_J)\rho - \frac{N_u}{\tau_u} \tag{6.1}$$

$$\frac{dN_\ell}{dt} = +g_\alpha c(n^u_{J-1} - n^\ell_J)\rho - \frac{N_\ell - N^e_\ell(T_1)}{\tau_1} \tag{6.2}$$

$$\frac{d(n^u_{J-1} - n^\ell_J)}{dt} = -2g_\alpha c(n^u_{J-1} - n^\ell_J)\rho - \frac{(n^u_{J-1} - n^\ell_J) - K(J)\Delta N}{\tau_R} \tag{6.3}$$

$$\frac{d\rho}{dt} = g_\alpha c(n^u_{J-1} - n^\ell_J)\rho - \frac{\rho}{\tau_c} \tag{6.4}$$

$$\frac{dE_{bs}}{dt} = \frac{E_u}{\tau_u} + \frac{E_\ell - E^e_\ell(T_1)}{\tau_1} - \frac{E_{bs} - E^e_{bs}(T)}{\tau_{VT}} \tag{6.5}$$

where $N_u(E_u)$, $N_\ell(E_\ell)$ are the populations (energies) in the upper and lower laser levels, $\Delta N = N_u - N_\ell$, n^u_{J-1} and n^ℓ_J are the populations of the particular rotational sublevels on which lasing occurs, and $K(J)\Delta N$ is the equilibrium value of the rotational inversion ($\sim$ 1/15 of the total inversion for P(18)). ρ is the in-cavity photon density and τ_c is the cavity decay time. The parameter E_{bs} is the energy in the combined BS modes, excluding the lower laser level, which is treated separately. (The energy E_{bs}, and its relationship to the temperature and populations of the BS modes,are treated in detail in Appendix B). When a parameter is written with the superscript e, e.g., $E_{bs}^{e}(T)$, it represents the equilibrium value of that parameter at a temperature T. The coefficient, g_α, is easily determined for any gas mixture and pressure using the data of Section 2.3. In general, g_α and K(J) have slightly different values for the upper and lower levels, but the average values can be used without any significant loss of accuracy. The other parameters occuring in these Equations are the relaxation times; τ_R is the rotational relaxation time and τ_u is the upper laser level decay time.

Observe that, provided the small-signal gain (which is a function of time) and the cavity decay time are known, the major unknown parameters are the relaxation times τ_R, τ_1 and τ_{VT}. It will be shown that by varying τ_R one obtains a single-parameter fit to the initial gain-switched spike, and that either τ_1 or τ_{VT} give a single-parameter fit to the laser pulse tail. A term was incorporated into the set of Equations 6.1 to 6.5 representing the pumping of the 00°1 level from combination levels such as 01'1. The rate constant determined by Burak et al. [69] was used for this purpose, but it turned out that this term made very little difference to the computed pulses. The same result was found for other similar pumping terms such as $CO_2(00°2) + CO_2(00°0) \rightarrow 2CO_2(00°1)$. The set of simultaneous equations were solved with a CDC 6400 computer, and the computer program accounted for the fraction of the cavity length which was actually filled by the gain medium.

In the following sections, we shall discuss experimentally observed laser pulses, and employ the above theory in their interpretation. Prior to proceeding with this plan, the predictions of the above theory for typical experimental circumstances are compared with those deduced by taking $\tau_R = 0$. That is, a comparison is made between the present and previously employed theories describing TE CO_2 lasers. Parameters typical of a 10% CO_2: 90% He gas mixture at a total pressure of 27 torr were employed for the calculations. This gas pressure is typical of those employed in the subsequent experiments. Similar differences between the two theories also occur at higher pressures. Figure 36 shows the predicted behaviour of the laser pulse and the gain in the P(18) transition as a function of time, obtained when the rotational levels maintain thermal equilibrium throughout the laser pulse. Observe that the laser pulse has a main peak which decays away rapidly, and is followed by a subsidiary peak. This reflects the behaviour of the inversion. The main laser pulse depletes the inversion almost to zero, and so (provided the cavity decay time is much faster than τ_1) the pulse decays away at a rate close to the cavity decay rate. The inversion then recovers as the excess population is removed from the lower laser level on a time-scale commensurate with τ_1. If this recovery produces a sufficiently large inversion, the radiation density will build up to another, smaller peak. This order of events may occur several times; a third pulse is in fact produced 3 μs after the main peak in this

FIGURE 36

Laser pulse and gain, calculated employing a model not including rotational coupling. All vibrational relaxation rates used in the calculations are chosen to correspond to a 10% CO_2: 90% He mixture at 27 torr total pressure; the values of Rate 1 and the V-T rate used are those determined in Section 6.5. All other parameters are chosen to correspond to the experimental cavity with an amplifier length of 92 cm. Lasing takes place at the peak of the time-dependent gain.

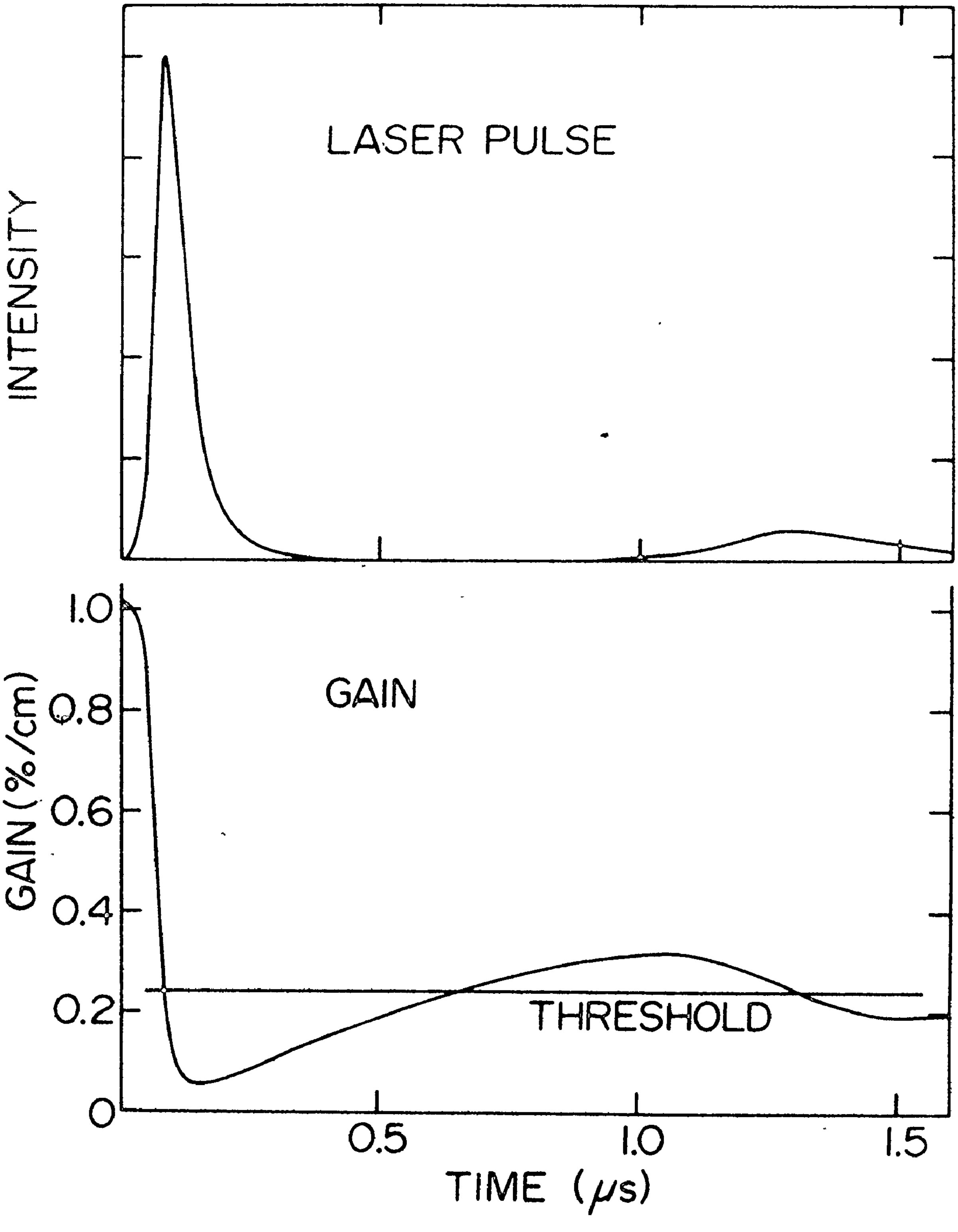
INTENSITY
LASER PULSE
GAIN (%/cm)
1.0
0.8
0.6
0.4
0.2
0
GAIN
THRESHOLD
0.5
1.0
1.5
TIME (μs)

case. Such behaviour has been predicted previously using similar laser models but has not usually been observed for gas mixtures without N_2 [36]. Figure 37 shows the behaviour of the laser pulse and gain predicted when the finite rotational level coupling time is taken into account. (The actual value used for the rotational relaxation rate is the one deduced in Section 6.4). For purposes of comparison, the gain corresponding to the thermal equilibrium inversion is also plotted for the same transition (dashed line). Observe that the laser output pulse now decays away monotonically,and that the P(18) inversion is reduced to a value considerably less than the equilibrium value. In this case, the transfer of energy from other rotational lines at a finite rate prevents the main peak of the pulse from depleting the entire inversion, and serves to hold the gain close to threshold at the start of the pulse tail. The inclusion of rotational coupling has a dramatic effect on the main laser pulse, its half width is increased by a factor of 3 and its peak intensity is reduced by a factor of 4.5. The tail decays at a rate determined by the emptying of the lower laser level. For the situation shown, the lower laser level emptying is controlled by τ_1. This is equivalent to the conditions of Pulse 2 in Figure 35, which bears a striking similarity to the theoretical pulse in Figure 37. The comparison of theoretical and experimental pulses is carried further in the next two sections. Section 6.4 deals specifically with the main laser pulse where the effect of τ_R is dominant, and Section 6.5 deals with the laser pulse tails which are controlled by τ_1 and τ_{VT}.

FIGURE 37

Laser pulse and gain calculated employing a model including the finite rotational level coupling time (τ_R = 10 ns). All other parameters are the same as for Figure 36. The dashed line indicates the time-dependence of $g_\alpha K(J)\Delta N$. Note the large departure from rotational equilibrium at the time of the laser pulse peak. The threshold gain is 0.24%/cm, the same as in Figure 36.

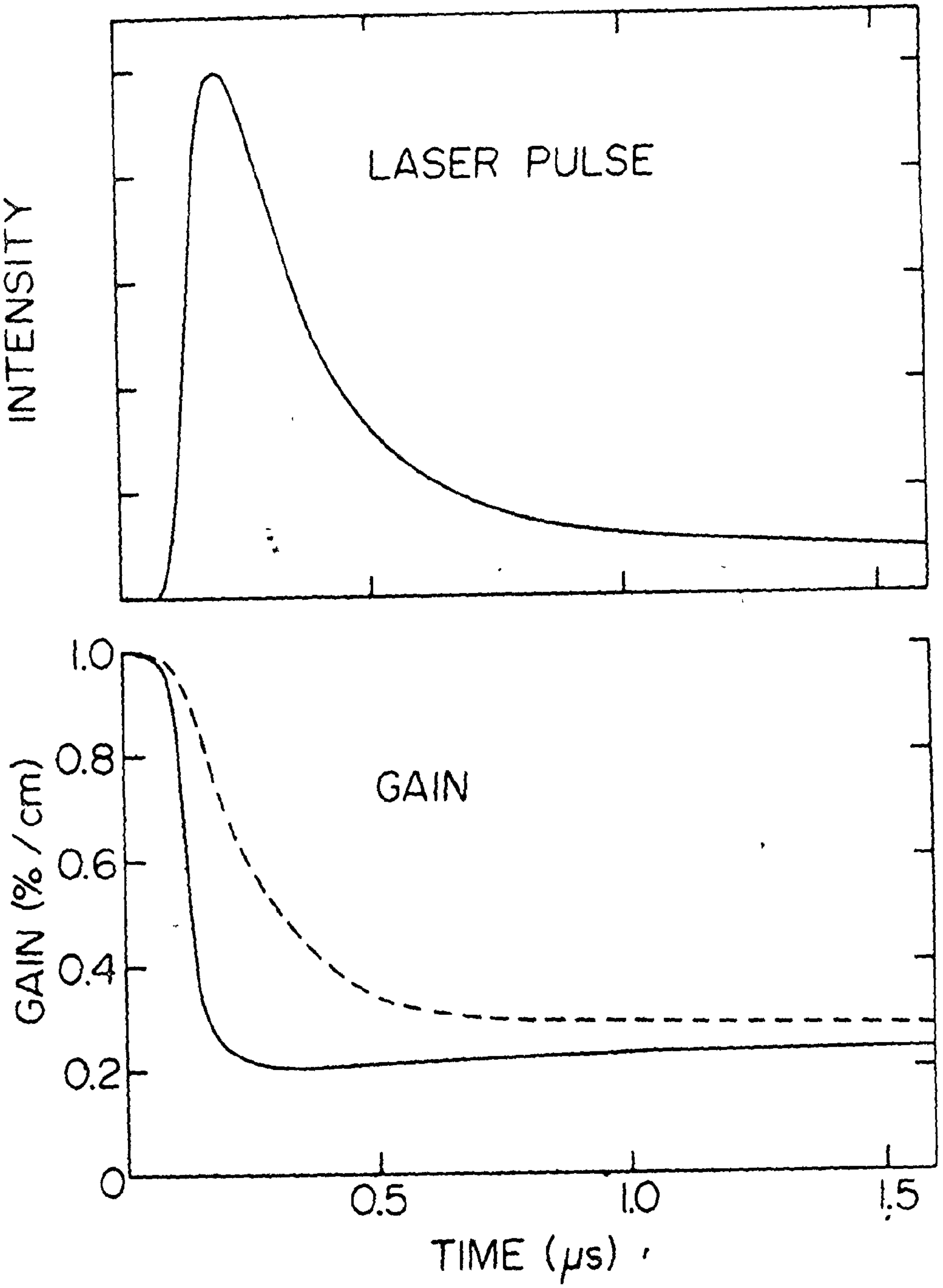
LASER PULSE
INTENSITY
GAIN
GAIN (% / cm)
1.0
0.8
0.6
0.4
0.2
0
0.5
1.0
1.5
TIME (μs)

6.4 Rotational Coupling and its Effect on the Main Laser Pulse

The possibility of significantly disturbing the rotational equilibrium in the CO_2 gain medium has been recognised previously in the case of amplification of nanosecond pulses [23-26]. In this case, there are not sufficient thermalising collisions to maintain the population equilibrium during the very brief period of interaction with the pulse. This is a transient effect. We show here that, even for very long pulses ($\sim 10^2$ rotational coupling times), the coupling between the rotational energy levels has a very significant impact on laser dynamics. In this case, the rotational distribution deviates from equilibrium on a quasi-steady state basis by an amount which depends on intensity. To see the potential impact of rotational coupling on the laser output, the theoretical model of Section 6.3 was employed to simulate the laser output for the conditions corresponding to Pulse 2 of Figure 35. Three different rotational coupling times were used. The results are displayed in the curves of Figure 38. Experimental points, taken from an oscilloscope trace photograph of Pulse 2, are indicated on each plot. The relevant laser parameters are given in the caption. Plot A shows the calculated laser output when the rotational distribution is undisturbed by coupling to the laser field. Once again, multiple output pulses are present. Plot B was calculated using a value of τ_R computed directly from previously reported values of the rotational coupling rates in CO_2: He mixtures [40,41]. Observe that multiple pulses no longer occur, and the pulse tail decays away on a time-scale much longer than

FIGURE 38

Computed laser pulses (solid lines) for a range of τ_R values. All other theoretical parameters are chosen to correspond to the experimental conditions appropriate to Pulse 2 of Figure 35. This pulse is indicated on each plot as a series of experimental points. The ratios of the initial inversion to the threshold inversion ($\Delta n_i : \Delta n_t$) is 4:1. The peak intensities of plots A, B and C are in the ratio 8:3:1.

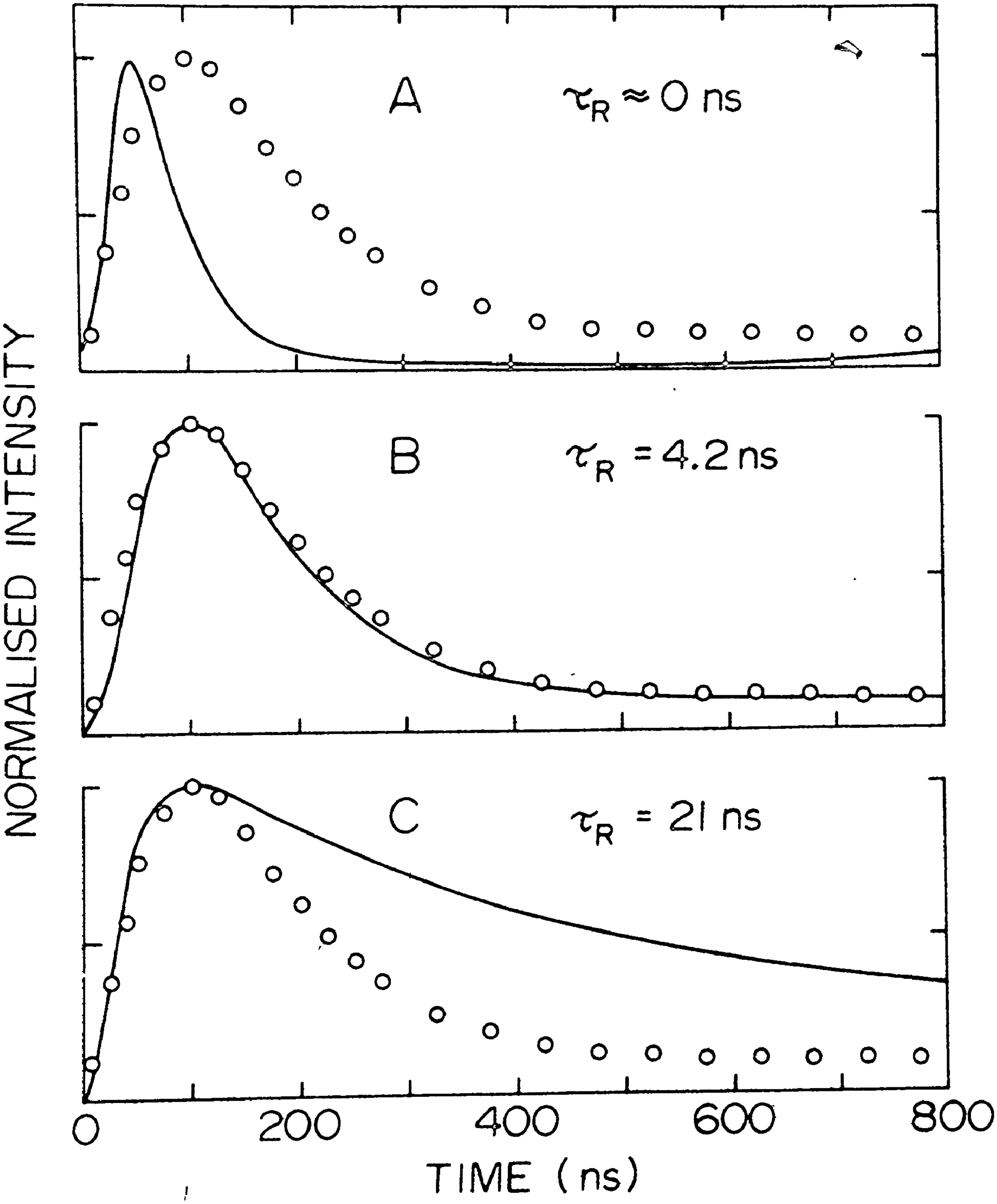
A
$\tau_R \approx 0$ ns
B
$\tau_R = 4.2$ ns
C
$\tau_R = 21$ ns
NORMALISED INTENSITY
0
200
400
600
800
TIME (ns)

that of the main peak. Plot C was computed using a value of τ_R five times larger than that used for B. As expected, increasing τ_R serves to increase the falltime of the main output pulse. Evidently, the behaviour of the laser pulse is quite sensitive to values of τ_R in the anticipated range. (The shape of the main laser pulse is not sensitive to the values of τ_1 and τ_{VT} employed in the model; the values determined in Section 6.5 are used). The similarity between the observed output and that displayed in Plot B is striking. The fit between theory and experiment in the main laser pulse can be optimised by varying the parameter τ_R. It is important to observe that this is the only adjustable parameter; all the other variables are known. Figure 39 shows the fit obtained in this way for two widely different gas pressures and ratios of gain to loss. It is noteworthy that the experimental change in the relative intensity of the laser pulse is also reproduced closely by the theory. No parameters are changed between these fits other than a scaling of all relaxation rates with pressure. The very good agreement between theory and experiment indicated in Figure 39 is typical of results obtained over pressures ranging up to 150 torr, and for many different values of gain and resonator loss. The present system could not be operated above 150 torr, since this marked the onset of intermittent air breakdown at the common focus of the two lenses employed in the Q-switch. Nevertheless, over the range of parameters studied, the output pulse is sensitive to the value of τ_R to the extent that it can be employed as a measure of the effective rotational relaxation rate. This

FIGURE 39

Comparison of computed (solid lines) and observed laser pulses for two widely different gas pressures in a 10% CO_2: 90% He mixture. At 72 torr, the experimentally measured $\Delta n_i:\Delta n_t$ ratio is 4:1, and at 27 torr it is 2:1, the cavity decay time is 33 ns. Identical values are used in the calculations. A rotational relaxation rate of 3.6×10^6 s^{-1} $torr^{-1}$ is used in each calculation, and all vibrational relaxation rates are similarly scaled with pressure.

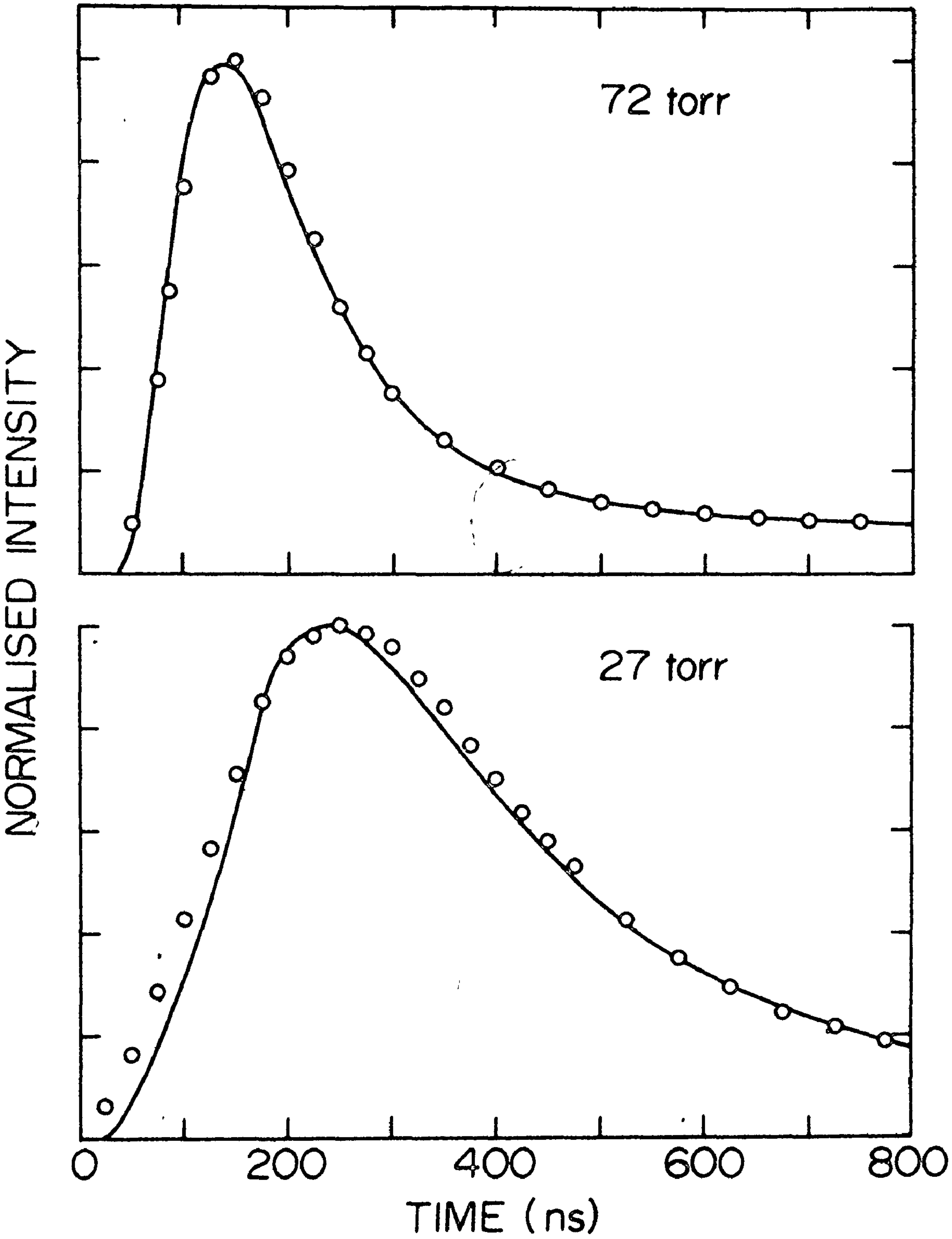
72 torr
27 torr
NORMALISED INTENSITY
0
200
400
600
800
TIME (ns)

rate was found to scale with pressure and had a value of $3.6\times10^{6}s^{-1}$ torr^{-1} for a 10% CO_2: 90% He mixture. Jacobs et al. [40,41] have directly measured the transient coupling rate into the single J = 19 level; they obtain a value of $6.6\times10^{6}s^{-1}$ torr^{-1}. This is in reasonable agreement with our measurement of an effective relaxation rate for the total energy in the rotational levels.

The model has been applied to calculate the change in output pulse obtained at high pressures for a 10% CO_2: 90% He mixture, due to the incorporation of rotational coupling. Figure 40 shows the results of such calculations (solid lines), compared with the outputs calculated for the same small-signal gain and resonator characteristics, but assuming the rotational level population always remains in thermal equilibrium (dashed lines). Observe that, at 300 torr, the effect of finite rotational energy transfer times is very large. The pulse intensity is approximately halved, and the pulse length is doubled. Even at atmospheric pressure, the effect of rotational coupling is still very significant. Clearly, the incorporation of a rotational coupling time into the laser dynamical equations is essential to the accurate modelling of gain-switched TE CO_2 laser pulses.

6.5 Laser Pulse Decay and Lower Level Relaxation Rates

In the previous section, we have demonstrated the importance of rotational coupling in the modelling of the main laser pulses. The proper incorporation of rotational level coupling also has a considerable

FIGURE 40

Computed laser pulses at high pressure in a 10% CO_2: 90% He mixture. The dashed lines are the results obtained from a model which does not include rotational coupling; the solid lines are the results obtained when a rotational relaxation rate of 3.6×10^6 s^{-1} $torr^{-1}$ is included. The cavity decay time is set at 15 ns (corresponding to a 1 m cavity with two mirrors of 80% reflectivity), and lasing occurs at the peak of the time-dependent gain. This peak gain is set at 1%/cm, and the amplifier length at 80 cm.

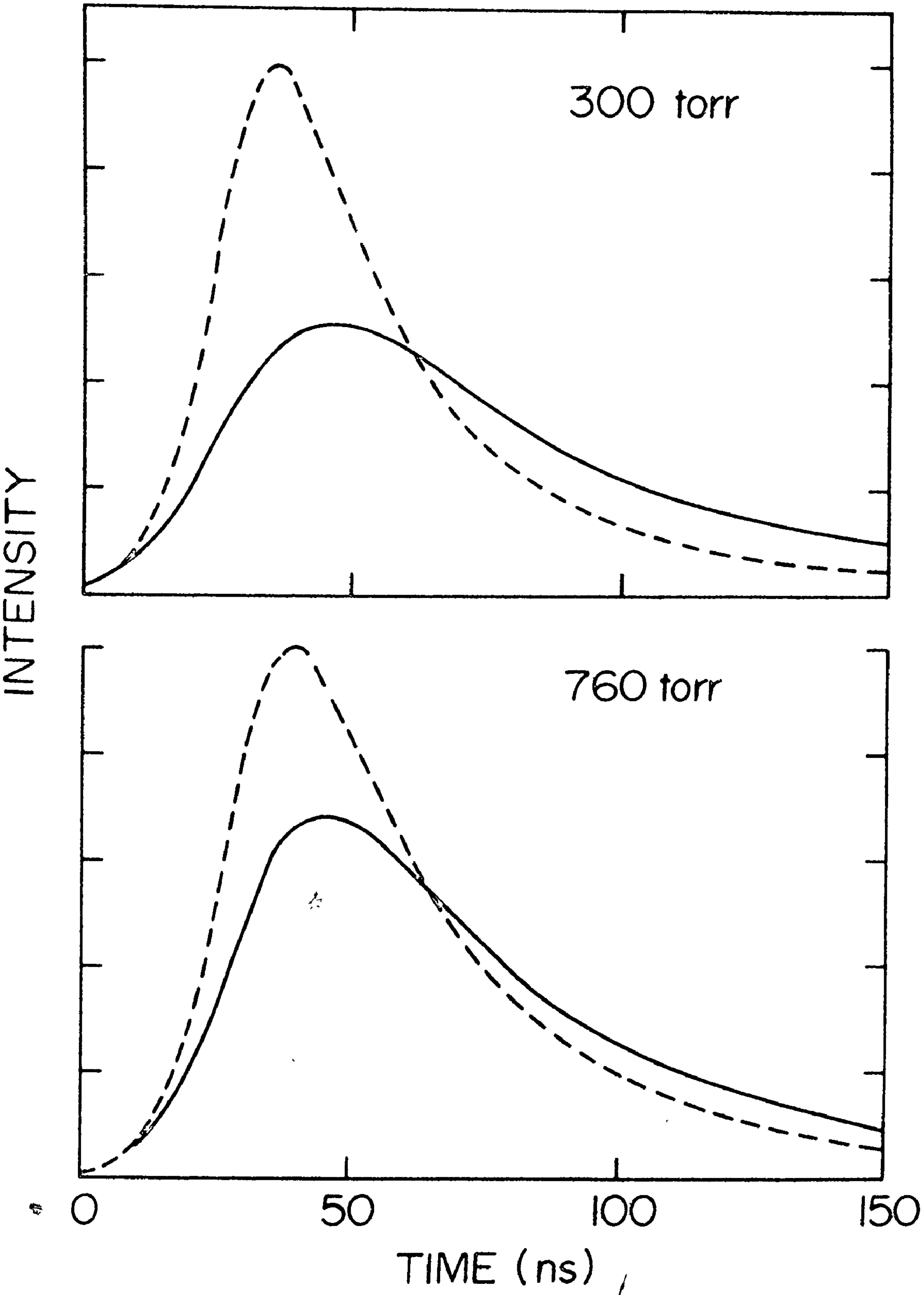
300 torr
760 torr
INTENSITY
0
50
100
150
TIME (ns)

impact on the modelling of the rate at which the laser energy decays away following the initial gain-switched peak. In this case, the impact of the rotational coupling rate is less direct; its importance lies mainly in the fact that the appropriate conditions of inversion and radiation density in the output pulse tail can be reproduced. We are now in a position to compare the observed laser pulse tails with those predicted by theory.

As described in Section 6.3, a proper choice of the time of lasing allows either τ_1 or τ_{VT} to dominate the laser decay. In essence, the fit to the gain-switched peak has been determined in the previous section, and only either τ_1 or τ_{VT}, whichever is appropriate, will be varied to obtain the correct behaviour of the laser pulse tail.

Figure 41 shows a typical example of an output pulse obtained for lasing during the risetime of the gain. The output pulse was displayed on an oscilloscope and then photographed. Experimental points, taken from such a photograph, are shown in the central plot of the figure. Also indicated are pulses predicted from the theory for different values of τ_{VT}. In order to provide a stringent test of the theory, τ_{VT} was not arbitrarily chosen to give the best fit. Instead, the value of τ_{VT} deduced from the data of Taylor and Bitterman [11] was used. For the gas mixture (10% CO_2: 90% He at 36 torr), τ_{VT} is 10 μsec. This value of τ_{VT} not only gives the excellent fit to the experimental laser pulse seen in Figure 41, but also accurately models the time-dependence of the experimental small-signal gain, when the lasing terms are removed from Equations

FIGURE 41

Computed laser pulses (solid lines) for a range of τ_{VT} values. All other parameters correspond to the experimental conditions appropriate to Pulse 1 in Figure 35; this pulse is indicated on the central plot as a series of experimental points.

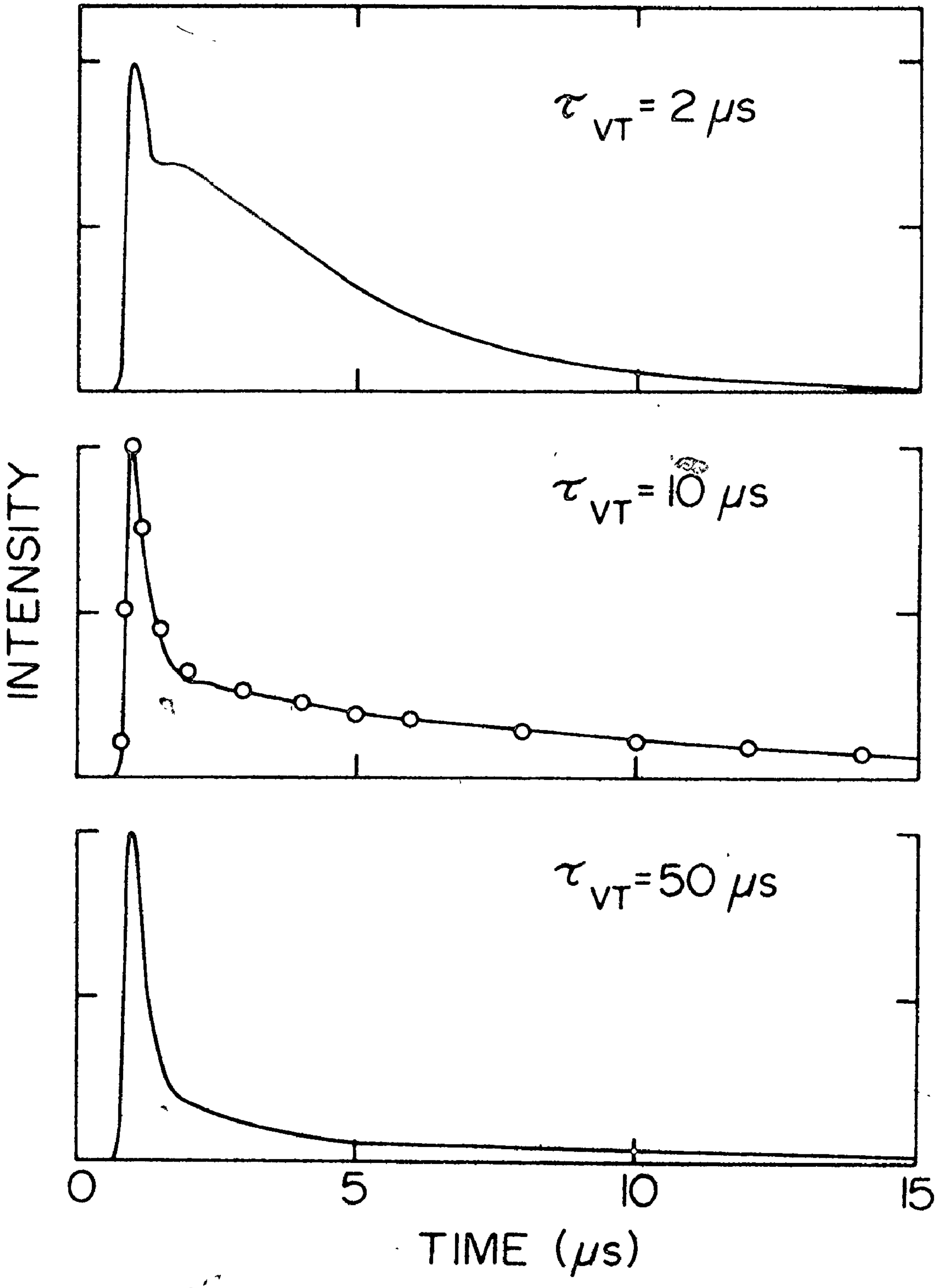
τ_{VT} = 2 μs
τ_{VT} = 10 μs
τ_{VT} = 50 μs
INTENSITY
0
5
10
15
TIME (μs)

6.1 to 6.5. (see Figure 21). The value of τ_1 used in the calculation is of little consequence provided it is faster than τ_{VT}.

Figure 42 shows an example of an output pulse, observed at a time just beyond the small-signal gain peak. Little change is observed in the general shape of the experimental pulse for later and later times during the decay of the gain. This indicates that once the gain has attained its peak value, all influence of extraneous discharge products has disappeared. In Figure 42, the experimental pulse is compared with pulses generated by employing several different values of τ_1 in the theoretical model. To better demonstrate the behaviour in the laser pulse tails, the laser intensities have been plotted on a logarithmic scale. Evidently, the pulse tail is very sensitive to the value of τ_1. As the discharge gas pressure is raised, τ_1 shortens, and eventually the laser pulse tail cannot be distinguished from the falling edge of the main peak. This occurs close to the upper operating pressure of the apparatus, i.e., 150 torr. Over the range of pressures studied, Rate 1 was found to scale with pressure and had a value of $4.6\text{x}10^4$ s^{-1} torr^{-1} for a 10% CO_2: 90% He mixture. Figure 43 shows the fits obtained, using this value, for two widely different gas pressures. It is a source of satisfaction that such excellent fits can be obtained by simply scaling all relaxation rates with pressure. Once again, the experimental change in the relative intensity of the laser pulse is also reproduced closely by the theory. In the following section, the significance of these observations is discussed, and the results are related to the work of others.

FIGURE 42

Computed laser pulses (solid lines) for a range of τ_1 values. All other relaxation rates are chosen to correspond to a 10% CO_2: 90% He mixture at the experimental pressure of 72 torr. The experimental pulse indicated in the central plot was obtained by Q-switching the cavity to give lasing at the gain peak (1%/cm, amplifier length 92 cm). To better demonstrate the behaviour in the laser pulse tails, the laser intensities have been plotted on a logarithmic scale.

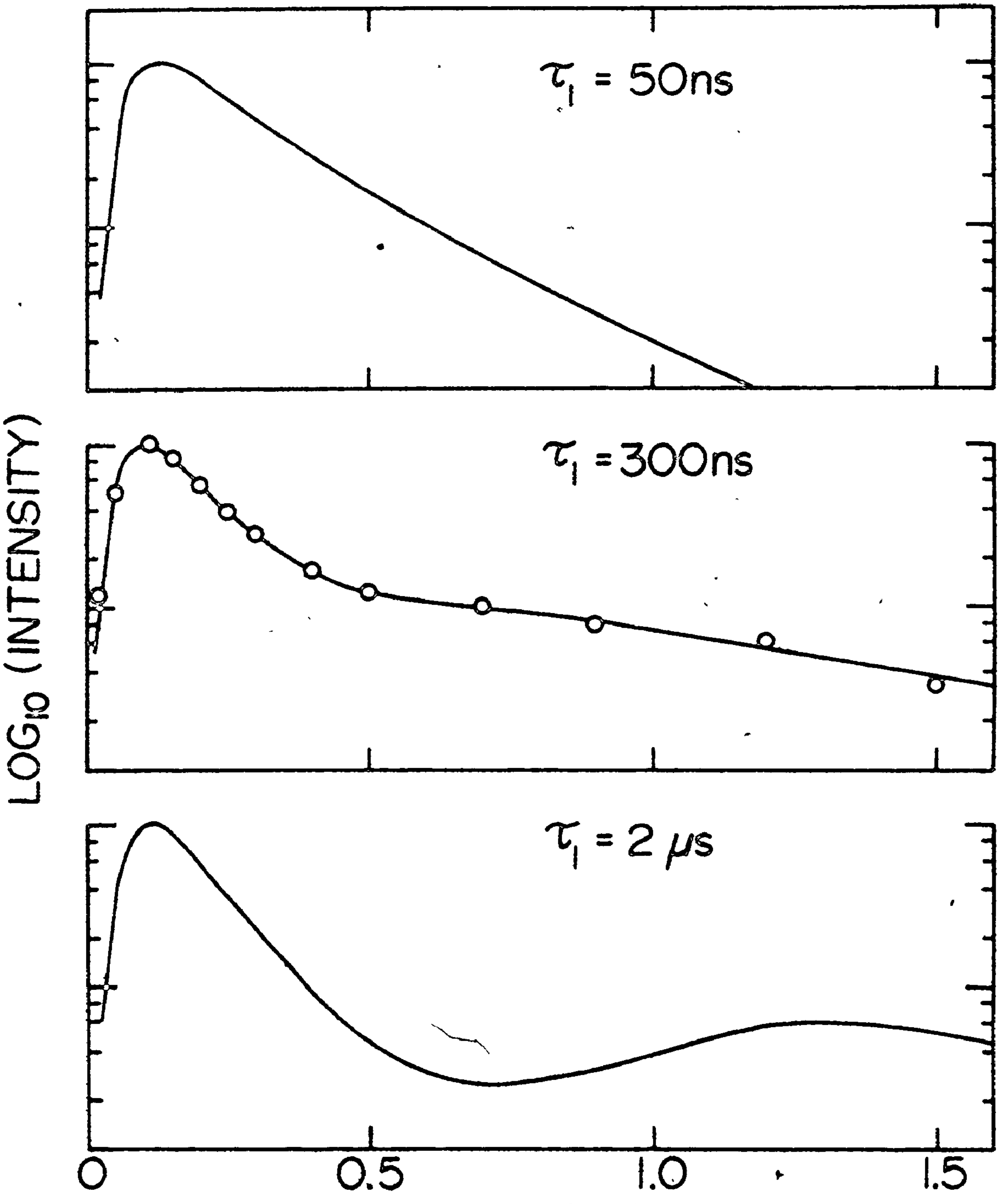
τ_1 = 50ns
τ_1 = 300ns
τ_1 = 2 μs
LOG$_{10}$ (INTENSITY)
0
0.5
1.0
1.5
TIME (μs)

FIGURE 43

Comparison of computed (solid lines) and observed laser pulses for two widely different gas pressures in a 10% CO_2: 90% He mixture. In each case, lasing took place just after the peak of the time-dependent gain (1%/cm, amplifier length 92 cm). Rate 1 is set at 4.6×10^4 s^{-1} $torr^{-1}$ in each calculation; and all other relaxation rates are similarly scaled with pressure.

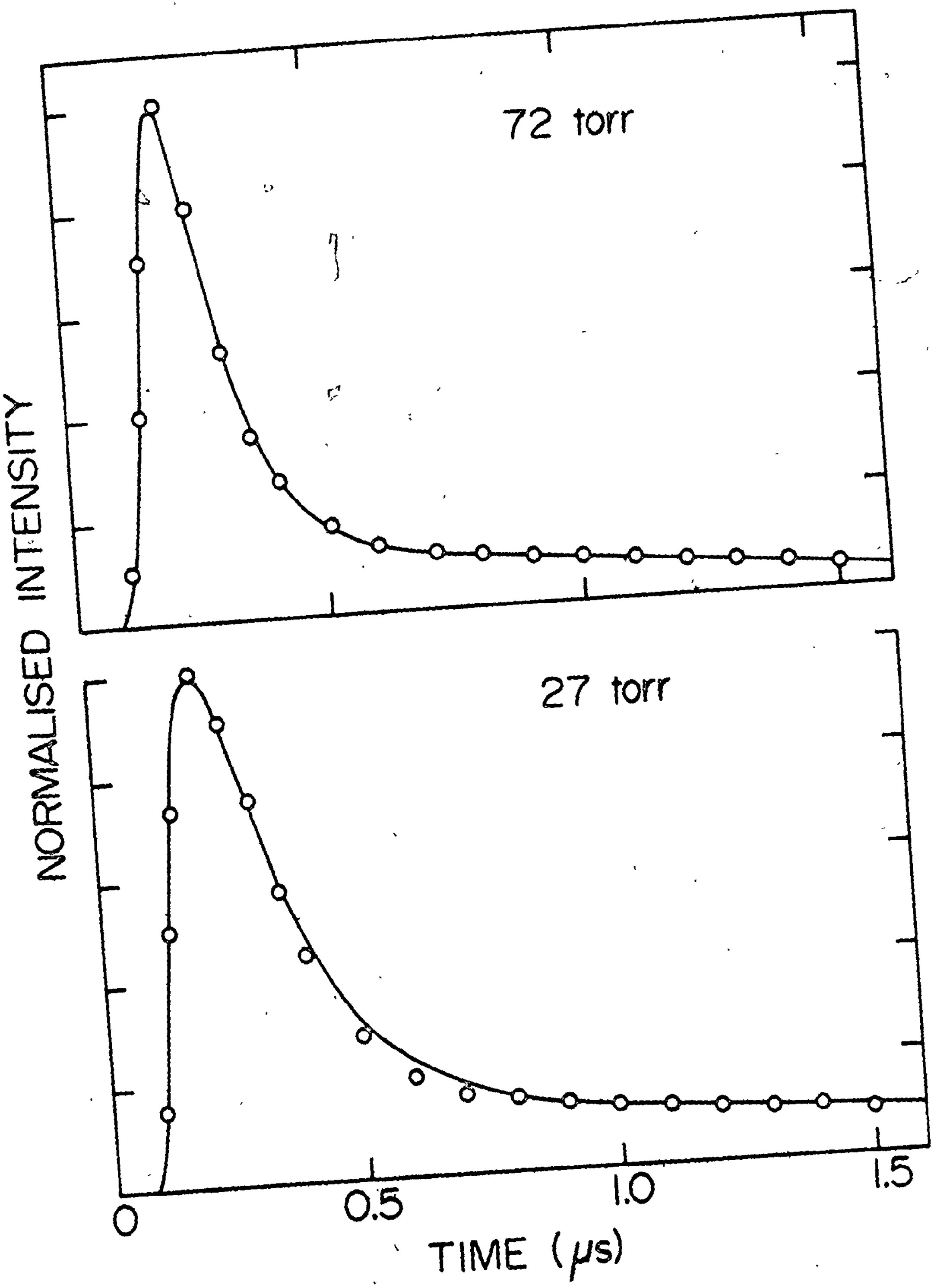
72 torr
27 torr
NORMALISED INTENSITY
0
0.5
1.0
1.5
TIME (μs)

6.6 Discussion and Conclusions

Previous models of gain-switched TE CO_2 lasers have not taken account of the finite coupling time between rotational sublevels of the 10.4 μ band [35-38]. We have demonstrated here that, in order to obtain good fits with experimentally observed laser pulses, it is necessary to include the effects of rotational coupling. The incorporation of a finite rotational coupling time into the laser dynamical equations immediately accounts for most of the difficulties obtained with previous models. First, it removes the predicted occurrence of multiple output pulses. Second, previously calculated laser pulses generally had peak intensities several times too large and falltimes much too short. Rotational coupling alone is sufficient to account for these discrepancies between theory and experiment. Even at atmospheric pressure, the effect of rotational coupling is very significant, and it dominates the laser pulse dynamics at pressures below 300 torr.

The laser model described in Section 6.3 not only fits the observed rise and fall-time of the main laser pulse, but also reproduces the appropriate conditions of inversion and radiation density in the initial part of the laser pulse tail. These correct starting conditions are essential for subsequent comparisons between the theoretical and experimental behaviour of the laser pulse tails. It is shown that the behaviour of the laser pulse tail is controlled by the emptying of the lower laser level. The relaxation of the lower laser level takes place in two stages: (1) A fast relaxation into the bending mode levels

(Rate 1), and a subsequent slower relaxation of the bending mode (V-T). By carefully controlling the experimental parameters, we have measured both these rates under actual lasing conditions. The results obtained for the V-T rate are in agreement with the data given by Taylor and Bitterman [11]. We have measured Rate 1 over a wide range of pressure for a 10% CO_2: 90% He mixture. The rate constant for the mixture is 4.6×10^4 s^{-1} $torr^{-1}$. Assuming that CO_2 is twenty times more effective than He for this relaxation [18], the effective relaxation rate for CO_2 is $\sim 3 \times 10^5$ s^{-1} $torr^{-1}$. This value is in good agreement with the calculations of Seeber [19] and Sharma [20], and with the experimental results of Stark [18]. Seeber calculates an effective value for Rate 1 of $\sim 2 \times 10^5$ s^{-1} $torr^{-1}$, while Sharma gives an estimate of $\sim 6 \times 10^5$ s^{-1} $torr^{-1}$. Stark has directly measured the 10°0 → 02°0 relaxation rate and obtains a value of 1.4×10^5 in CO_2. Manes and Seguin [37] have used a technique somewhat akin to the method reported here to estimate the coupling rate between the symmetric stretching mode and the bending mode in CO_2. By comparing experimental laser pulses at atmospheric pressure with a theoretical model, they determined that the intermode coupling rate was $\sim 1.4 \times 10^6$ $s^{-1}torr^{-1}$. However, their theoretical model did not explicitly include rotational relaxation, with the result that their estimated coupling rate is probably too fast.

It follows from the above that the lower laser level in CO_2 is very strongly coupled to the bending mode levels, with a coupling rate certainly greater than 10^5 $s^{-1}torr^{-1}$. This is much greater than the results reported by Bulthuis [12] and Rosser et al. [13], who obtain coupling rates of 1.5 x 10^4 and 10^3 $s^{-1}torr^{-1}$ respectively. Undoubtedly, these rates are incorrect for the lasing conditions reported here. The source of the very large disagreement is not clear and merits further investiation.

We have chosen to determine relaxation rates by fitting to the shape of the experimental pulses. In principle, the rates can be obtained by fitting to the absolute intensity of the pulses, but this requires a calibrated detector and an accurate knowledge of cavity mode and active medium volumes. These additional complications make intensity comparisons inherently less accurate than pulse shape comparisons. This is particularly true in the pulse tails, which contain only a small fraction of the total energy of the pulse. (An estimate was in fact made of the cavity mode and active medium volumes, and satisfactory agreement was obtained between experimental and theoretical intensities).

Although the relaxation rates reported here were measured in a 10% CO_2: 90% He mixture, the technique can easily be extended to measure rates in other He:CO_2 mixtures. Preliminary observations using other mixtures indicate that the V-T rate is helium-controlled, as is expected from the data of Taylor and Bitterman [11]. Preliminary results on the variation of Rate 1 with mixture indicate that CO_2 is roughly an order of magnitude more effective than He at relaxing the lower laser level into the bending mode. The addition of N_2 to the laser gas mixture produces laser pulses with very long tails which obscure the CO_2 relaxation rates. Nevertheless, by extending the theoretical model to include a nitrogen (ν = 1) pump term, the CO_2-N_2 coupling rate can, in principle, be determined.

The in-cavity laser technique described in this report is an extremely versatile method of measuring relaxation rates. We have employed it to measure relaxation times in CO_2 which differ by more than three orders of magnitude; from V-T times of tens of microseconds to rotational coupling times of nanoseconds. This method has the additional advantage that it measures directly relaxation rates which are relevant to the laser dynamics.

6.7 Summary

In this Chapter, the interaction between the CO_2 gain medium and intense laser radiation is studied. It is shown that rotational coupling is an extremely important aspect of the laser dynamics; and a theoretical model is developed which explictly includes the finite rotational relaxation time. This model gives an excellent fit between theory and experiment, which enables several important relaxation rates in CO_2 to be determined under conditions relevant to the laser dynamics.

CHAPTER 7

CONCLUSIONS

In this final Chapter, we shall outline the important conclusions that can be drawn from the work reported in this thesis. As detailed in Chapter 1, there are many shortcomings and areas of uncertainty in the generally accepted model of laser dynamics in CO_2. The work in this thesis was aimed at resolving some of these problems, and has, to a large extent, succeeded in this aim. Each of the last three Chapters contains a section giving a detailed discussion of the significance of the observations of that Chapter, and their relationship to the work of others. All the important conclusions are, in fact, covered in those sections; this Chapter is concerned with giving a brief account of the overall significance of the research.

The relaxation rates controlling the emptying of the lower laser level of CO_2 (10°0) were the first areas investigated in this thesis. The 10°0 level was thought to be strongly coupled to the bending mode levels, but previous authors have obtained relaxation rates into the bending mode which varied by more than three orders of magnitude, from $<10^3$ s^{-1} $torr^{-1}$ to $>10^6$ s^{-1} $torr^{-1}$. It was not even clear if the lower laser level emptied during the risetime of the small-signal gain. We have shown that the relaxation of the lower laser level is controlled by two different rates; (1) A fast relaxation into the bending mode levels (Rate 1),and (2) a slower V-T relaxation of the bending mode via the 01'0 level. In general, the V-T rate determines the risetime of the small-signal gain, whereas Rate 1 dominates the decay of the laser intensity. We showed that the V-T rate is controlled by the helium in the discharge mixture, and obtained a relaxation rate of $\sim 3.2\times10^{3}$ s^{-1} $torr^{-1}$, in good agreement with previous determinations. We have also demonstrated that the 10°0 level empties during the gain risetime, and is near equilibrium with the He thermal bath at the time of the gain peak. The fast relaxation rate is mainly controlled by CO_2-CO_2 collisions, and we obtained a relaxation rate of $\sim 3\times10^{5}$ s^{-1} $torr^{-1}$ for this process. Calculations have shown that the fast relaxation into the bending mode can take place via several alternative routes [19,20]. The actual relaxation mechanisms were not determined. However, we have obtained the overall relaxation rate, which is precisely that relevant to laser dynamics. It is this rate which controls the extraction of energy from the lasing medium during the gain-switched laser pulse. The measured rate is in good agreement with calculated values [19,20] and also is in accord with a recent direct determination of the 10°0 → 02°0 relaxation rate [18]. Our value of 3×10^{5} s^{-1} $torr^{-1}$ is much greater than the results reported by Bulthuis [12] and Rosser et al. [13], who obtain coupling rates of 1.5×10^{4} and 10^{3} s^{-1} $torr^{-1}$ respectively. Undoubtedly, these rates are incorrect for the conditions occurring in pulsed TE CO_2 lasers. The source of the very large disagreement is not clear, and merits further investigation of their experimental techniques.

To optimise the energy extraction per unit volume from TE CO_2 lasers, it is essential to know the limitations on the maximum useful input energy density. Gain saturation with increasing discharge energy has generally been observed in all TE laser systems, but it has usually been ascribed to secondary effects such as discharge deterioration or temperature increases. In Chapter 5, we have reported careful investigations of the gain saturation effect, and have clearly demonstrated that it is a fundamental property of CO_2 discharges. The saturation effect occurs in a manner consistent with the existence in the discharge of an electronic de-excitation process for the upper laser level. If such a de-excitation process indeed accounts for these observations, then the cross-section must be an order of magnitude larger than the corresponding excitation process. Evidence for the existence of de-excitation processes of this magnitude has also been obtained in work on low pressure CO_2 laser amplifiers. The theoretical basis for such a large value of the de-excitation cross-section is at present unclear; this cross-section is generally predicted to be only of the same order of magnitude as the excitation cross-section. It is evident that further investigation is required of the role of electrons in de-exciting vibrationally excited molecules in CO_2 lasers. The results of such investigations may lead to methods of dramatically increasing the energy per unit volume extractable from TE CO_2 lasers.

For many applications of TE CO_2 lasers, the peak intensity of the laser pulse, rather than the total energy, is the most important consideration. In Chapter 6, we have investigated the effect of rotational coupling on the peak intensity obtainable in a gain-switched laser pulse. Previous models of gain-switched laser pulses have ignored the impact of the finite rotational relaxation time. We have demonstrated, on the contrary, that a proper account of rotational coupling is crucial to the laser dynamical modelling at pressures below 300 torr. Rotational coupling has a very significant effect even at atmospheric pressure. We have included a rotational coupling term in a theoretical model of the laser pulse, and obtained an excellent fit between theory and experiment. This was not previously possible. It is shown that, during the intense laser pulse, the rotational distribution deviates from equilibrium on a quasi-steady state basis by an amount which depends on intensity. The effective rotational relaxation rate under these conditions was determined to be $3.6\text{x}10^6$ s^{-1} $torr^{-1}$ for a 10% CO_2: 90% He mixture. This is in reasonable agreement with the directly measured transient coupling rate of $6.6\text{x}10^6$ s^{-1} $torr^{-1}$. The model of rotational coupling used in Chapter 6 assumes that all rotational levels are coupled to the lasing level with the same time constant, τ_R. This assumption enables us to obtain an excellent fit between theory and experiment. However, it takes no account of the possible existence of selection rules governing rotational transitions [39-41]. This type of selection rule would result in slower effective rotational coupling rates for rotational levels far removed from the lasing transition. The next step in the accurate modelling of TE CO_2 laser dynamics would be an investigation of the potential importance of such rules. However, this would require more complicated experiments than those described here. For example, much information concerning these processes could be gathered by monitoring the inversion in one rotational transition while lasing occurs between two other rotational levels. The mechanism of rotational coupling in molecular systems is of fundamental interest, and such investigations are important for their own sake. Nevertheless, by demonstrating that rotational coupling in TE CO_2 lasers is much more important than previously suspected, we have provided an added incentive for the undertaking of such experiments.

APPENDIX A

THE PARTITION FUNCTION OF CO_2 AND ITS INFLUENCE ON THE LASER LEVEL POPULATIONS

The vibrational partition function of CO_2 can be readily calculated, using elementary statistical mechanics, provided that each normal mode of vibration of CO_2 is treated as an harmonic oscillator. This model assumes that the influences of Fermi resonance, vibrational-rotational interaction, and ℓ-doubling are all negligible. According to Gray and Selvidge [91], these simplifications result in errors of less than 2% in the computation of the partition function for temperatures up to 1200°K.

We shall calculate the partition function in the most general case, i.e., when the asymmetric stretching, symmetric stretching, and bending modes all have different temperatures. These temperatures are represented by T_a, T_s and T_b respectively. ξ_a, ξ_s and ξ_b represent the energy spacings of the three normal modes, and x_a, x_s and x_b correspond to the exponential factors: $\exp(-\xi_a/kT_a)$, $\exp(-\xi_s/kT_s)$ and $\exp(-\xi_b/kT_b)$. The simplified partition function, Q, is given by [95]:

$$Q = \left(\frac{1}{1 - x_a}\right)\left(\frac{1}{1 - x_s}\right)\left(\frac{1}{1 - x_b}\right)^2 \qquad (A.1)$$

The squared term associated with the bending mode takes account of the double degeneracy of this mode.

Gray and Selvidge have calculated the partition function of CO_2 from 150°K to 1200°K [91]. They consider the case when all the modes of CO_2 are in thermal equilibrium, i.e., $T_a = T_s = T_b$ = translational temperature, T. Some of their results are given in Table 3. Note that even when all the anharmonic and resonance factors are accounted for, the accurate partition function differs little from the simplified form given by Equation (A.1). This is particulary true for temperatures below 500°K.

In this thesis we are concerned with the effect of the partition function upon the laser level populations; in particular its influence during the risetime of the small-signal gain. In the simple harmonic oscillator approximation, the population densities of the upper and lower laser levels (N_u and N_ℓ) are given by:

$$N_u = \frac{N_o x_a}{Q} \tag{A.2}$$

$$N_\ell = \frac{N_o x_s}{Q} \tag{A.3}$$

where N_o is the total density of CO_2 molecules. It should be emphasised that only molecules in the 00°1 and 10°0 states contribute to the gain in the 10.4 μ band; molecules in combination states such as 01'1 and 11'0 do not, in general, affect the gain. In Chapters 4 and 5, we studied the effect of the changing partition function during the risetime of the gain. During the gain risetime, very little energy

TABLE 3

Vibrational Partition Function of CO_2 (from Reference 91)

Temperature °K	Vibrational Partition Function as given by (A.1)	Accurate Vibrational Partition Function
200	1.017	1.017
300	1.088	1.089
400	1.218	1.220
500	1.400	1.405
600	1.634	1.643
700	1.920	1.936
800	2.264	2.287
900	2.670	2.703
1,000	3.144	3.191
1,100	3.693	3.756
1,200	4.325	4.408

decays away from the asymmetric stretching mode, and hence x_a is relatively constant. The bending and symmetric stretching modes are in equilibrium, i.e. $T_b = T_s = T_1$, and T_1 relaxes at the V-T rate. Hence the gain at any instant of time is given by

$$\alpha(J) = g_\alpha(J)\,(N_u - N_\ell) \tag{A.4}$$

$$= g_\alpha(J)\,\frac{N_o}{Q\,(T_1)}\left[x_a - \exp(-\frac{\xi_s}{T_1})\right]$$

The coefficient, $g_\alpha(J)$, is readily determined from the data given in Section 2.3. During the risetime of the gain, the time-dependence of $\alpha(J)$ is controlled by the time-dependence of T_1. At the gain peak, the BS modes are near equilibrium with the translational temperature and the subsequent time development of the gain is determined by the slow decay of x_a. In Chapter 5, we use (A.4) to determine x_a from a knowledge of $\alpha(J)$ and T_1 at the gain peak.

Further use of (A.4) is made in Chapter 4. By extrapolating the falltime of the gain to the time of the current pulse, the initial value of x_a can be determined. The initial value of $\alpha(J)$ is obtained directly from the measured gain "step" and hence T_1 is the only unknown in (A.4). Note that T_1 occurs twice in Equation (A.4), with the result that $\alpha(J)$ is very sensitive to the value of T_1.

In Chapter 4, an alternative model is postulated to explain the gain risetime. In this model, it is assumed that the bending and symmetric stretching modes are not strongly coupled, and that the increase in gain during the risetime is caused mainly by relaxation from the bending mode. Consequently, x_a and $x_s(T_s)$ are relatively constant during the risetime, and only T_b is strongly time-dependent. To clearly demonstrate the relative time-dependencies we can re-write (A.4) as:

$$\begin{aligned} \alpha(J) &= g_\alpha(J)\ (N_u - N_\ell) \\ &= g_\alpha(J)\ \frac{N_o}{Q(T_b)} \left[x_a - x_s \right] \end{aligned} \qquad (A.5)$$

During the gain risetime, the only large change is in the value of T_b, and consequently in Q.

We shall conclude this Appendix with a specific example of the use of the partition function. From the data of Figure 21 (page 76) it can be seen that the small-signal gain increases by approximately a factor of three during the risetime. If the two models represented by (A.4) and (A.5) are used to interpret this increase, the results obtained are

$$T_1 = 630°\text{K} \qquad (A.4)$$

$$T_b > 1200°\text{K} \qquad (A.5)$$

These very different results are used in Chapter 4 as evidence that Equation (A.4) correctly represents the gain dynamics.

APPENDIX B

THE ENERGY IN THE COMBINED BENDING AND SYMMETRIC STRETCHING MODE

In Chapter 6, the parameter E_{bs} is introduced to represent the energy in the combined BS mode. This energy is calculated under the assumption that the bending and symmetric stretching modes have a common temperature T_1. In the simple harmonic oscillator approximation, E_{bs} is given by the sum of the energies in the two modes [96]

$$E_{bs} = \xi_s \left[\frac{x_s}{(1-x_s)^2}\,\frac{N_o}{Q}\right] + 2\xi_b \left[\frac{x_b}{(1-x_b)^3}\,\frac{N_o}{Q}\right] \qquad (B.1)$$

using the nomenclature of Appendix A. We make the further approximation that the symmetric stretching energy levels have exactly double the energy spacing of the bending mode levels, i.e., $\xi_s = 2\xi_b$. Consequently, $x_s = x_b{}^2$, and we can use Equation (A.1) to simplify (B.1), thus

$$E_{bs} = 2\xi_b N_o (1-x_a) \; x_b \left[\frac{3x_b+1}{x_b+1}\right] \qquad (B.2)$$

where x_b is equal to $\exp(-\xi_b/kT_1)$. Equation (B.2) is used extensively in the computer program described in Chapter 6. It relates E_{bs} to T_1 and vice versa.

REFERENCES

[1] C.K.N. Patel, W.L. Faust, and R.A. McFarlane, Bull. Am. Phys. Soc. 9, 500 (1964), and Phys. Rev. Lett 12, 588 (1964).

[2] C.K.N. Patel, Phys. Rev. 136A, 1187 (1964).

[3] A.J. Demaria, Proc. IEEE 61, 731 (1973).

[4] A.E. Hill, Appl. Phys. Lett. 16, 423 (1970).

[5] R. Dumanchin and J. Rocca-Serra, C.R. Acad. Sci. Paris 269, 916 (1969).

[6] A.J. Beaulieu, Appl. Phys. Lett. 16, 504 (1970).

[7] M.C. Richardson, A.J. Alcock, K. Leopold, and P. Burtyn, IEEE J. of Quantum Electronics QE-9, 236 (1973).

[8] O.R. Wood, Proc. IEEE 62, 355 (1974), and cited references.

[9] P.K. Cheo, J. Appl. Phys. 38, 3563 (1967).

[10] P.K. Cheo, IEEE J. Quantum Electronics QE-4, 587 (1968).

[11] R.L. Taylor and S. Bitterman, Rev. Mod. Phys. 41, 26 (1969).

[12] K. Bulthuis, J. Chem. Phys. 58, 5786 (1973).

[13] W.A. Rosser, E. Hoag, and E.T. Gerry, J. Chem. Phys. 57 4153 (1972).

[14] L.J. Denes and L.A. Weaver, J. Appl. Phys. 44, 4125 (1973).

[15] H. Brinkschulte and R. Lang, Phys. Lett. 47A, 455 (1974).

[16] C.K. Rhodes, M.J. Kelly, and A. Javan, J. Chem. Phys. 48, 5730 (1968).

[17] T.A. DeTemple, D.R. Suhre, and P.D. Coleman, Appl. Phys. Lett. 22, 349 (1973).

[18] E.E. Stark, Appl. Phys. Lett. 23, 335 (1973).

[19] K.N. Seeber, J. Chem. Phys. 55, 5077 (1971).

[20] R.D. Sharma, J. Chem. Phys. 49, 5195 (1968).

[21] W.L. Nigham, Phys. Rev. A 2, 1989 (1970).

[22] J.J. Lowke, A.V. Phelps, and B.W. Irwin, J. Appl. Phys. 44, 4664 (1973).

[23] J.F. Figueira, W.H. Reichelt, G.T. Schappert, T.F. Stratton, and C.A. Fenstermacher, Appl. Phys. Lett. 22, 216 (1973).

[24] G.T. Schappert, Appl. Phys. Lett. 23, 319 (1973).

[25] E.E. Stark, W.H. Reichelt, G.T. Schappert, and T.F. Stratton, Appl. Phys. Lett. 23, 322 (1973).

[26] B.J. Feldman, IEEE J. Quantum Electronics QE-9, 1070 (1973).

[27] W.L. Nigham, Appl. Phys. Lett. 15, 355 (1969).

[28] C.B. Mills, J. Appl. Phys. 45, 1336 (1974).

[29] W.P. Allis and H.A. Haus, J. Appl. Phys. 45, 781 (1974).

[30] A.M. Robinson, Can. J. Phys. 50, 2138 (1972).

[31] J.L. Lachambre, J. Gilbert, F. Rheault, R. Fortin and M. Blanchard, IEEE J. Quantum Electronics QE-9, 459 (1973).

[32] J.F. Figueira, Opt. Commun. 11, 220 (1974).

[33] W.T. Leland, M.J. Nutter, J.P. Rink and C.A. Fenstermacher, "Characteristics of high pressure CO_2 laser amplifiers pumped with electron beam", presented at the 25th Gaseous Electronics Conference, London, Ontario, Canada (1972).

[34] J.M. Hoffman, F.W. Bingham, and J.B. Moreno, J. Appl. Phys. 45, 1798 (1974).

[35] G.C. Vlases and W.M. Moeny, J. Appl. Phys. 43, 1840 (1972).

[36] J. Gilbert, J.L. Lachambre, F. Rheault, and R. Fortin, Can. J. Phys. 50, 2523 (1972).

[37] K.R. Manes and H.J. Seguin, J. Appl. Phys. 43, 5073 (1972).

[38] D.L. Lyon, IEEE J. Quantum Electronics QE-9, 139 (1973).

[39] R.L. Abrams and P.K. Cheo, Appl. Phys. Lett. 15, 177 (1969).

[40] R.R. Jacobs, K.J. Pettipiece, and S.J. Thomas, Appl. Phys. Lett. 24, 375 (1974).

[41] R.R. Jacobs, S.J. Thomas, and K.J. Pettipiece, IEEE J. Quantum Electronics QE-10, 480 (1974).

[42] P.K. Cheo, "CO_2 lasers" in Lasers, Vol. 3, A.K. Levine and A.J. Demaria Eds. New York: Marcel Dekker, 1971 p.111.

[43] G. Herzberg, "Spectra of diatomic molecules", 2nd Edition, Van Nostrand Reinhold Co., New York: 1950.

[44] E. Fermi, Z. Phys. 71, 250 (1931).

[45] G. Herzberg, "Infrared and Raman spectra", Van Nostrand Co., Princeton, 1945.

[46] A.C.G. Mitchell and M.W. Zemansky, "Resonance radiation and excited atoms", University Press, Cambridge, 1961, p. 95.

[47] J.C. Polanyi, Appl. Opt. Supp. 2, Chemical Lasers, 109 (1965).

[48] C. Cousin, C. Rossetti, and C. Meyer, C.R. Acad. Sc. Paris 268B, 1640 (1969).

[49] R.R. Patty, E.R. Manring, and J.A. Gardner, Appl. Opt. 7, 2241 (1968).

[50] R. Ely and T.K. McCubbin, Appl. Opt. 9, 1230 (1970).

[51] T.Y. Chang, Opt. Commun. 2, 77 (1970).

[52] A.D. Devir and U.P. Oppenheim, Appl. Opt. 8, 2121 (1969).

[53] B. Hartmann and B. Kleman, Can. J. Phys. 44, 1609 (1966).

[54] J.A. Howe and R.A. McFarlane, J. Mol. Spectroscopy 19, 224 (1966).

[55] C.K.N. Patel, Phys. Rev. Lett 13, 617 (1964).

[56] T. Holstein, Phys. Rev. 70, 367 (1946).

[57] J.P. Rink, J. Appl. Phys. 43, 2441 (1972).

[58] L.J. Denes and J.J. Lowke, Appl. Phys. Lett. 23, 130 (1973).

[59] R.D. Hake and A.V. Phelps, Phys. Rev. 158, 70 (1967).

[60] M.J.W. Boness and G.J. Schulz, Phys. Rev. Lett. 21, 1031 (1968).

[61] M.J.W. Boness and G.J. Schulz, Phys. Rev. 9A, 1969 (1974).

[62] A. Andrick,D. Danner, and H. Ehrhardt, Phys. Lett. 29A, 346 (1969).

[63] C.R. Claydon, G.A. Segal, and H.S. Taylor, J. Chem. Phys. 52, 3387 (1970).

[64] G.J. Schulz, Phys. Rev. 125, 229 (1962).

[65] G.J. Schulz, Phys. Rev. 135, A988 (1964).

[66] A.G. Engelhardt, A.V. Phelps, and C.G. Risk, Phys. Rev. 135, A1566 (1964).

[67] O.P. Judd, J. Appl. Phys. 45, 4572 (1974).

[68] H. Statz, C.L. Tang and G.F. Koster, J. Appl. Phys. 37, 4278 (1966).

[69] I. Burak, Y. Noter, and A. Szoke, IEEE J. Quantum Electronics, QE-9, 541 (1973).

[70] J. Reid, B.K. Garside, and E.A. Ballik, IEEE J. Quantum Electronics QE-9, 602 (1973).

[71] B.K. Garside, E.A. Ballik and J. Reid, J. Appl. Phys. 43, 2387 (1972).

[72] J. Reid, B.K. Garside, and E.A. Ballik, IEEE J. Quantum Electronics, QE-8, 449 (1972).

[73] R. Fortin, M. Gravel,and R. Tremblay, Can. J. Phys. 49 1783 (1971).

[74] A.M. Robinson, J. Appl. Phys. 42, 4098 (1971).

[75] R.R. Jacobs, Rev. Sci. Instrum 44, 1146 (1973).

[76] G. Otis and R. Tremblay, Can. J. Phys. 52, 257 (1974).

[77] M.C. Fowler, J. Appl. Phys. 43, 3480 (1972), and cited references.

[78] A.M. Robinson, Can. J. Phys. 50, 2471 (1972).

[79] J.Y. Coester and Ph. Vautier, Infrared Physics 7, 173 (1967).

[80] S. Singer, IEEE J. Quantum Electronics QE-10, 829 (1974).

[81] C. Meyer, C. Rossetti, and P. Barchewitz, IEEE J. Quantum Electronics, QE-6, 179 (1970).

[82] A.A. Mikaberidze, V.N. Ochkin, and N.N. Sobolev, Sov. J. Quant. Electronics 3, 21 (1973).

[83] D. Gaultier, D. Bailly, E. Arie, and C. Rosetti, C.R. Acad. Sc. Paris B272, 269 (1971).

[84] D. Bailly, D. Gaultier, C. Rossetti, and P. Barchewitz, Can. J. Phys. 50, 2605 (1972).

[85] S.J. Kast and C. Cason, J. Appl. Phys. 44, 1631 (1973).

[86] T.W. Johns and J.A. Nation, Appl. Phys. Lett. 20, 495 (1972).

[87] O.P. Judd and J.Y. Wada, IEEE J. Quantum Electronics QE-10, 12 (1974).

[88] R.W. O'Neil, R.J. Carbone, H. Granek, and H. Kleiman, Appl. Phys. Lett. 20, 461 (1972).

[89] W.J. Weigand, M.C. Fowler and J.A. Benda, Appl. Phys. Lett. 16, 237 (1970).

[90] K.K. Corvin and S.J.B. Corrigan, J. Chem. Phys. 50, 2570 (1969).

[91] L.D. Gray and J.E. Selvidge, J. Quant. Spectrosc. Radiat. Transfer 5, 291 (1965).

[92] M.C. Gower and A.I. Carswell, Appl. Phys. Lett. 22, 321 (1973).

[93] B.M. Christophe and A.A. Offenberger, Can. J. Phys. 50, 368 (1972).

[94] W.J. Witteman, J. Chem. Phys. 35, 1 (1961).

[95] A.L. Hoffman and G.C. Vlases, IEEE J. Quantum Electronics, QE-8, 46 (1972).

[96] B.F. Gordietz, N.N. Sobolev, V.V. Sokovikov, and L.A. Shelepin, IEEE J. Quantum Electronics QE-4, 796 (1968).